

ABSTRACT

Title of Document: SINGLE MOLECULE FRET OF LACI-DNA-
IPTG LOOP CONFORMATIONS

Kathy A. Goodson, Doctor of Philosophy, 2012

Directed By: Associate Professor, Jason D. Kahn, Department
of Chemistry & Biochemistry

This work focuses on the *Escherichia coli* lactose repressor protein (LacI) which represses expression of the *lac* operon. In order to repress transcription, the tetrameric LacI protein binds a primary promoter-proximal operator, O₁, and one of two auxiliary operators, O₂ or O₃. The binding of these two sites to a single LacI molecule occurs via DNA loop formation. Induction of the *lac* operon by allolactose reduces the affinity of LacI for DNA, but induction does not completely prevent looping *in vivo*. The synthetic inducer isopropyl-β-D-thiogalactoside (IPTG) acts similarly to allolactose. Model DNA constructs have been used to demonstrate, through fluorescence resonance energy transfer (FRET) analysis, that LacI may change conformation in order to form more than one loop structure. This work employs single molecule FRET to investigate LacI-induced loop formation in DNA looping constructs, as a function of IPTG concentration, on freely diffusing LacI-DNA complexes. The results include evidence for the persistence of DNA loop

formation under at saturating IPTG concentration, and they provide a detailed view of how LacI conformation affects DNA loop formation. In addition, this work explores possible changes in geometry in LacI-induced DNA loops through the use of model DNA constructs that produce alternative loop topologies. We propose that inducer-bound LacI-DNA looped complexes may control the kinetics of induction and repression of the operon.

SINGLE MOLECULE FRET OF LACI-DNA-IPTG LOOP CONFORMATIONS

By

Kathy A. Goodson

Dissertation submitted to the Faculty of the Graduate School of the
University of Maryland, College Park, in partial fulfillment
of the requirements for the degree of
Doctor of Philosophy
2012

Advisory Committee:
Associate Professor Jason D. Kahn, Chair
Associate Professor Douglas S. English
Professor Dorothy Beckett
Professor David Fushman
Associate Professor Srinivasa Raghavan

© Copyright by
Kathy A. Goodson
2012

Dedication

I dedicate this to my mother, Trina, who believed in me before I even knew how to believe in myself. She inspires me to be more.

Acknowledgements

I would like to thank my advisors Dr. Jason Kahn and Dr. Douglas English. They have both taught me the meaning of the phrase “to think,” how to always be excited about science, and encouragement on saying what I mean, and meaning what I say. I thank my Independent Proposal advisor Dr. Dorothy Beckett. She taught the true meaning of communicating my science. I would also like to thank Dr. David Fushman for optimistic encouragement. Thank you Dr. Srinivasa Raghavan for serving as part of the committee for my dissertation work. I would also like to thank Dr. Squire Booker for my introduction to Biochemistry and Dr. Jim Watson for always asking if this was my “best.” I appreciate the generous support of NOBCChE and the CLFS Board of Visitors.

V.S.U....I love it...I love it (repeat). Without my undergraduate education at Virginia State University I would not have found my way through graduate education at the University of Maryland. While there are indeed many persons who influenced my time there, in brief I would like to thank Dr. Ralph Gatrone and Dr. Michael Shackleford.

It takes a village. I would like to thank the Kahn, English, and Rokita labs (you have a thermocycler like no other) for being the absolute best. Working with them has made them more like family than friends. I would like to thank Aaron, Dan, Lucas, Sarah, Xiayou, Jason, Sara, Zifan, Patrick, Petrina, and Jen. I would like to give a special thanks to Sara for watching our favorite show together on the one molecule at a time channel. To Jen...just 'cause we're in lab doesn't mean we can't cause any trouble. Thanks to the NOBCChE crew. Petrina thank you for the pure

comedy and Caedmon for not so randomly and repetitiously asking me about those NOBCChE meetings.

I would like to thank my family and my friends who are family for their love and support. I thank my parents, Trina and Ernest, and my sister and brother, Lisa and David, and my Uncle Alvin and Aunt Denise. Thank you to Aretha for being everyone's (yes everyone's) mom away from home. To A, my best friend, thank you for being my, sister, friend, conscience, and more. Philippians 4:13.

Table of Contents

Dedication	ii
Acknowledgements	iii
Table of Contents	v
List of Tables	vii
List of Figures	viii
Chapter 1: Single Molecule Analysis of LacI-DNA Loop Conformation	1
<u>1.1 Introduction: DNA Morphology</u>	1
1.1.1 Implications of DNA Loop Complexes in Gene Regulation	3
<u>1.2 Lac Repressor System: Model for Gene Regulation and DNA Looping</u>	4
1.2.1 lac Operon	4
1.2.2 Lac Repressor Protein	7
1.2.3 DNA Looping	10
<u>1.3 Lac Repressor-DNA Loop Complexes</u>	13
1.3.1 Hyperstable Looped Complexes	13
1.3.2 Effector Molecules and Lac-Repressor-DNA Loop Complexes	15
<u>1.4 Single Molecule Spectroscopy, Confocal Microscopy, and SM-FRET</u>	17
<u>1.5 Single Molecule Confocal Microscopy and SM-FRET Analysis of Freely Diffusing LacI-DNA Loop Complexes</u>	19
1.5.1 Introduction	19
<u>1.6 Methods of Single Molecule Study: FRET and Single Molecule Spectroscopy</u>	20
<u>1.7 Experimental Design: Synthesis and Characterization of Fluorophore Labeled Model DNA Constructs (9C14)</u>	27
<u>1.8 Previous Studies of DNA-LacI Looped Complexes</u>	29
1.8.1 FRET Evidence for Open/Closed Loop Preference	29
1.8.2 SM-FRET Evidence for a Single Population	29
<u>1.9 Research Objectives</u>	32
Chapter 2: SM-FRET Analysis of Freely Diffusing 9C14 DNA with IPTG	35
<u>2.1 Introduction</u>	35
<u>2.2 Materials and Methods</u>	35
<u>2.3 Results</u>	41
2.3.1 Electrophoretic Mobility Shift Assay Results for LacI-9C14-IPTG Complexes	41
2.3.2 Bulk FRET Studies	43
2.3.2 SM FRET LacI-9C14 Results for Titration with IPTG	46
2.3.3 SM-FRET Results on LacI-9C14 with LacI Pre-Incubated with IPTG	51
<u>2.4 Discussion</u>	55
Chapter 3: SM-FRET Analysis of Freely Diffusing DNA-LacI Molecules with Proposed Alternative Loop Geometries	57
<u>3.1 Introduction</u>	57
<u>3.2 Materials and Methods</u>	62
<u>3.3 Results</u>	64

3.3.1 Selection of Samples Based on Bulk FRET Results for LacI-Landscape Complexes.....	64
3.3.2 SM-FRET Results for LacI-Landscape Complexes	65
<i>3.4 Discussion</i>	77
Chapter 4: Implications of Presented Studies and Areas of Future Work	81
<i>4.1 Introduction</i>	81
<i>4.2 Biological Consequences of DNA-Protein Complexes, DNA Looping, and DNA Loop Topology</i>	82
<i>4.3 Systems Biology Applications</i>	85
Appendices.....	87
<i>Appendix I LacI Purification</i>	87
<i>Appendix II Data Analysis and Error Propagation</i>	90
<i>Appendix IV Immobilization of Model DNA Constructs</i>	99
Bibliography	106

List of Tables

Table 1: Selection of molecules for SM-FRET analysis based on bulk FRET landscapes.	65
--	----

List of Figures

Figure 1.1 Control of expression by allolactose.	5
Figure 1.2 DNA loops resulting from Lac repressor binding in the <i>lac</i> operon.	7
Figure 1.3 LacI with and without IPTG.....	8
Figure 1.4 DNA looping trajectories.	12
Figure 1.5 Layout of the 9C14 and 11C12 model constructs.	13
Figure 1.6 Transcriptional periodicity of DNA looping.	16
Figure 1.7 Structure of Alexa 647.....	21
Figure 1.8 Excitation (solid lines) and emission (dotted lines) spectra of donor and acceptor labeled primers.	22
Figure 1.9 Microscope set up.....	26
Figure 1.10 DNA looping construct 9C14 and models for LacI-DNA loops.....	28
Figure 1.11 Freely diffusing single molecule studies of 9C14-LacI loop complexes.	31
Figure 1.12 Model for LacI-DNA loops.	33
Figure 2.1 Amine modified thymine (IDT).	37
Figure 2.2 EMSA of IPTG binding to LacI-DNA complexes demonstrates stable LacI-DNA-IPTG loops.	42
Figure 2.3 Bulk FRET of LacI-9C14 complexes in the presence and absence of IPTG.	44
Figure 2.4 Establishing equilibrium among looped and unlooped states.	46
Figure 2.5 Single-molecule fluorescence experiments on freely diffusing LacI-9C14-IPTG complexes.....	49
Figure 2.6 Single-molecule fluorescence titration experiments	50
Figure 2.7 Binding cycle of LacI to IPTG and DNA.....	51
Figure 2.8 Single-molecule fluorescence experiments on freely diffusing LacI-9C14-IPTG complexes in which LacI was pre-incubated with IPTG.	53
Figure 2.9 Single-molecule fluorescence experiments on freely diffusing LacI-9C14-IPTG complexes.....	54
Figure 3.1 Layout and schematic of the model construct landscape.	58
Figure 3.2 Top view of LacI bound to extended operator DNA with highlighted Alexa Flour® 555 donor (green) and Alexa Fluor® 647 acceptor (red) fluorophore points of attachment.	59
Figure 3.3 Models for LacI-DNA loops with fluorophores.....	60
Figure 3.4 Bulk FRET population maps of LacI-landscape complexes.	61
Figure 3.5 SM-FRET histograms of LacI-landscape complexes.....	65
Figure 3.6 Single-molecule FRET experiments on freely diffusing LacI-landscape complexes.	73
Figure 3.7 Single-molecule diffusing FRET experiments on freely diffusing 13C14 DIAI and 13C14 DIAE LacI-landscape complexes.....	75
Figure 3.8 Single-molecule diffusing FRET experiments on freely diffusing 7C16 DIAI and 7C16 DEAI LacI-landscape complexes.....	76
Figure 3.9 Model of LacI-DNA looped complex differential response to DNA expansion for antiparallel and parallel loop topologies.	78

Figure 4.1 Schematic of proposed loop formation at the apex of a negatively supercoiled plectoneme.....	83
Figure 4.2 Stochastic model for the functions of alternative DNA loops during repression, induction, and re-repression.	85

Abbreviations

APD	avalanche photodiode
AI or AE	Acceptor flurophore attachment inside (AI) or outside (AE) of the operator sequence.
A	Antiparallel loop (A1 or A2)
BSA	bovine serum albumin
Cy5	Cyanine 5
DCLP	dichroic long pass
DTT	dithiothreitol
DI or DE	Donor flurophore attachment inside (DI) or outside (DE) of the operator sequence.
EMSA	electrophoretic mobility shift assay
EDTA	ethylenediaminetetraacetic acid
FPLC	Fast protein liquid chromatography
FRET	Förster/fluorescence resonance energy transfer
iAmMC6T	Internal Amino Modifier C6 dT (IDT ordering code)
IDT	Integrated DNA Technologies
IPTG	isopropyl- β ,D-thiogalactoside
LacI	Lac repressor
NEB	New England Biolabs
P	Parallel loops (P1 or P2)
PCR	polymerase chain reaction
SM-FRET	single molecule fluorescence resonance energy transfer

SMS	single molecule spectroscopy
SPCM	single photon counting modules
TAMRA	tetramethylrhodamine

Chapter 1: Single Molecule Analysis of LacI-DNA Loop Conformation

1.1 Introduction: DNA Morphology

DNA is the molecular building block of genetic information. DNA is a water soluble macromolecule made up of four basic structural units, the adenine (A), thymine (T), guanine (G), and cytosine (C) nucleotides. The double helical structure of DNA is derived from Watson-Crick base pairing, A:T and G:C of the nucleotides (Chargaff, 1950; Watson and Crick, 1953). DNA possesses the ability to self organize, which allows DNA to have specific regions of coordinated structure or topological domains (Condon, 2006).

DNA morphology is its mode of communication in the cell and can influence recognition, binding, and packing. DNA itself is described as a polymer (Hagerman, 1988). Polymers may be described in terms of their inherent stiffness defined as persistence length which approximates the distances between one bend to another bend along the length of the molecule. At lengths below its persistence length a polymer acts as a flexible elastic rod (Eslami-Mossallam and Ejtehadi, 2009) and at lengths much greater than the persistence length polymers behave like a random coil. The persistence length of double stranded DNA is ~50 nm (approximately 150 bp); however, the overall length of chromosomal DNA much longer (Hagerman, 1988).

The length of DNA in a cell can be up to a hundred thousand times that of the actual cell's diameter. The 1 mm length of chromosomal DNA of *E. coli* occupies a cell that is 2 μm long and between 0.5 and 1 μm wide (Lodish, 2000). One method of compression of chromosomal DNA in a bacterial cell is DNA supercoiling. The

predicament of packaging of DNA in eukaryotes is assisted through the use of proteins, known as histones, allowing formation into highly supercoiled, tightly compacted complexes called chromatin (Lodish et al., 2000).

The compaction of chromosomal DNA to fit into the cell is associated with DNA supercoiling in which two or more distinct DNA sequences which are distant from each other are brought together (Vologodskii et al., 1992). The distance between binding sites for activator proteins and promoters can be on the order of kb in eukaryotes (Blackwood and Kadonaga, 1998). The bridging of two distinct sites on DNA molecules is characterized by DNA loop formation in which a protein (or protein complex) simultaneously binds to each individual DNA site (Schleif, 1992; Whitson et al., 1987). The effective concentration increase of distinct DNA sequences as allowed by DNA supercoiling facilitates DNA loop formation (Schleif, 1992). The juxtaposition of two distinct DNA sites is approximately 2 fold higher in supercoiled DNA than of relaxed DNA (Vologodskii and Cozzarelli, 1996). Specific reactions may be promoted by the conformation of supercoiled DNA. For example, the mode of action of eukaryotic topoisomerases distinctively recognize juxtaposed helices (Zechiedrich and Osheroff, 1990).

DNA looping is a regulatory factor in transcription, recombination, and replication. In short DNA loops, with lengths that are less than the DNA persistence length of 150 bp, as depicted here, the major factor influencing of looping is DNA elasticity including DNA bending and twisting. The free energy of looping indicates the ease of loop formation and thus predicts the effect of DNA sites far removed from one another. The most important free energy component as presented in our studies

is that of DNA elasticity.

1.1.1 Implications of DNA Loop Complexes in Gene Regulation

Regulation and cellular behavior are linked to the physical properties of DNA. *In vivo*, one finds a variety of loop types and thus a variety of intrinsic properties related to these loops including DNA elasticity and plasticity of looped complexes. A complete and thorough characterization of the dependence of DNA looping free energy on the molecular properties of the proteins, the DNA, and the protein-DNA complexes is critical in developing quantitative models for DNA looping (Kuhlman et al., 2007). The theory may be incorporated to algorithms to predict changes in gene expression, but the treatment so far has been simplistic. The study of looping complexes begins with the classic definition of the biological function of looping as seen in the *lac* operon.

The Lac Repressor (LacI) homotetramer, consisting of a dimer of dimers, has the ability to bind two operator sites simultaneously, forming a DNA loop (Bellomy et al., 1988; Friedman et al., 1995; Lewis et al., 1996; Mossing and Record, 1986; Müller et al., 1996). In part, the biological function of looping is that binding of one dimer to its operator increases the effective local concentration of the other operator around the other dimer, leading to increased occupancy of the second operator (Oehler et al., 1994). In *E. coli*, the *lac* operon is regulated by an inducer, allolactose, which binds the repressor protein, causing a conformational change in the repressor, which then releases the DNA. The synthetic inducer isopropyl- β -D-thiogalactoside (IPTG) acts similarly to allolactose (Lewis et al., 1996), and up-regulates transcription of the *lac* operon (Jacob and Monod, 1961b). The focus here is the

evaluation of conformational dynamics in gene repression. In particular, this work explores the impact that IPTG binding has on the destabilization of the LacI-induced DNA loop. Single molecule fluorescence resonance energy transfer (SM-FRET) is used to investigate the dynamics of the LacI-DNA system. FRET is the mechanism of energy transfer between two fluorophores (a donor and acceptor molecule) (Periasamy, 2001).

Single molecule spectroscopy (SMS) utilizes the distance dependent phenomenon of FRET to quantify and elucidate biochemical conformation of the species (Deniz et al., 1999). SMS uses the measurement of single photons from an individual molecule as a reporter of an environment. In SMS, only an individual molecule is in resonance with the volume probed by the laser, thus allowing depiction of a single conformational state. SM-FRET eliminates ensemble averaging by measuring the signal from a single molecule at a time, thus providing a probability distribution for a molecular property related to the measured signal (Deniz and Mukhopadhyay, 2007). The detection of fluctuation of signals from individual molecules by SMS allows one to monitor trajectories of protein folding and unfolding (Chung et al., 2009) and protein binding kinetics (Elf et al., 2007).

1.2 Lac Repressor System: Model for Gene Regulation and DNA Looping

1.2.1 *lac* Operon

The control of the *lac* operon in *E. coli* by LacI is a classic example of negative gene regulation (Jacob and Monod, 1961a). The tetrameric protein binds a primary promoter-proximal operator, O_1 , and one of two auxiliary operators, O_2 and

O₃, in order to repress transcription of the *lac* operon (Figure 1.1). The presence of either O₂ or O₃ or both operators is critical for maximal repression at cellular levels of LacI, which are generally low. These operators cause repression through the binding of these two sites to a single LacI molecule via DNA loop formation (Oehler et al., 1994).

Repression: (-) lactose

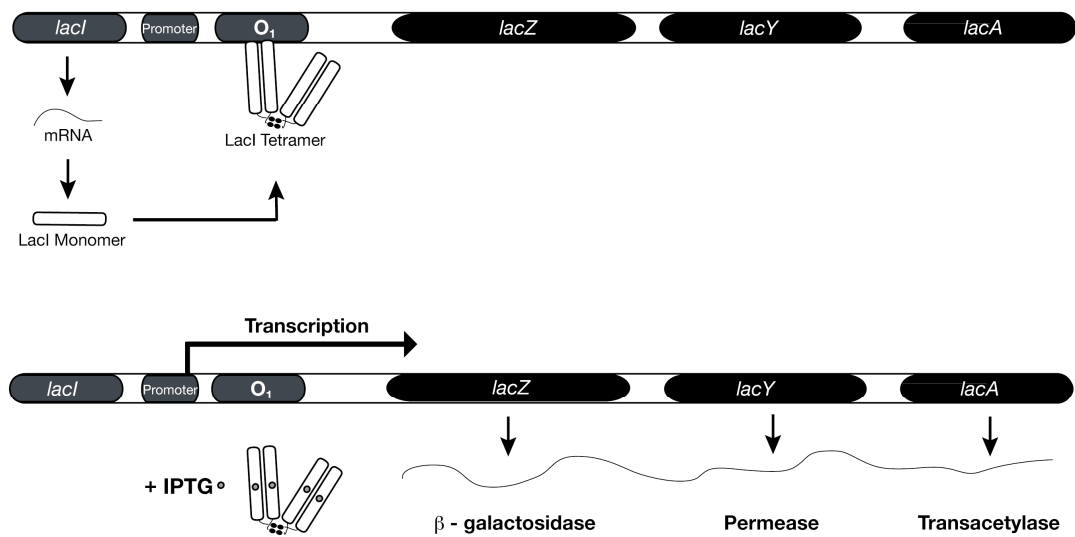


Figure 1.1 Control of expression by allolactose.

Repression of the *lac* genes in *E. coli* in the absence of lactose. In the absence of lactose, the artificial inducer (IPTG) binds to the repressor protein. This dislocates LacI from the DNA which then allows the enzymes responsible for lactose metabolism to be transcribed from the *lac* genes. Transcription is further activated by the CAP protein (not shown).

The *lac* operon works by a control mechanism in which transcription of genes can only take place upon dissociation of LacI, the product of the *lacI* gene in *E. coli* (Figure 1.1). Thus, initiation of transcription of the *lac* operon is achieved through the use of an inducer. In the presence of lactose, residual β-gal activity leads to production of allolactose, an inducer that reduces the affinity of the LacI for DNA, via

a conformational change in the repressor. IPTG serves as a synthetic inducer of the *lac* operon. It is believed that the structural changes in LacI induced by binding of IPTG diminish DNA binding affinity, ultimately resulting in the transcription of the *lac* genes. The wild type *lac* promoter is weak, so transcription is low. Another regulatory component of the *lac* operon, which stimulates *lac* transcription, is the catabolite activator protein (CAP) (Emmer et al., 1970) that bends DNA. In the absence of glucose, CAP forms a complex with cAMP (cyclic-AMP), which promotes binding the RNAP, leading to transcription. The studies discussed here are not inclusive of the regulatory components of CAP.

The natural operator sequence of the *lac* operon is composed of ~ 20 bp and is somewhat symmetric in the center, while highly symmetric at its ends (Gilbert and Maxam, 1973). This symmetry and the spacing between the two halves of the operator play an important role in the efficacy of LacI binding (Sadler et al., 1983; Sasmor and Betz, 1990). Our work uses a perfectly symmetric operator (O_{sym}).

The *lac* operon contains a primary operator sequence adjacent to the promoter at position +11 bp, which is accompanied by two secondary operators with similar sequences; one located 401 bp downstream and the other located 92 bp upstream (Pfahl et al., 1979; Reznikoff et al., 1974). RNA polymerase is sterically hindered from occupancy of the primary operator from the binding of LacI (Jacob and Monod, 1961a). Although LacI binds to the auxiliary operators with less affinity, the auxiliary operators play a major role in maximal repression of the *lac* operon system. In experiments by Oehler et al. (Oehler et al., 1990), it was shown that removal of one of the auxiliary operators minimally reduced repression; however, removal of both

auxiliary operators significantly reduced repression as outlined in Figure 1.2. Auxiliary operators increase the local concentration of repressor in the neighborhood of the primary operator via DNA looping, leading to maximum repression efficiency.

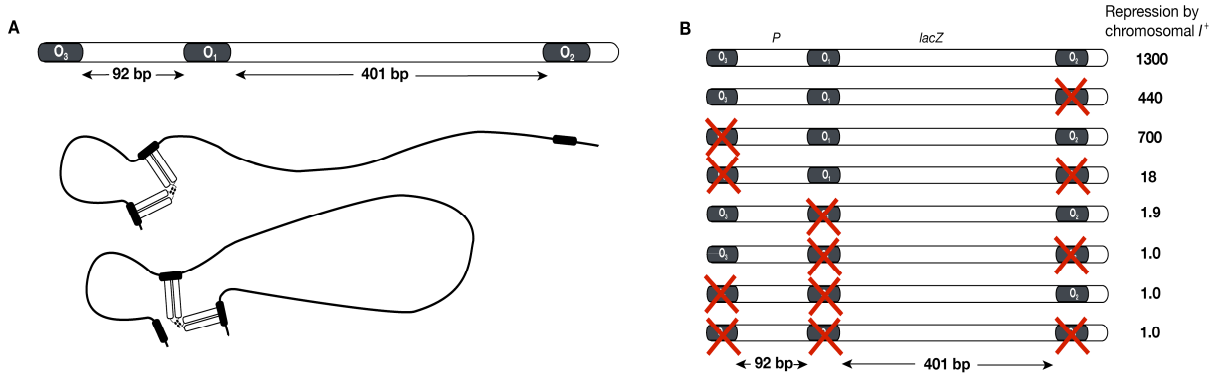


Figure 1.2 DNA loops resulting from Lac repressor binding in the *lac* operon.

(A) Possible DNA loops obtained from binding a primary promoter-proximal operator, O₁, and one of two auxiliary operators, O₂ or O₃, in order to repress transcription of the *lac* operon. (B) Maximum repression of the *lac* genes is observed when all three operator sites are present and is at a minimum when the O₁ site is not present. From the work of Oehler et al., 1990.

1.2.2 Lac Repressor Protein

The V-shaped Lac repressor tetramer protein is defined by its four structural regions: the DNA binding domain (headpiece), a hinge region, the core domain including an N-terminal domain, and a C-terminal domain, and the C-terminal tetramerization domain (Lewis, 2005; Matthews et al., 2007) (Figure 1.3). The DNA binding domain and the core of the protein are connected by a flexible linker denoted as the hinge region of the protein. In addition, there is flexibility between the C-terminal domain, and the C-terminal tetramerization domain. These flexible domains

may play an important role in allowing the LacI tetramer to loop DNA under a variety of conditions and allowing the protein to stabilize various loop geometries and topologies. Upon binding of DNA to the protein the hinge region becomes

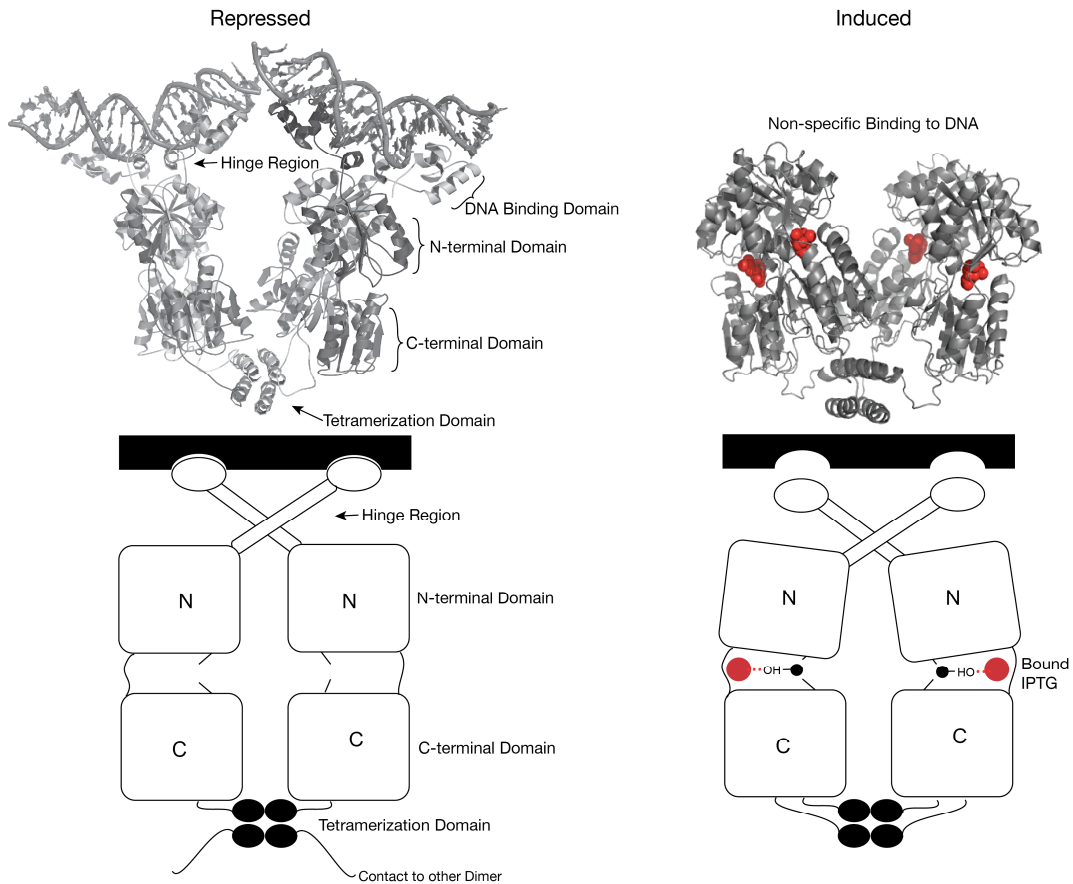


Figure 1.3 LacI with and without IPTG.

The cocrystal structure of a LacI tetramer-DNA “sandwich” complex with and without IPTG based on the work of the Lewis lab (Lewis, 1996) and the Steitz lab (Friedman et al., 1995) Protein Data Bank entry 1LBG and 1TLF. The crystal structure of LacI reveals the presence of two flexible regions: the region connecting the DNA binding domains to the core domain and the region before the four-helix bundle of the tetramerization domain. A schematic of the domains (adapted from Lewis, 2005) within one dimer is shown below to emphasize the location of effector binding, conformational shift of NH₂-terminal subdomains, as well as disassociation from DNA. This dissociation is the conversion of LacI binding from specific to non-specific (Kao-Huang et al., 1977). The headpiece is disordered in 1TLF.

structurally ordered. Effector molecules bind at the interface of the N-terminal and C-terminal domains within the core of the monomers (Daber et al., 2007). Overall,

the asymmetry of the protein along with strong dimer contacts and weak tetramer contacts classifies the protein as a dimer of dimers (Bell and Lewis, 2000; Lewis, 2005; Lewis et al., 1996).

Distinct structural changes occur in the dimer interface in the transition between the induced and repressed forms of the Lac repressor. The rearrangement upon inducer binding involves clamping and rotation of the NH₂-terminal domain of the core leading to disruption of the network of interactions in the monomer-monomer interface of the NH₂-terminal and COOH domains and between the two NH₂-terminal subdomains (Flynn et al., 2003; Lewis, 2005; Lewis et al., 1996). The reorientation of the core domain increases the distance between DNA binding headpieces in a dimer, destabilizing the strong interactions between the headpiece and the DNA operator (Bell and Lewis, 2000; Lewis, 2005).

The minor groove of the center of the operator sequence makes specific contacts with the antiparallel hinge helices, which leads to operator bending toward the major groove (Kalodimos et al., 2004; Lewis et al., 1996; Spronk et al., 1999). Upon inducer binding, the hinge helices of the dimers are separated, causing them to unfold, and affinity for the operator DNA is lost (Spronk et al., 1999). NMR studies show that the formation of the alpha helix of the hinge region is prevented when LacI is bound to non-specific DNA. The protein and major groove DNA contacts remain while the minor groove contacts are lost with non-specific binding (Kalodimos et al., 2004). Formation of the hinge helix is thought to be a mechanism for transitioning between specific and non-specific DNA binding.

1.2.3 DNA Looping

Loop geometry and stability is modulated by DNA bending strain, protein flexibility, and specific versus non-specific protein-DNA interactions. In a looped protein-DNA complex vs. a singly bound complex, the thermodynamic stability is affected by the DNA deformation energy required for looping, and the protein deformation energy required for a change in protein conformation. In terms of the Lac repressor, where one must account for a simultaneous reaction of two DNA binding domains and two operator sites, the free energy includes contributions for the conformation of the LacI protein (ΔG_{pos}), interaction with each individual operator site ($\Delta G_{int O_1}$, $\Delta G_{int O_2}$), and the deformation energy cost for looping the intervening DNA between operator sites (ΔG_{loop}) (Vilar and Saiz, 2005), and the anticooperative effects of binding a second operator (ΔG_{coop}) (Levandoski et al. 1996). The free energy of a looped state is represented by the sum of individual free energies of the interacting components as defined by equation 1.1 (Vilar and Saiz, 2005).

$$\Delta G_{O_1-O_2} = \Delta G_{pos} + \Delta G_{int O_1} + \Delta G_{int O_2} + \Delta G_{loop} + \Delta G_{coop} \quad (1.1)$$

Shape, twist, and local concentration effects of binding domain and binding sites characterize looping efficiency (Bellomy and Record, 1990; Rippe et al., 1995). Cyclization requires DNA deformability and is modeled with the same previously mentioned looping efficiency parameters. Thus, DNA cyclization has been used to interpret and model DNA looping in particular to undertake the length dependence of ΔG_{loop} . In order to alter the deformation energy in regard to the DNA and the protein, one can change the deformation of the DNA by altering its length. Cyclization

efficiency is measured with a J factor, which is experimentally determined as the ratio of the equilibrium constants for cyclized DNA product to the bimolecular product (Shore et al., 1981). In cyclization experiments by Shore and Baldwin (Shore and Baldwin, 1983), the J factor was shown to be dependent upon DNA length and helical phasing, which is a function of the twist of DNA. For DNA molecules of shorter length (less than 500 base pairs), phasing is significant for cyclization. As a whole, changing the length, *i.e.* the twist of DNA and the magnitude of DNA bending has a large impact on energy required for DNA deformability. The free energy of looping fluctuates with the helical periodicity of DNA (Horowitz and Wang, 1984; Müller et al., 1996; Vilar and Saiz, 2005).

Adhya and coworkers (Semsey et al., 2005) have shown that both parallel and antiparallel trajectories for DNA loops must be considered, and the choice between loop topologies can be dictated by sequence-directed DNA bending (Kahn et al., 2006; Lillian et al., 2008) (Figure 1.4). Some of the early indications of the importance of DNA bending strain came from the work of the Matthews and Müller-Hill labs, where it was shown that LacI binding was stabilized by negative DNA supercoiling, which brings the two pieces of DNA into close contact (Kramer et al., 1988; Whitson et al., 1987).

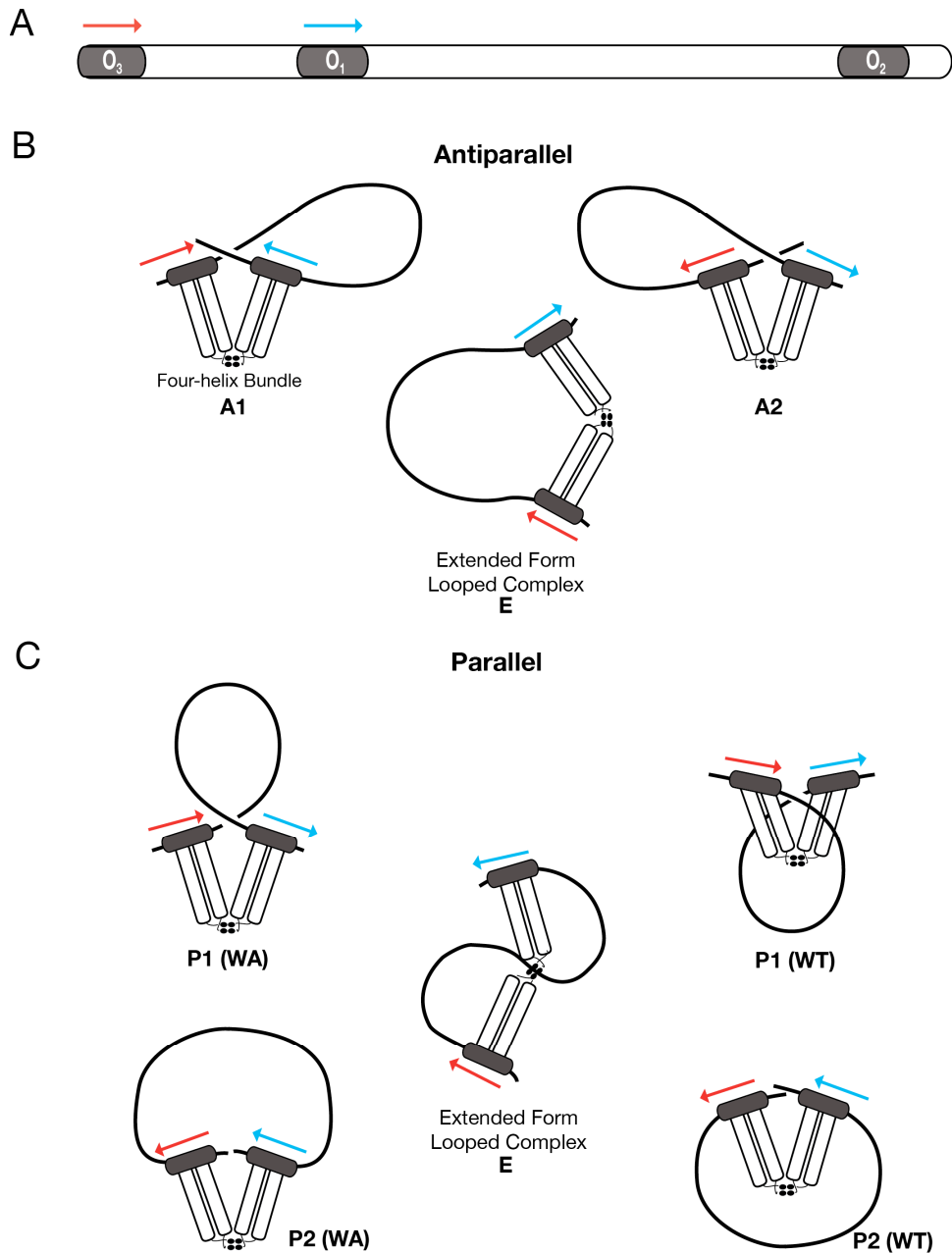


Figure 1.4 DNA looping trajectories.

Schematic of DNA loops with different topologies (Semsey et al., 2005; Swigon et al., 2006) in the lac system based on the direction of LacI binding sites (direction is indicated by arrows) (A) Parallel and antiparallel refer to the directions defined by the operators indicated by the arrows. (B) Antiparallel DNA trajectories formed from the V-shaped and extended conformations of LacI. (C) Parallel DNA trajectories formed from the V-shaped conformation of LacI including the wrapping away (WA) and wrapping toward (WT) loops (based on the relative position of LacI in regard to the DNA loop). The 9C14 DNA model construct is a parallel, wrapping away looped complex (P1).

In addition to the character of the DNA, protein shape and/or conformation may facilitate protein-DNA looped complexes. Evidence for multiple conformations of the Lac repressor has been provided by x-ray scattering and electron microscopy, which suggested that LacI could open up from its closed V-shape in solution (McKay et al., 1982; Ruben and Roos, 1997). Tethered particle microscopy experiments monitoring the effective length of DNA upon looping by LacI have shown distinct loop states ascribed to multiple conformations of Lac repressor (Wong et al., 2008).

1.3 Lac Repressor-DNA Loop Complexes

1.3.1 Hyperstable Looped Complexes

The natural O₁-O₃ loop is not very stable (Brenowitz et al., 1991), which is biologically beneficial, but make the loop difficult to study. Our introduction of designed LacI-DNA looped complexes whose shape and stability depend on DNA sequence allows the study of alternative loop geometries, DNA binding topologies, and protein conformational changes (Mehta and Kahn, 1999). The DNA constructs contain a sequence directed A-tract bend (Crothers et al., 1990) positioned between two perfectly symmetric operators (O_{sym}) (Lewis et al., 1996) (Figure 1.5). Loop geometry is controlled by changing the phasing of the operator axis dyads relative to the A-tract bend by changing the length of the two DNA linkers. The designed model DNA constructs have been shown to be hyperstable, with half-lives measured in days based on EMSA experiments (Mehta and Kahn, 1999).

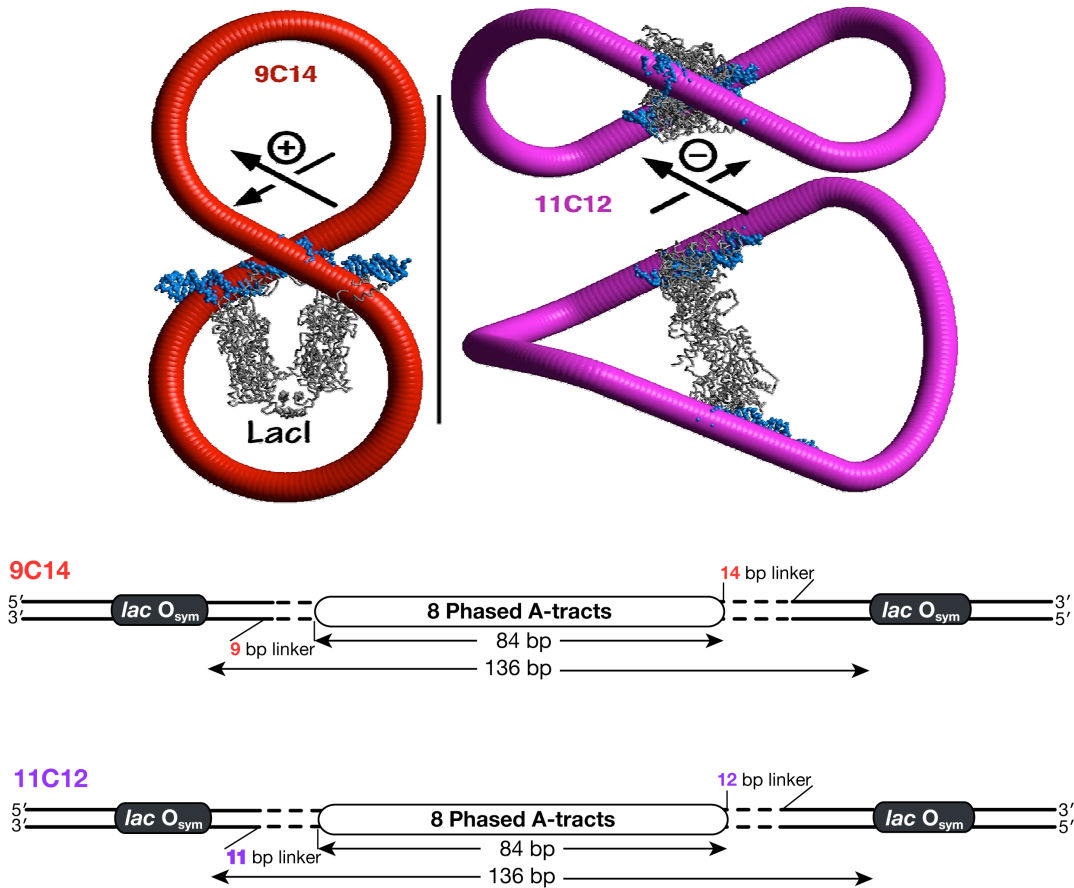


Figure 1.5 Layout of the 9C14 and 11C12 model constructs.

Model of the 9C14 and 11C12 proposed minicircles based on the positive and negative topoisomers induced in cyclization experiments (Mehta and Kahn, 1999). A more closed form of the LacI tetramer was proposed for the 9C14-LacI loop and a more open or extended form of the LacI tetramer was suggested for the 11C12 model construct. Hyperstable looping constructs and proposed loop topologies for LacI induced DNA looping from Mehta and Kahn, 1999.

The two DNA constructs that have been most carefully characterized are denoted as 9C14 and 11C12. The 9C14 model DNA construct was designed to form a wrapping away loop, with an outward operator direction in regard to the sequence induced bend. This DNA construct was designed to assume a closed form where the

heads of LacI are closer together with the DNA positioned in a tight positive supercoil. In contrast, the wrapping toward/simple loop DNA constructs have the operators directed toward the center of curvature and were designed to assume an open form where LacI was more extended. The 11C12 construct forms a simple loop/wrapping towards loop with an inward or perpendicular operator direction. Cyclization experiments revealed that the 11C12 model construct gave a relaxed topoisomer as predicted; however, the 9C14 loop was a mixture of relaxed, positive, and negative topoisomers (Mehta and Kahn, 1999).

1.3.2 Effector Molecules and Lac-Repressor-DNA Loop Complexes

A single IPTG molecule binds to the core domain of one monomer of LacI with a $K_D \sim 5.0 \times 10^{-6}$ M (Donner et al., 1982; O’Gorman et al., 1980; Ohshima et al., 1974). von Hippel and coworkers explained derepression as the redistribution of IPTG-bound LacI onto non specific DNA (Kao-Huang et al., 1977). Early *in vivo* studies of LacI interaction with the lac operators demonstrated a sigmoidal curve for derepression as a function of IPTG concentration. This led to a belief in either a cooperative or a two-step mechanism, requiring two molecules of inducer to dissociate LacI from the operator (Boezi and Cowie, 1961; Yagil and Yagil, 1971). Oehler et al. (2006) showed that if IPTG binding decreases DNA binding by one dimer, the sigmoidal curve can be explained by stabilization of binding to the primary operator via binding of an auxiliary operator through DNA looping. *In vivo* experiments confirmed incomplete IPTG induction of the operon (Becker et al., 2005). Figure 1.6 displays that *in vivo* IPTG-saturated LacI reserves its ability to bind DNA and formulate functional repression loops. The curves demonstrate that the

efficiency even of induced transcription varies periodically with DNA spacing (Figure 1.6), diagnostic of loop formation (Becker et al., 2005; Mossing and Record, 1986).

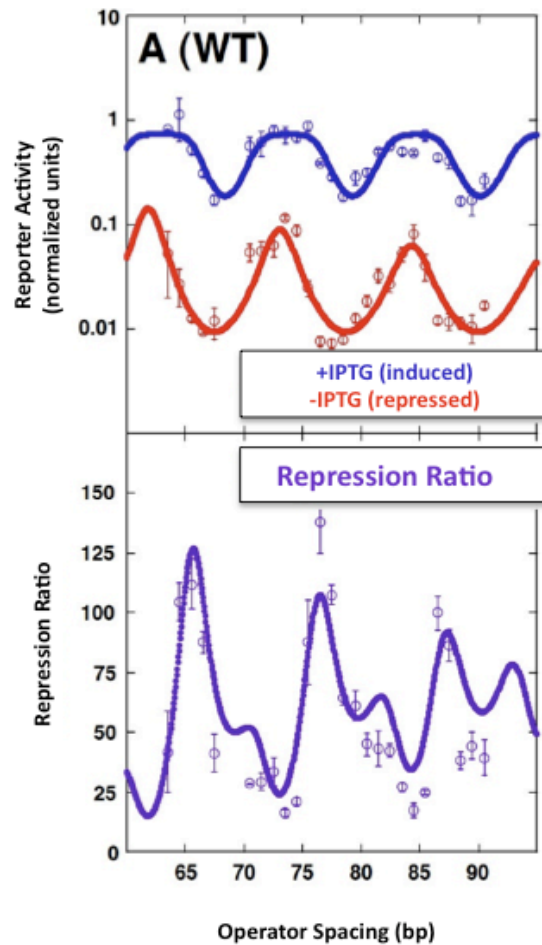


Figure 1.6 Transcriptional periodicity of DNA looping.

Expression in *E. coli* cells from the work of Becker et al. (Becker et al., 2005). Top: β -galactosidase expression as a function of operator spacing in the absence and presence of inducer. Bottom: Repression ratios of induced to uninduced β -galactosidase activity.

The secondary peaks in the repression ratio are attributed to the difference in the apparent physical properties in the loop with and without IPTG. The noted increase in the optimal operator spacing upon induction suggested a change in LacI conformation (Becker et al., 2005).

1.4 Single Molecule Spectroscopy, Confocal Microscopy, and SM-FRET

Single molecule studies have been at the forefront of nanotechnology research on exploring biological molecular processes. Several research methods aimed at individual study of species including scanning tunneling microscopy (Binnig et al., 1982), atomic force microscopy (Binnig et al., 1986), and tethered particle microscopy (Schafer et al., 1991) have been successful. SMS (Moerner, 2002) has had great influence in interdisciplinary study through its uniting of physics, chemistry, and biology. SMS involves optical radiation of an individual molecule. The conditions under which this is achieved are when only a single molecule is in resonance with probed laser volume and a low signal to noise level (SNR). SMS allows for detection of a molecule of interest on the order of $\sim 1.66 \times 10^{-24}$ moles (Moerner, 2002). Rapid technical advancements in microscopy, photon detection, and dye chemistry have made SMS a prevailing technique in the study of biological phenomena.

One of the emerging techniques for improving the SNR levels in SMS has been that of using confocal microscopy (Ha et al., 1997). In confocal microscopy, a high numerical aperture (N.A.) lens is used to focus a laser beam which reduces the excitation volume. Confocal fluorescence microscopy, versus other single molecule

methods such as AFM or EM, has allowed for less perturbation of the systems under study since probe and sample are at a greater proximity and the samples may be free in solution. To this end, optical spectroscopy of single diffusing molecules, which monitors a molecule as it diffuses in and out of the focal volume, has allowed for the preservation of equilibrium reaction conditions during experimental acquisition.

Success in SMS in general also requires that the probe molecule have a high fluorescence quantum yield. Over time several single molecule studies have used varying probe molecules including fluorescent proteins and quantum dots. However, higher photostability and monovalent conjugation have made small organic dyes the fluorescent molecules of choice (Kapanidis and Weiss, 2002). Early single molecule experiments were dependent on photomultiplier tubes (PMT) for detection of events; however, advancement in semiconductor photodectors has driven the field to the use of single photon avalanche photodiodes (SPADs) (Eisaman et al., 2011). SPADs have a higher quantum efficiency for visible light than a PMT.

Accompanying the advancement of the SMS field itself is the use of emerging fluorescent techniques such as FRET (Ha et al., 2008). FRET is the non-radiative transfer of energy between fluorophores. The ratiometric method of FRET in collaboration with SMS has allowed for measurement in terms of molecular distance. FRET has the ability to observe intermolecular distances of 1-10 nm (Harekrushna, 2011), allowing for structural study of biochemical processes.

1.5 Single Molecule Confocal Microscopy and SM-FRET Analysis of Freely Diffusing LacI-DNA Loop Complexes

1.5.1 Introduction

Single molecule studies by our group and others have explored DNA looping through single molecule methods (Finzi and Gelles, 1995; Morgan et al., 2005; Vanzi et al., 2006; Wang et al., 2005). The most widely used optical method for single molecule spectroscopy is fluorescence. However, since most biological macromolecules are not inherently fluorescent in the wavelength ranges that are most suited for SMS, it is usually necessary to modify them with the addition of a suitable fluorophore. FRET has become a powerful tool in the measure of distances in single molecules (Deniz et al., 1999; Ha et al., 1996; Purohit and Nelson, 2006; Weiss, 1999). The greatest asset of single molecule spectroscopy (Ambrose et al., 1999; Bell et al., 2001; Dahan et al., 2001; Deniz et al., 1999; Moerner and Orrit, 1999; Nie and Zare, 1997; Weiss, 2000; Xie and Trautman, 1998) is that it is devoid of the confounding effects of heterogeneity seen in conventional ensemble measurements. It allows for the investigation of copious structural distributions and for the evaluation of real time and stochastic dynamics.

Previous work by our lab reported the geometric analysis of LacI-induced DNA loops using FRET. Steady state and time resolved bulk fluorescence measurement employing FRET were performed on LacI-9C14 and LacI-11C12 complexes (Edelman et al., 2003). The bulk FRET studies confirmed the existence of the 9C14 closed loop form indicated by the cyclization studies and were in agreement with the open form loop prediction for the 11C12 loop (Mehta and Kahn, 1999). SM-FRET studies on the LacI-9C14 and LacI-11C12 complexes have provided a method

for understanding the exact geometry of protein-induced DNA looping. The result of the LacI-9C14 SM-FRET study unequivocally determined the geometry of the LacI-induced 9C14 loops as a closed form with a V-shape tetramer (Morgan et al., 2005). Studies conducted on DNA loop formation geometries, as proposed herein, will be a continuation of this previous work and will explore induced form of LacI mediated DNA loops.

1.6 Methods of Single Molecule Study: FRET and Single Molecule Spectroscopy

FRET occurs between fluorophores when there is a transition dipole interaction between the fluorophores. This requires spectral overlap between the donor emission spectrum and acceptor absorption spectrum. Dipole-dipole interaction dictates that distance plays a strong role in energy transfer. FRET is a valuable technique for measuring distances between donor and acceptor fluorophores. The most widely used Alexa Fluor® family (Figure 1.7) of cyanine fluorophore were used in SM-FRET studies presented here because of their excellent photostability (Berlier et al., 2003; Cordes et al., 2011) (Figure 1.8).

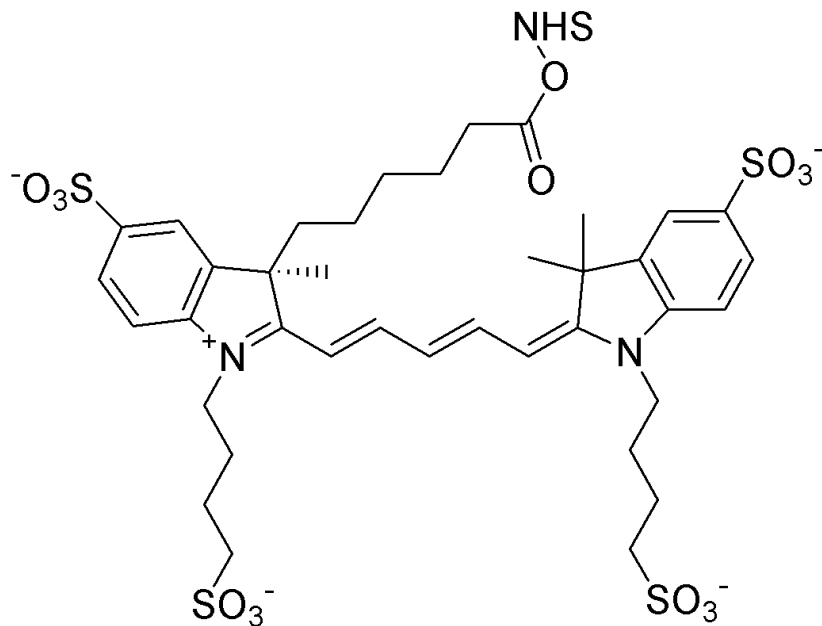


Figure 1.7 Structure of Alexa 647.

The Alexa 647 fluorophore is a carbocyanine type dye and is similar in both structure and photophysics to the Cy5 dye. NHS represents N-Hydroxysuccinimide. Alexa 555 is proprietary but it resembles Cy3.

In FRET, the rate of energy transfer, and hence its efficiency, has a steep dependence (inverse sixth power) on dye separation and is therefore sensitive to small deviations around the Förster distance R_0 , the distance at which the efficiency of transfer is 50%. The rate of energy transfer (k_T) is given by:

$$k_T(r) = \frac{1}{\tau_D} \left(\frac{R_0}{r} \right)^6 \quad (1.1)$$

where τ_D is the decay time of the donor in the absence of the acceptor, r is the inter-dye (donor to acceptor) distance and R_0 is the Förster distance. The Förster distance, (Lakowicz, 2006) is given by equation 1.2.

$$R_0 = 0.211(\kappa^2 n^{-4} Q_D J(\lambda))^{\frac{1}{6}} \quad (\text{in } \text{\AA}) \quad (1.2)$$

where κ^2 describes the orientation of transition dipoles of the fluorophores (equation 1.4 below), n is the solvent refractive index, Q_D is the quantum yield of the donor,

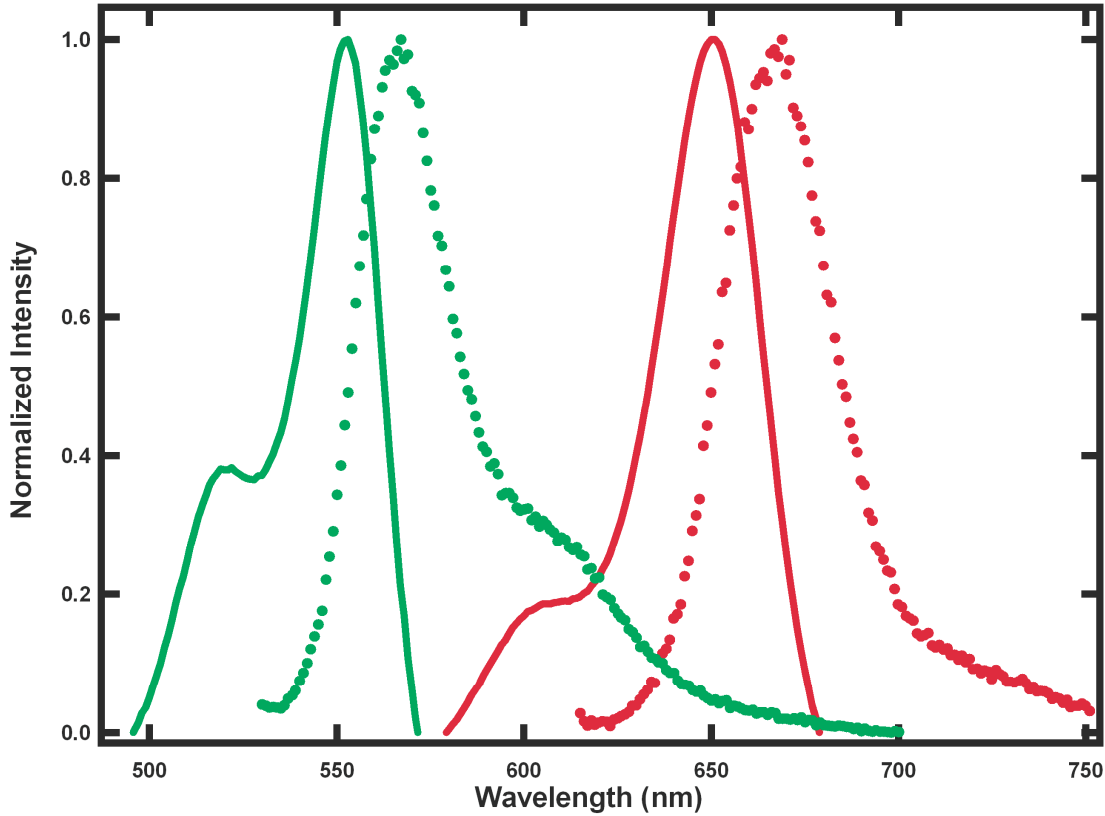


Figure 1.8 Excitation (solid lines) and emission (dotted lines) spectra of donor and acceptor labeled primers.

Alexa Fluor® 555 (donor, shown in green) and Alexa Fluor® 647 (acceptor, shown in red) fluorophore labeled primers (56 oligonucleotides in length) for the 9C14 model DNA construct. Emission spectra were obtained with excitation at 514 nm and 600 nm, for donor and acceptor labeled molecules respectively.

and $J(\lambda)$ is the amount of spectral overlap between donor emission and acceptor absorption as represented by the following:

$$J(\lambda) = \int_0^{\infty} F_D(\lambda) \epsilon_A(\lambda) \lambda^4 d\lambda \quad (1.3)$$

where $F_D(\lambda)$ is the corrected intensity of the donor fluorescence and $\varepsilon_A(\lambda)$ is the acceptor absorption spectrum.

In equation 1.4 the angle between the donor emission transition dipole and acceptor absorption transition dipole is represented by θ_T , and the angle between the dipoles are referred to as θ_D and θ_A :

$$\kappa^2 = (\cos \theta_T - 3 \cos \theta_D \cos \theta_A)^2 \quad (1.4)$$

κ^2 is taken to generally be $2/3$ which is the value of the expression averaged over θ 's and is equivalent to assuming that on the timescale of the measurement the dyes are freely rotating (van der Meer, 2002). However, in terms of a fluorophore's ability to interact with themselves (a dye may fold upon itself) and with the biomolecules they may be conjugated to, other factors such as electrostatic and hydrophobic interactions may play a significant role. The average value of $2/3$ for κ^2 may be an underestimation of an instantaneous orientation, which may generally be assumed to range in value from 0-4, since the dye may not always be freely rotating. Furthermore, with regard to single molecule events, sampling of the κ^2 orientation may be incomplete during the fluorescent burst event. Thus, FRET is a measure of relative distances because of all the uncertainties and is represented in terms of distributions (Hoeftling et al., 2011; van der Meer, 2002).

Energy transfer between the donor and acceptor is characterized by a decrease in donor fluorescence intensity that is accompanied by the appearance or increase of acceptor fluorescence. FRET efficiency (E) measures the likelihood that a photon absorbed by a donor will lead to excitation energy transfer to an acceptor. The fraction of molecules for which this is successful is given by:

$$E = \frac{k_T(r)}{\tau_D^{-1} + k_T(r)} \quad (1.5)$$

Given eq. (1.1), efficiency of this transfer may be rearranged as the following:

$$E = \frac{1}{1 + \left(\frac{r}{R_0}\right)^6} \quad (1.6)$$

FRET efficiency may be determined experimentally through microscopy by measuring the number of emitted donor and acceptor photons. This method reflects the decrease in the fluorescence intensity of the donor when some portion of energy is transferred to the acceptor as noted by an enhancement of fluorescence emission. The observed or apparent FRET efficiency is calculated using equation 1.7:

$$E = \frac{I_A}{I_A + I_D} \quad (1.7)$$

where I_A and I_D represent the intensity of the signal from the acceptor and donor emission respectively. This equation may be extended to incorporate background for the acceptor (B_A) and donor (B_D) and photophysical and instrumentation factors as follows:

$$E = \frac{I_A - B_A}{(I_A - B_A) + \left[\left(\frac{\eta_A Q_A}{\eta_D Q_D} \right) I_D - B_D \right]} \quad (1.8)$$

Correction factors η_A and η_D account for photodiode detection efficiencies. Q_A/Q_D is the ratio of the dye quantum yields for the acceptor and donor fluorophores. Details of interpreting experiments are described below in the context of our previous work.

Here we employ confocal microscopy using continuous wave laser light to excite fluorophores conjugated to DNA samples. Single molecule sensitivity through confocal microscopy is achieved from optical filtering of out of focus light (and undesired excitation) and allowing for femtoliter observed detection volumes through use of a high N.A. lens (Lakowicz, 2006; Sandison et al., 1995). As fluorophore conjugated DNA samples (nM) diffuse in and out of the focal volume of the laser beam the emitted fluorescence is collected. In our experiment, the excitation is performed at 514 nm with an argon ion laser focused 10 μm into the sample from the glass-liquid interface (Figure 1.9).

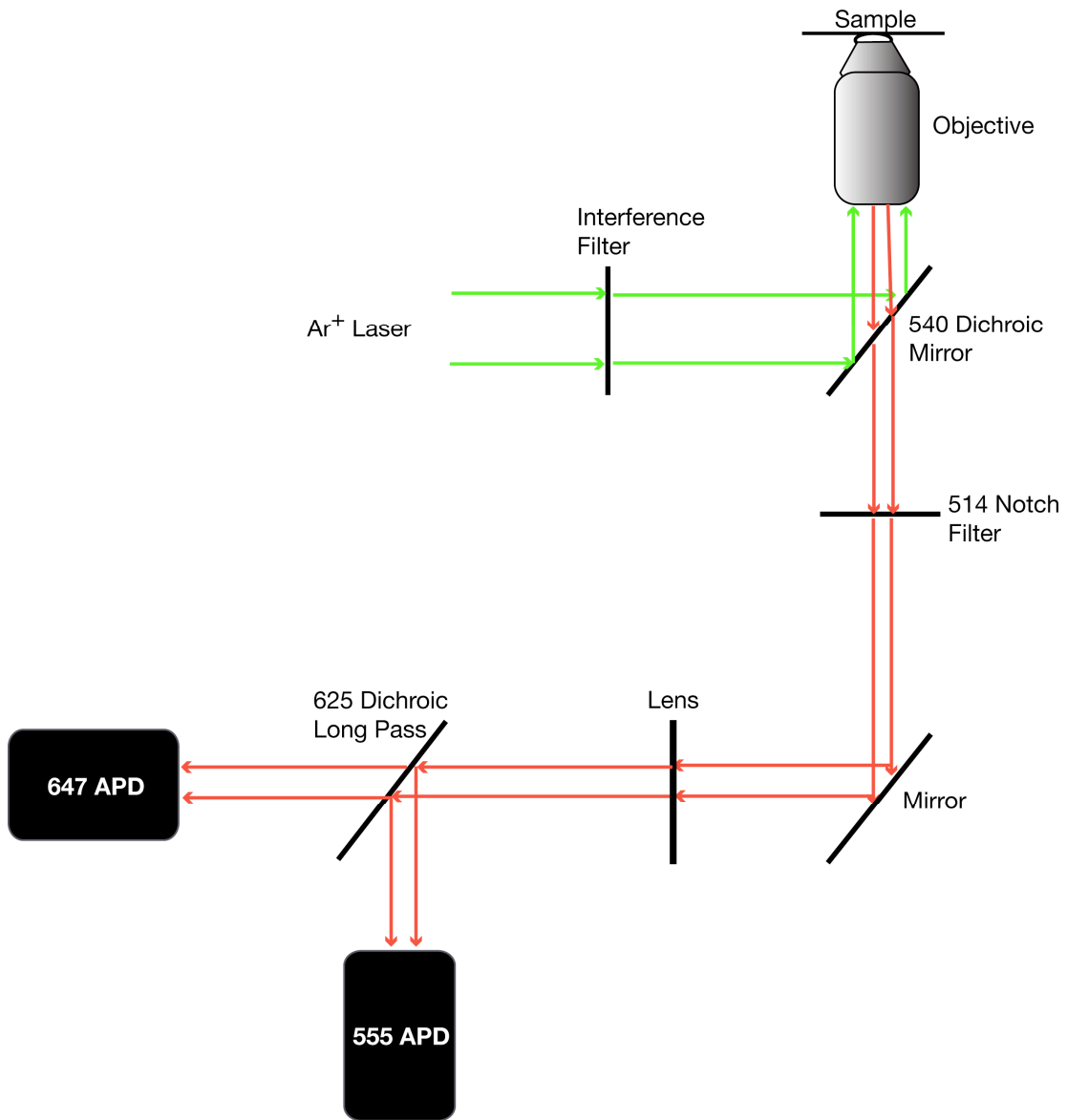


Figure 1.9 Microscope set up.

The objective collects the fluorescence burst photons as the molecules travel through the beam, and the light is then directed through a notch filter to remove the excitation wavelength of the laser. The emitted light is subsequently split between two avalanche photodiode single photon counting modules using a dichroic beam splitter.

1.7 Experimental Design: Synthesis and Characterization of Fluorophore Labeled Model DNA Constructs (9C14)

Experiments presented here focus on the dynamics of LacI-DNA complexes. LacI-induced DNA loops in this system have been proposed to form a variety of loops, which include an extended loop, a wrapping toward loop, and a wrapping away loop based on the position of the loop in regard to the protein core (Friedman et al., 1995) (Figure 1.4). The looping constructs were synthesized to facilitate protein and DNA deformation and thus control geometry and stability of the LacI mediated looping. The constructs include a phased A-tract bend (Crothers et al., 1990) flanked by two operator sites, which allows the DNA to bend more easily, assisting in loop structure formation (Figure 1.10) (Mehta and Kahn, 1999). A-tracts are defined by 4-6 adenines repeated in phase with a helical repeat, which in turn induces a bend of approximately 18 degrees per A-tract. The adaptor region of the model constructs is the region between the central bend created by the A-tracts region and the operator sites. The operator phasing relative to the central bend is mediated by changing the length of the adaptor region (Mehta and Kahn, 1999). The overall model design is such that the operator symmetry axis may have different orientations in regard to the sequence induced bend.

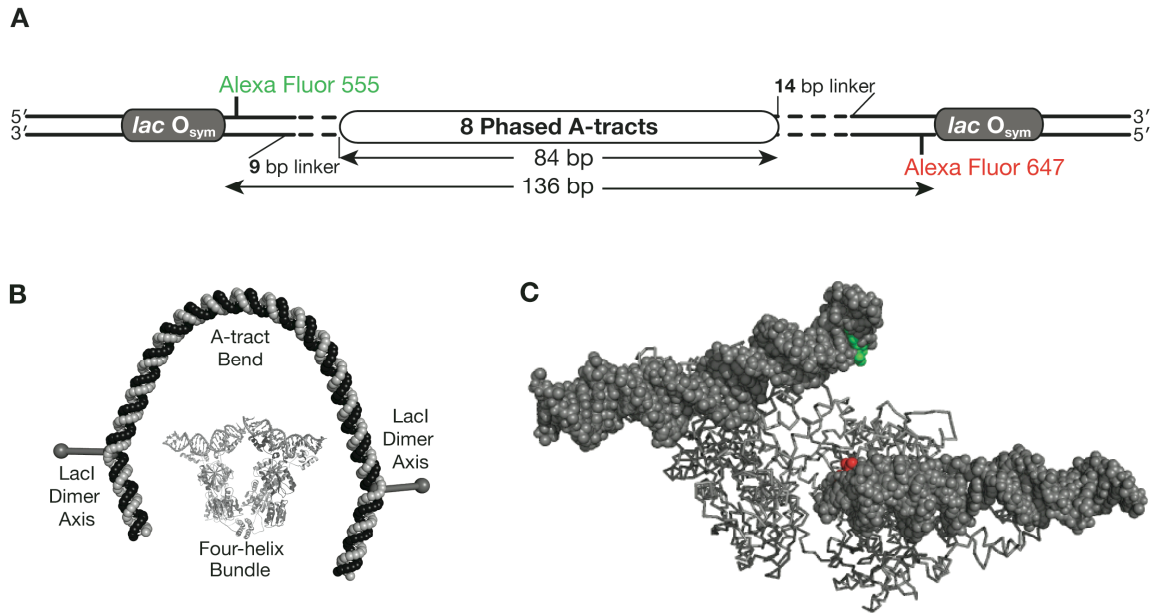


Figure 1.10 DNA looping construct 9C14 and models for LacI-DNA loops.

(A) Schematic of the dual fluorophore 9C14 construct, which is the same as in previous work (Crothers et al., 1990; Edelman et al., 2003; Mehta and Kahn, 1999) except for the use of Alexa Fluor® 555 and Alexa Fluor® 647 fluorophores ($R_0 = \sim 51 \text{ \AA}$). The sequence induced A-tract bend is flanked by symmetrical operator binding sites. (B) Model for the lowest-energy structure of unbound 9C14 based on the junction model for A-tract DNA bending (Koo et al., 1990), assuming a DNA helical repeat of 10.45 bp per turn outside the A-tracts. The thick rods indicate the dyad axes of the lac operators and hence the LacI dimers within the tetramer. The structure of LacI bound to operator DNA is from PDB file 1LBG (Lewis et al., 1996), shown approximately to scale. (C) Top view of LacI bound to extended operator DNA with highlighted donor (green) and acceptor (red) points of attachment without the intervening loop. The approximate distance between donor and acceptor fluorophores is 35 Å in a closed form loop (Morgan et al., 2005).

1.8 Previous Studies of DNA-LacI Looped Complexes

1.8.1 FRET Evidence for Open/Closed Loop Preference

Bulk FRET experiments using the 9C14 and 11C12 constructs suggested that the lac repressor protein may change conformation to form different DNA loop complexes. Low FRET values were observed for the 11C12 simple loop, suggesting a more open *lac* repressor, while high FRET values were calculated for the wrapping away loop, revealing a more closed *lac* repressor. The bulk FRET experiments demonstrated a closed form of 9C14 giving an apparent FRET efficiency of approximately 70% (Edelman et al., 2003), but could not distinguish if this was a uniform population. This led to the hypothesis that either 70% of the molecules were exhibiting 100% FRET efficiency or 100% of the molecules were exhibiting 70% FRET efficiency. In order to directly assess loop geometry single molecule fluorescence resonance energy transfer (SM-FRET) was employed.

1.8.2 SM-FRET Evidence for a Single Population

Previous 9C14 SM-FRET diffusing experiments (Figure 1.11) showed that the fully bound form of LacI-9C14 exhibited two peaks: one at an approximate energy transfer (ET) of 10% (zero ET) and a high FRET peak at an approximate ET of 90%. The zero ET transfer peak was analyzed using laser excitation at 514 and 543 nm, the latter of which directly excites acceptor molecules. Two zero-ET difference histograms were constructed by subtracting a SM-FRET histogram of a fully titrated sample (Lac-9C14) from a DNA only (9C14) histogram from samples excited at each wavelength, 514 and 543 nm. The Gaussian fits of each of the zero-ET difference

histograms were compared to that of donor only 9C14 molecules. The zero-ET peak as shown in figure 1.11D could be decomposed into a Gaussian that had the same center and width as donor only molecules and a second Gaussian that disappeared upon titration with protein at 543 nm. Based on the analysis of the zero FRET peak shape, it was determined that only a single conformer was present and the zero FRET peak came from molecules lacking a FRET acceptor. Every double-labeled molecule is shifted to the high-FRET peak upon the addition of protein. The high FRET 90% ET peak from the fully bound 9C14 molecules were fit to a β -distribution function (Dahan et al., 2001). Gaussian functions are symmetric, thus showing a better fit to data points that are mirror images of each other. β -distribution functions do not have to display symmetry and are used for data with mean values between 0 and 1 (Dahan et al., 2001). The β -distribution function fitting showed that only noise contributed to the width of the high efficiency peak meaning that only one value was present (Morgan et al., 2005). This led to a hypothesis of loop rigidity.

The single molecule experiments on the 9C14 induced loop structure demonstrate that the two heads of LacI must be close together to form the wrapping away loop (Morgan et al., 2005), and that the LacI-induced loop from the 9C14 complex mirrors the extrapolated loop seen in the Lewis *et al.* crystal structure (Lewis et al., 1996). The formation of the 9C14-LacI induced DNA loop is strongly stabilized by the increased curvature of 9C14.

The bulk and single molecule fluorescence resonance energy transfer studies verified that 9C14 does exist in a closed form. Very low FRET efficiencies detected from 11C12 are consistent with an open LacI-DNA looped complex (Edelman et al.,

2003; Morgan et al., 2005). Direct interpretation about the loop states were hard to decipher based on the calculated efficiencies from the bulk FRET studies, this in part was the motivation of study through the use of single molecule studies. As a whole, evidence from cyclization (Mehta and Kahn, 1999), bulk FRET, and SM-FRET experiments lead us believe that open (and closed) loop forms exist based on opening of the LacI tetramer.

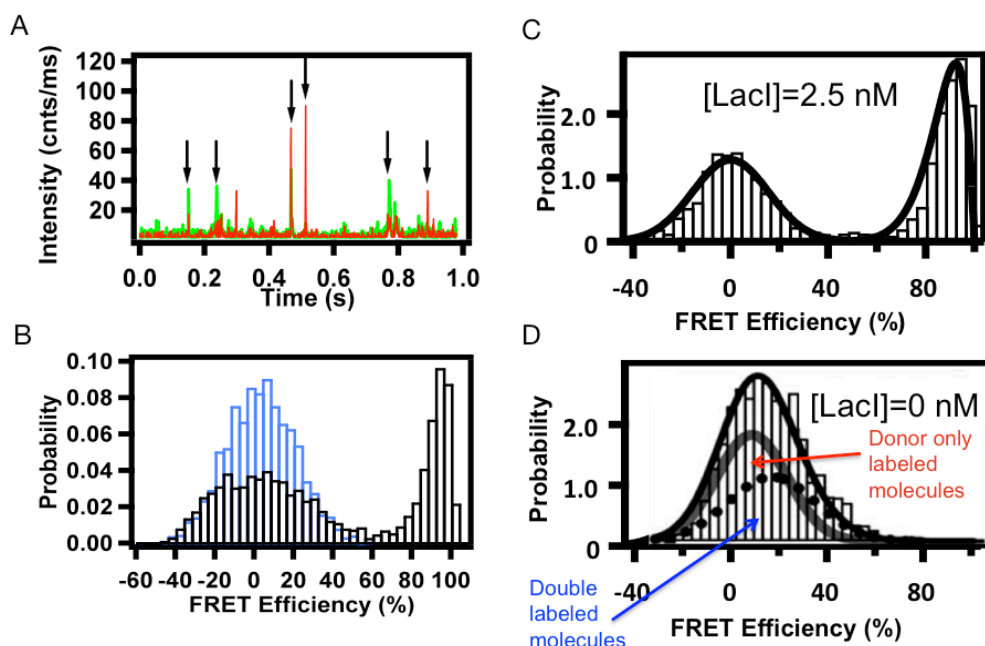


Figure 1.11 Freely diffusing single molecule studies of 9C14-LacI loop complexes.

Work from (Morgan et al., 2005) (A) SM transient from freely diffusing 1 nM 9C14 with 2.5 nM LacI and excitation at 514 nm. The arrows mark total intensities above 30 counts per ms. (B) Burst data as seen in (A) was analyzed by calculating the observed energy transfer efficiency (E) for each burst that has a donor and acceptor intensity above the defined threshold. The energy transfer efficiency is used to build a histogram describing the probability distribution of FRET values. SM-FRET histograms of freely diffusing 9C14 only (blue bars) and LacI bound 9C14 (black bars). (C) SM-FRET histogram LacI bound 9C14 acquired with 543 nm excitation. The zero ET peak is fit to a Gaussian and the high FRET peak is fit to β -distribution distribution function. The negative efficiency values arise from the case where the background in the acceptor channel was higher than that of the collected intensity. (D) SM-FRET histogram of freely diffusing 9C14 DNA acquired with 543 nm excitation with the overlaid Gaussian fits of donor-only labeled 9C14 and donor and acceptor labeled 9C14.

1.9 Research Objectives

The initial single molecule studies also begged the question of the open and closed loop forms in not only the repressed state of the LacI tetramer, but also the induced state. Induction has been described as redistribution to non-specific DNA (von Hippel and Berg, 1989) and there is evidence for *in vivo* to support incomplete induction and suggestion of change in LacI conformation in the presence of inducer (Becker et al., 2005). Single molecule studies in subsequent chapters in aim to explore and compare the geometries of both the induced and uninduced loop, which includes studies of the 9C14-LacI DNA, loop in the presence of IPTG. Bulk and SM-FRET experiments are used to investigate conformational changes caused by the addition of IPTG to pre-looped LacI-induced DNA complexes.

Modeling studies from the Perkins laboratory have shown that our experimental results from Mehta and Kahn, 1999, Edelman, Cheong et al. 2003, and Morgan et al., 2005 which suggest open and closed conformations of the Lac repressor may also be explained with a V-shaped Lac repressor only (Lillian et al., 2008). This signifies namely that the open or extended loop form for 11C12 model construct could be explained by a V-shaped Lac repressor with an antiparallel loop geometry. Ultimately, suggesting that different placement of fluorophores could shed further light on the loop geometries, thus motivating the importance of synthesis of bent sequences for the extension of experimental studies, and further expansion of alternative loop geometry characterization via single molecule studies.

Here, hyperstable looping constructs are used to investigate the effects of IPTG on LacI-DNA looped complexes (Figure 1.12). SM-FRET on freely diffusing LacI-DNA loops allows us to analyze population distributions directly as opposed to the average properties measured in a bulk experiment, and the efficiency of energy transfer is sensitive to changes in loop geometry.

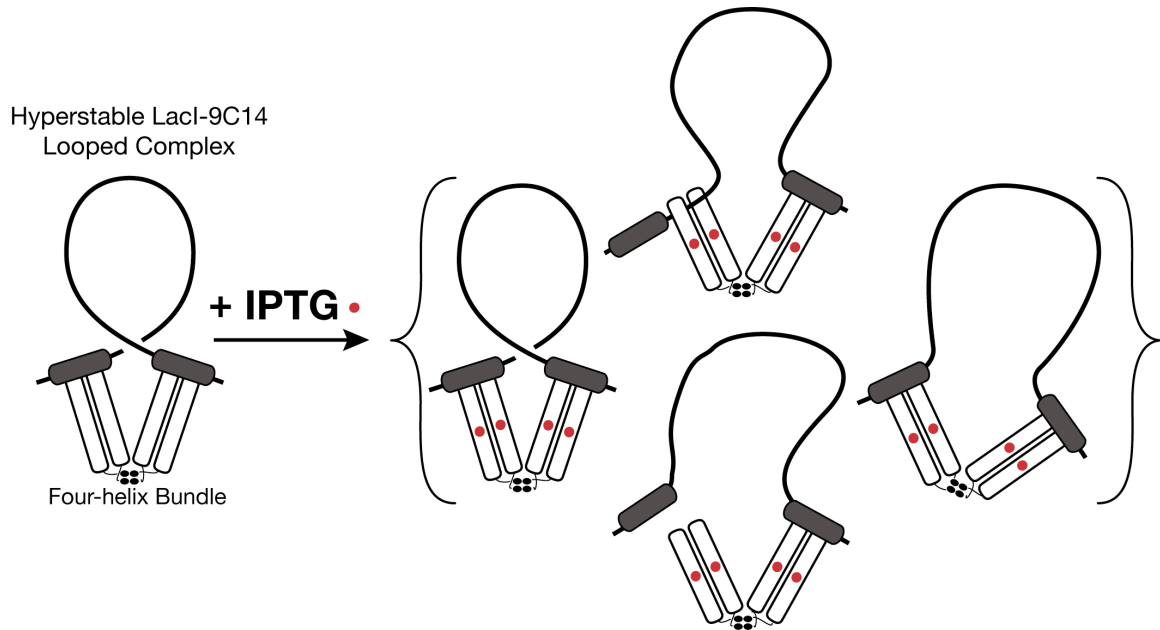


Figure 1.12 Model for LacI-DNA loops.

Proposed conversion of the uniform LacI-DNA loop to a set of possible looped complexes upon binding inducer. LacI may change conformation and/or bind DNA non-specifically resulting in the formation of various different loops. In addition, single-bound complexes may form.

There are potentially hundreds of LacI-DNA-IPTG species considering ligand free and induced LacI conformations, DNA binding states including single-bound, double-bound, and loops, multiple loop shapes, and possible nonspecific LacI-DNA interactions. The Kahn Lab interest is in mutual interactions among inducer binding, DNA site selection, and DNA loop stability, and therefore the focus here is on conditions where inducer is saturating, the DNA is designed to form exceptionally stable loops, and the protein:DNA ratio is ~ 1 . A complete quantitative understanding

of the *lac* operon, and by extension all genes regulated by ligand-responsive DNA looping proteins, will require confronting a more complete structural and thermodynamic characterization of all of the possible protein-DNA-effector complexes.

To further address possible looping conformations, two additional experimental factors were explored: repositioning of fluorophores and development of a matrix of pre-bent DNA constructs to investigate variations with LacI geometry based on the design of 9C14. The donor and acceptor fluorophores have been repositioned from inside the operators to outside the operators on the model constructs to identify possible looping conformations. The matrix (Haeusler et al., 2010) was developed by rotating the operators relative to the operator bend phasing in 9C14 and is described in more detail in Chapter 3. The pre-bent DNA matrix will allow examination of multiple states of looping in a single molecule which has previously not been shown.

Chapter 2: SM-FRET Analysis of Freely Diffusing 9C14 DNA with IPTG

2.1 Introduction

Recent *in vivo* studies, demonstrating β -galactosidase expression varying periodically with DNA spacing in presence of inducer, have shown that LacI-DNA-IPTG loops are capable of repressing transcription (Becker et al., 2005), but they have provided little insight into the geometry of the induced loop. Bulk FRET studies on LacI-induced DNA loops showed that addition of IPTG resulted in lower observed FRET efficiency, but population distributions could not be obtained (Edelman et al., 2003). Previous SM-FRET work investigated uninduced loops only and revealed the formation of a closed form loop supporting efficient energy transfer (Morgan et al., 2005). The analysis of loop population distributions for LacI-DNA-IPTG is the purpose of the work presented in this chapter. We use bulk and SM-FRET experiments to investigate conformational changes caused by the addition of IPTG to pre-looped LacI-induced DNA complexes. This work is an expansion of a paper that was originally submitted to Biophysical Journal (Goodson, Kathy A.; Haeusler, Aaron R.; Wang, Zifan; English, Douglas S.; and Kahn, Jason D. LacI-DNA-IPTG Loops: Equilibria among Conformations by Single-Molecule FRET).

2.2 Materials and Methods

Materials

Restriction enzymes and the Phusion™ High-Fidelity PCR kit were from New England Biolabs and used as directed except as indicated. dNTPs were from USB.

Alexa Fluor® labeling kits were from Molecular Probes/Invitrogen and were used as directed. DNA oligonucleotides were purchased from IDT. LacI buffer is 25 mM Bis-Tris pH 7.9, 5 mM MgCl₂, 100 mM KCl, 2 mM DTT, 0.02% IGEPAL CA-630 (Sigma; replaces nonionic detergent Nonidet P-40), and 50 µg/ml acetylated BSA. IPTG was from Fisher Scientific. The concentration of LacI is expressed as active tetramer throughout, as determined by EMSA titration against excess DNA. LacI protein expression and purification as well as the determination of specific activity is described in Appendix I.

9C14 Template

A ~420 bp PCR template was prepared by digesting plasmid pRM9C14 (Mehta and Kahn, 1999) with BstN I overnight. The fragment was purified on a 7.5 % polyacrylamide (40:1 (w/w) acrylamide: bis-acrylamide), native gel and stained with ethidium bromide. The DNA template was excised, eluted overnight into 50 mM NaOAc (pH 7.0) and 1 mM EDTA, phenol-chloroform extracted, ethanol precipitated, and stored in TE buffer.

Fluorescently labeled 9C14

Fluorescently labeled oligonucleotides 56 nucleotides in length were used as PCR primers for synthesis of the 9C14 DNA with Alexa Fluor® 555 (donor) and Alexa Fluor® 647 (acceptor) fluorophores. Fluorophores were conjugated to oligonucleotides synthesized with an amino dT C-6 internal (Figure 2.1) modification (T* below: iAmMC6T).

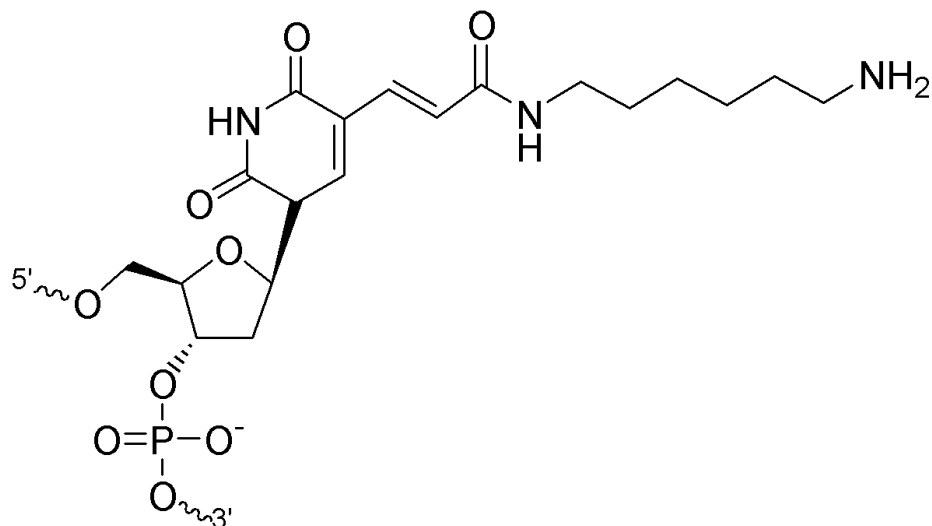


Figure 2.1 Amine modified thymine (IDT).

The Alexa fluorophore is attached to 5 position of the amine modified thymine via a six carbon linker.

Fluorescently labeled oligonucleotides were purified on a 12% polyacrylamide (40:1 (w/w) acrylamide: bis-acrylamide), 8 M urea gel. The primers were excised, eluted, phenol-chloroform extracted and ethanol precipitated. The PCR primers are 5'-CTGCAGGTCAGTCTAGGTAAATTGTGAGCGCTCACAATTAT*ATCTCAATTCGTACGG-3' and 5'-CAAGCTTTACCATCAACGAAATTGTGAGCGCTCACAATTAT*CTAGCTTCGATTCTAG-3', with the *lac* operator underlined. Dual fluorophore labeled DNA constructs were synthesized using the Phusion™ High-Fidelity PCR with the template described above. PCR reactions (50 µL) contained 40 pg of template, 200 µM of each dNTP, 1 µM each labeled primer, 1X Phusion HF Reaction Buffer, and 2 units of Phusion™ High-Fidelity DNA Polymerase. PCR cycling conditions were the

following: 94.0 °C for 1 min, 55.0 °C for 30 s, 60.0 °C for 30 s, 72 °C for 1 min, for 35 cycles.

Fluorophore labeling efficiencies

Labeling efficiencies for Alexa Fluor® 555 and Alexa Fluor® 647 fluorophore labeled primers were determined by measuring the ratio of dye concentration to DNA concentration, using the dye extinction coefficients reported by Invitrogen: Alexa555(555 nm) = 150,000 M⁻¹ cm⁻¹ and Alexa647(647 nm) = 239,000 M⁻¹ cm⁻¹. The dye contributions to absorption at 260 nm were calculated based on their concentrations and their correction factors to 260 nm (CF₂₆₀). The Alexa Fluor® 555 CF₂₆₀ = 0.04 and Alexa Fluor® 647 has no contribution at 260 nm. The absorbance of the dye at 260 nm was subtracted, and the concentration of DNA in each sample was then determined using extinction coefficients from IDT for single stranded DNA (33 µg/OD260 unit).

Bulk FRET studies on 9C14

Acceptor and donor labeled 9C14 constructs at 2 nM were incubated for 2 min with 0 or 2 nM LacI in LacI buffer. Fluorescence emission was collected from 550 to 750 nm, with excitation at 514 nm, using a Varian Cary Eclipse Fluorescence Spectrophotometer with a 10 nm slit width. Following incubation and scanning, 5 mM IPTG was added, allowed to incubate for 2 min, and the emission spectrum was acquired again. Additional LacI was added to 8 nM and the spectrum was acquired a third time.

SM-FRET measurements

Single-molecule FRET was carried out essentially as described (Morgan et al., 2005). Initial LacI titration experiments were used to determine the optimum concentration of LacI to be used. SM-FRET IPTG measurements were conducted at 1 nM 9C14 and 1-1.5 nM LacI in LacI buffer. IPTG was added at various concentrations and stages as described in the text. Samples were allowed to equilibrate at room temperature (20 °C) for at least 5 min. Because of the photostability of the Alexa-labeled DNA, it was not necessary to use an oxygen scavenging system. In addition, we did not observe power-dependence effects previously noted with Cy3-Cy5 that were ascribed to triplet state conversion or blinking (Morgan et al., 2005).

Single molecule studies were performed with an oil immersion objective inverted microscope (Fluar, 100X, N.A.=1.3, Carl Zeiss, Oberkochen, Germany) with standard methods (Dahan et al., 2001; Deniz et al., 2001; Schuler et al., 2002). Excitation at 514 nm was from an argon ion laser focused 10 µm into the sample from the glass-liquid interface. The objective collects the fluorescence burst photons as the molecules travel through the beam, and the light is then directed through a notch filter (Kaiser Optical, Ann Arbor, MI) to remove the excitation wavelength of the laser. The emitted light is subsequently split between two avalanche photodiode single photon counting modules (SPCM-AQR-15, PerkinElmer Optoelectronics, Vaudreuil, Quebec) using a dichroic beam splitter (625DCLP, Chroma, Rockingham, VT). The photon counts are recorded on separate channels of a counter/timer board (PCI 6602,

National Instruments, Austin, TX) in 1 ms time bins. The SPCMs are connected to the counter/timer board directed by Labview 6.0 (National Instruments) software.

SM-FRET data analysis

The fluorescence intensities for each bin were corrected for background, and bursts that exceeded a threshold total (donor plus acceptor) intensity were selected; the threshold value was chosen so that small changes do not affect the results. The apparent FRET efficiency of bursts above the defined threshold is calculated using the following equation:

$$Efficiency = \frac{I_A}{I_A + I_D} \quad (2.1)$$

where I_A and I_D are the background-corrected intensities of the acceptor and donor channels. To minimize peak broadening and to retain sensitivity to low-efficiency FRET we chose not to perform leakthrough correction, because the correction adds to the noise. Without the leakthrough correction, the peak apparent FRET efficiency for the zero ET population is 25%. Leakthrough correction has very little effect on the measured efficiency for the high-efficiency FRET peak. The probability of observing bursts as a function of the apparent FRET efficiency is binned and displayed in SM-FRET histograms.

2.3 Results

2.3.1 Electrophoretic Mobility Shift Assay Results for LacI-9C14-IPTG Complexes

An electrophoretic mobility shift assay (EMSA) was performed in the absence and presence of inducer (Figure 2.2). The mobilities of uninduced 9C14-LacI loop, doubly-bound LacI₂-DNA, and LacI-DNA₂ sandwich mirror those in our previous studies, which identified the bands using titrations of protein and DNA (Mehta and Kahn, 1999). If we consider initial formation of a singly-bound complex, the high local concentrations of the remaining headpiece of the LacI tetramer and the DNA operator potentiates loop formation. Thus, as expected, the uninduced complex is primarily found as a DNA loop that appears to be a single species. Doubly-bound DNA and sandwich complex are formed upon addition of excess LacI or DNA respectively. The mobility of our doubly-bound LacI₂•DNA complex is decreased by DNA bending, so it moves more slowly than the looped complex. The sandwich complexes have much slower mobility.

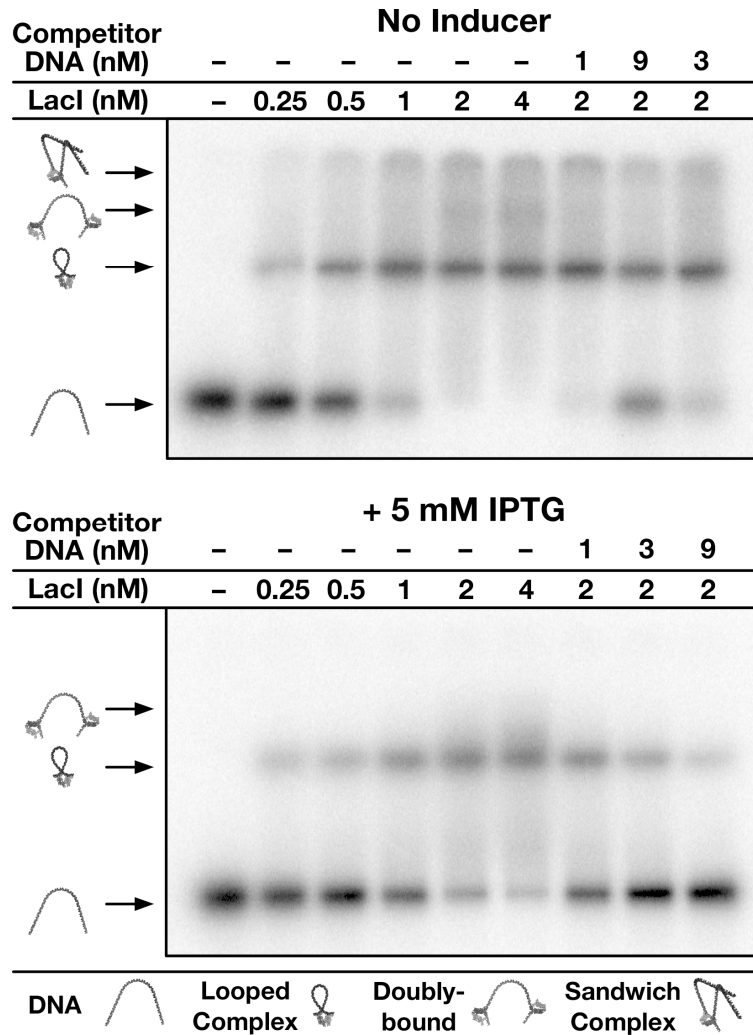


Figure 2.2 EMSA of IPTG binding to LacI-DNA complexes demonstrates stable LacI-DNA-IPTG loops.

Electrophoretic mobility shift studies were performed with 1 nM of ^{32}P -labeled 9C14. The DNA was mixed with 0, 1, 2, and 4 nM of tetrameric LacI for 30 min at room temperature. Following this incubation, 1, 3 or 9 nM of unlabeled 9C14 competitor DNA was added and incubated for an additional 30 min. The upper gel shows controls without IPTG, showing free DNA, a stable looped complex, a smear corresponding to doubly-bound DNA that appears at excess LacI, and faint sandwich complexes running near the well that appear with excess DNA. The lower gel, run with 5 mM IPTG in the sample and the gel, shows that the looped complex remains relatively stable but the doubly-bound and especially the sandwich complex do not survive electrophoresis.

The EMSA in the presence of saturating [IPTG] (5 mM, added to both the binding reaction and the gel) demonstrates that the LacI-DNA looped complex is still formed. The predominant loop does not change in electrophoretic mobility, suggesting that the induced and uninduced loops have similar geometries. The kinetic stability of the induced loop is clearly less than that of the uninduced loop: the addition of competitor DNA to an induced, preincubated complex displaces labeled DNA readily, presumably through a sandwich intermediate. The sandwich and the doubly-bound complexes are destabilized by inducer binding or the electrophoresis process, so the loop is the only bound species observed. Free DNA is observed in the presence of IPTG even at increased [LacI], suggesting that a kinetically less stable induced loop breaks down in the gel to some extent.

While the EMSA results demonstrate the existence of a relatively stable LacI-DNA-IPTG loop, the results are not informative as to the loop conformation or solution stability. Caging effects in the gel may alter the stability of the different bound forms and may change the distribution of loop shapes. In contrast, FRET reports on the solution shape, and the remainder of this work applies FRET to the analysis of loop structure and stability in solution.

2.3.2 Bulk FRET Studies

FRET studies on Alexa Fluor® 555 and Alexa Fluor® 647 double-labeled 9C14 DNA with LacI and IPTG (Figure 2.3) show that addition of saturating inducer to a LacI:DNA loop decreases the sensitized emission of the acceptor to approximately 40% of its original value. DNA labeled with the Alexa dyes ($R_0 = \sim 51 \text{ \AA}$) behaves similarly to the fluorescein/TAMRA ($R_0 = \sim 55 \text{ \AA}$) and Cy3/Cy5 (R_0

= $\sim 60 \text{ \AA}$) pairs used in previous bulk (Edelman et al., 2003) and single-molecule FRET (Morgan et al., 2005). Control experiments confirm that maximal sensitized emission of the acceptor is observed at approximately equimolar active LacI and DNA (as in Figure 2.3) and decreases at higher LacI concentrations. This decrease

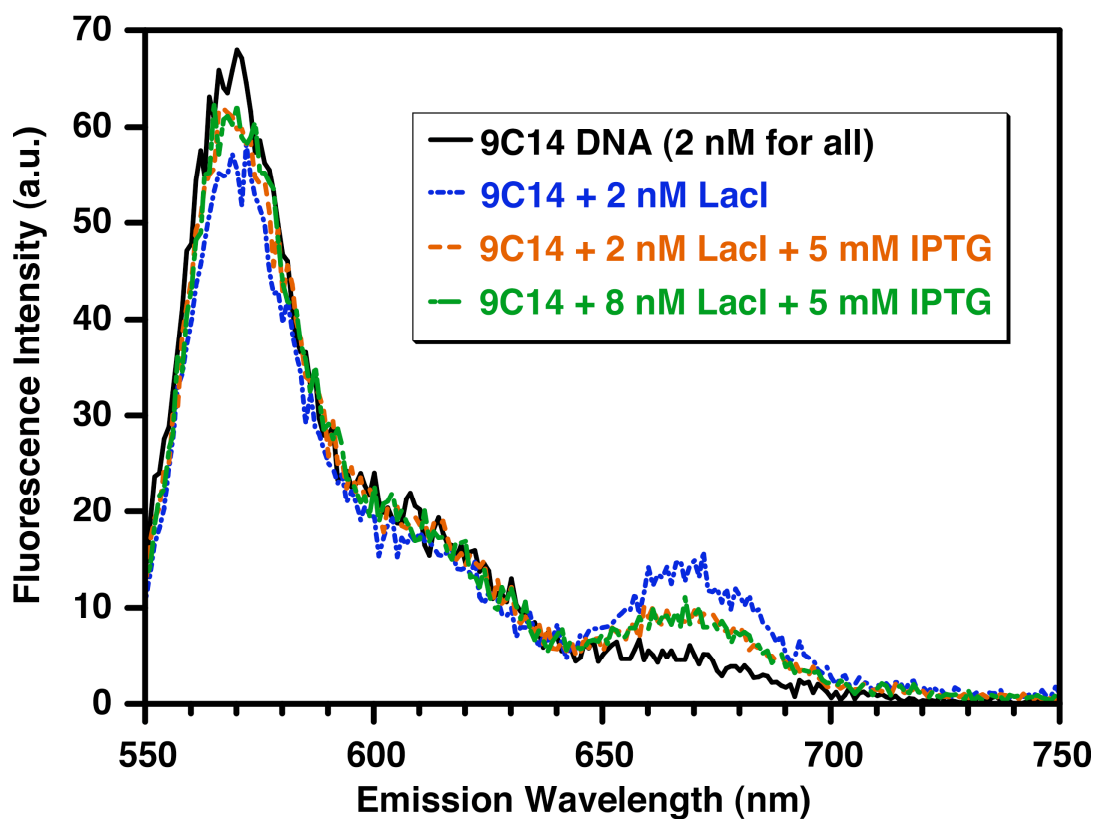


Figure 2.3 Bulk FRET of LacI-9C14 complexes in the presence and absence of IPTG.

Samples were prepared with 2 nM doubly-labeled DNA and 0 or 2 nM LacI. After 2 min, IPTG was added to 5 mM final concentration when used, and after a further 2 min, LacI was added to 8 nM to one sample. The samples were excited at 514 nm and the emission spectra was scanned from 550-750 nm. The enhanced emission of the Alexa Fluor® 647 acceptor at 670 nm is due to DNA looping. The enhancement is decreased ~ 2 -fold in the presence of IPTG. Excess LacI has no further effect, suggesting that there is no free DNA released during the initial incubation with IPTG and that there is no free singly bound DNA. SM-FRET experiments (Figure 2.6) confirm that 5 mM IPTG is saturating.

may be attributed to specific-nonspecific looping or conversion to doubly-bound complexes as seen in the EMSA. The decrease in FRET upon IPTG binding indicates that either a new equilibrium among looped and unlooped states is established (Figure 2.4), or the transfer efficiency of a stable loop is perturbed.

Since FRET does not disappear completely, at least a portion of the DNA must still be bound by protein. To test whether any free 9C14 DNA is present, the LacI concentration was quadrupled at saturating IPTG. The additional LacI should re-bind and loop any free 9C14, increasing the energy transfer efficiency, but no such effect was observed, suggesting that IPTG had not caused the dissociation of the original LacI-9C14 complexes. In contrast, any singly-bound, unlooped DNA should have been converted to doubly-bound upon addition of excess LacI (Figure 2.4), shifting the equilibrium to unlooped forms and thereby decreasing FRET efficiency; no such decrease was observed. All of these observations suggest that the LacI-9C14-IPTG complex exists as a mixture of stable loops and the drop in FRET efficiency with IPTG addition suggests that a structural rearrangement does take place. To identify this putative structural rearrangement, single-molecule FRET studies were pursued.

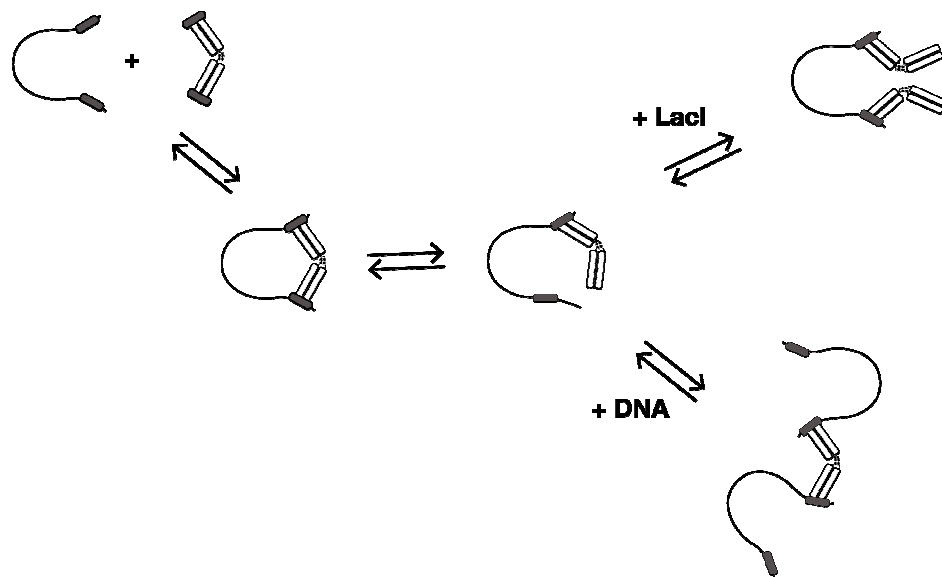


Figure 2.4 Establishing equilibrium among looped and unlooped states.

The additional LacI to the protein-DNA system would bind and loop any free 9C14. However, in the case of presence of singly-bound, unlooped DNA would be converted to doubly-bound upon addition Lac repressor in excess concentrations.

2.3.2 SM FRET LacI-9C14 Results for Titration with IPTG

The 9C14 DNA bound to LacI exists substantially in a closed loop form. Based on the inter-fluorophore distance estimated from the known attachment sites and the LacI-DNA co-crystal structure (Lewis et al., 1996), the closed loop has an expected FRET efficiency of 0.9 (Morgan et al., 2005). Control histograms (Figures 2.5 A and 2.8 A) show that 9C14 alone exhibits no FRET. Addition of IPTG to the free DNA has no effect on the FRET histogram (Figure 2.5 A and B).

Single-molecule FRET for LacI-9C14 complexes confirms a peak at 90 % efficiency (Figure 2.5 B). As IPTG is added to the LacI-9C14 loop, the high-efficiency FRET peak decreases in amplitude, but the maximum of the peak does not shift, and significant high-efficiency FRET remains at saturating IPTG concentrations

(Figure 2.5 B-F). After the addition 0.15 mM IPTG there is no further change at concentrations up to 30 mM IPTG (Figure 2.5 C-F). IPTG binding is expected to be less favorable when it is coupled to disruption of a very stable loop, but this effect should simply increase the apparent dissociation constant for IPTG, and the data show that saturation has been reached. Repeated experiments show that intermediate amplitudes of the high-efficiency peak can be observed, but trends as a function of IPTG are variable (Figure 2.6); the maximum of the peak is never observed to shift to lower efficiency. The persistence of the high-efficiency FRET peak indicates that some of the LacI-DNA-IPTG still exists as a closed form loop, presumably with a geometry similar to the original LacI-9C14 loop.

As the amplitude of the high-FRET peaks decreases, the amplitude of the zero-FRET peak increases, but in agreement with the bulk results, the addition of more LacI does not change its amplitude further (not shown). This confirms that the molecules that do not support FRET are still looped. Other studies on 9C14 suggest that, in fact, some of the molecules that contribute to the zero-FRET peak even in the absence of IPTG are stable loops with alternative topologies or an open form of LacI (Lillian et al., 2008). The FRET results presented here do not directly bear on the population of zero FRET loops in the absence of IPTG. The histograms also show bins that depend on LacI and show intermediate apparent FRET. However, a detailed analysis that includes the photon counting statistics underlying the histograms suggests that these values do not reflect possible alternative looped complexes with intermediate FRET efficiencies; rather, the intermediate values are due to photophysical effects discussed in Appendix II.

The data in Figure 2.6 are the results from IPTG titration experiments conducted with 1 nM 9C14, 1.5 nM LacI, and varying concentrations of IPTG. DNA looping is demonstrated by the presence of a high FRET efficiency due to the closed loop form of the LacI-9C14 complex. The SM-FRET experiments reveal high FRET populations from LacI-9C14 molecules in the absence and presence of inducer. Figure 2.6 C is a plot of the average fraction of molecules exhibiting a FRET efficiency above 60% versus IPTG concentration. Overall, even at saturation with IPTG, ~20% of LacI-9C14 complexes exist in a looped state. The plot shows that saturation with inducer is reached at approximately 2 mM, which is well above the ~5 μM K_D for IPTG-LacI binding (and the $\sim 8 \times 10^{-5}$ K_D for LacI binding in the presence of operator DNA (O'Gorman et al., 1980)). IPTG binding does not prevent stable loop formation. This suggests a shift in equilibrium toward stable IPTG-LacI-DNA complexes. In terms of the thermodynamic cycle as shown in Figure 2.7, we measure binding equilibrium constants $K_3 \ll K_1$. This is because binding of inducer is coupled to the disruption of specific LacI-DNA interface contacts. The reduction in the high-FRET loop population means that the high-FRET is loop less stable with respect to other protein-DNA complexes. There is another state that now competes with the loop that we can observe. A more quantitative treatment of the thermodynamics would require an expansion of the MWC model of O'Gorman including the parameters of multiple binding of IPTG and inclusion of ΔG_{coop} (discussed in Chapter 1).

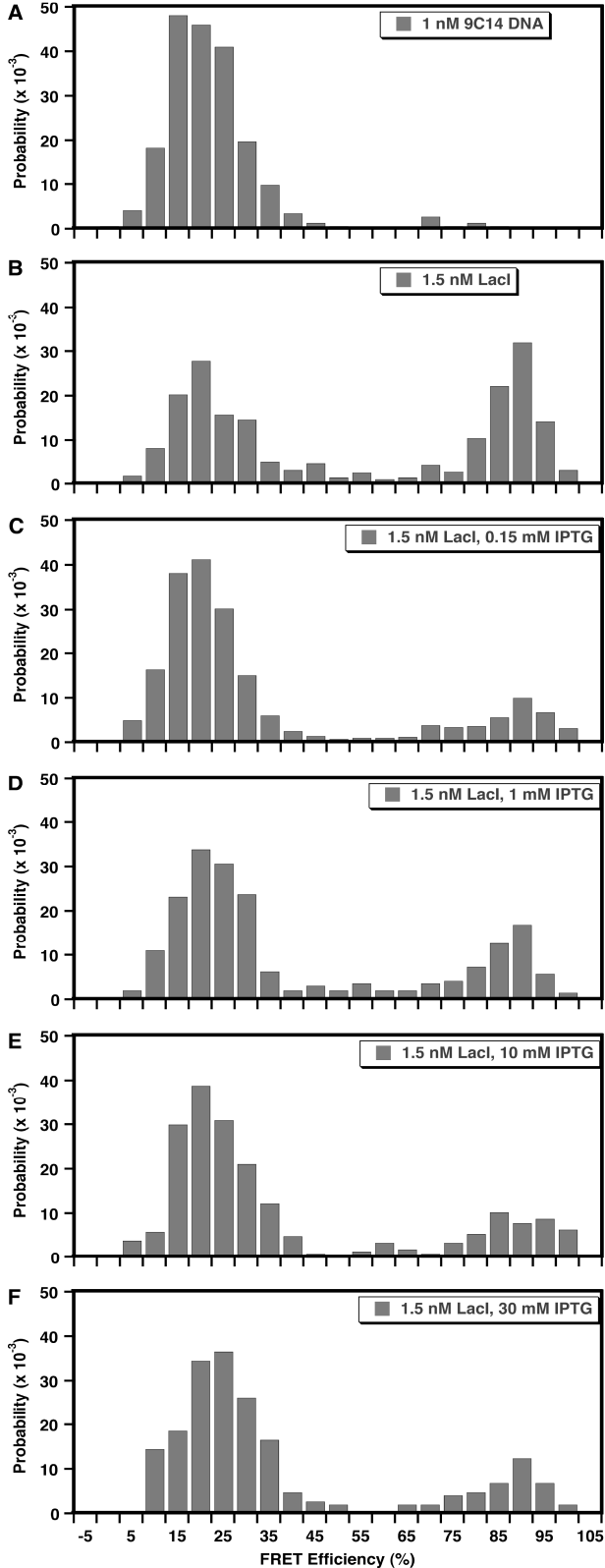


Figure 2.5 Single molecule fluorescence experiments on freely diffusing LacI-9C14-IPTG complexes. LacI was incubated with DNA and then IPTG was added to give the indicated final concentrations. The histograms are normalized distributions of FRET efficiencies calculated from fluorescence collected in donor and acceptor channels upon 514 nm laser excitation of Alexa Fluor® 555 and Alexa Fluor® 647 dual-labeled samples. (A) Control showing no FRET in freely diffusing 9C14 DNA alone. (B) LacI-9C14 looped complexes show a population with high FRET. The 1.5 nM LacI concentration is saturating under these conditions, so the zero-efficiency peak is mainly composed of molecules with bleached acceptors (Morgan et al., 2005). (C-F) Histograms obtained from LacI-9C14 complexes with the indicated concentrations of IPTG, ranging from 0.15 – 30 mM. The amplitude of the high-efficiency peak is decreased but not eliminated at saturating IPTG. As discussed in the text, the zero-efficiency peak probably includes LacI-DNA-IPTG loops that are not FRET active. The low-probability intermediate apparent FRET efficiencies seen here and in Figure 2.9 are probably due to photophysical effects, not to loops with actual intermediate levels of FRET.

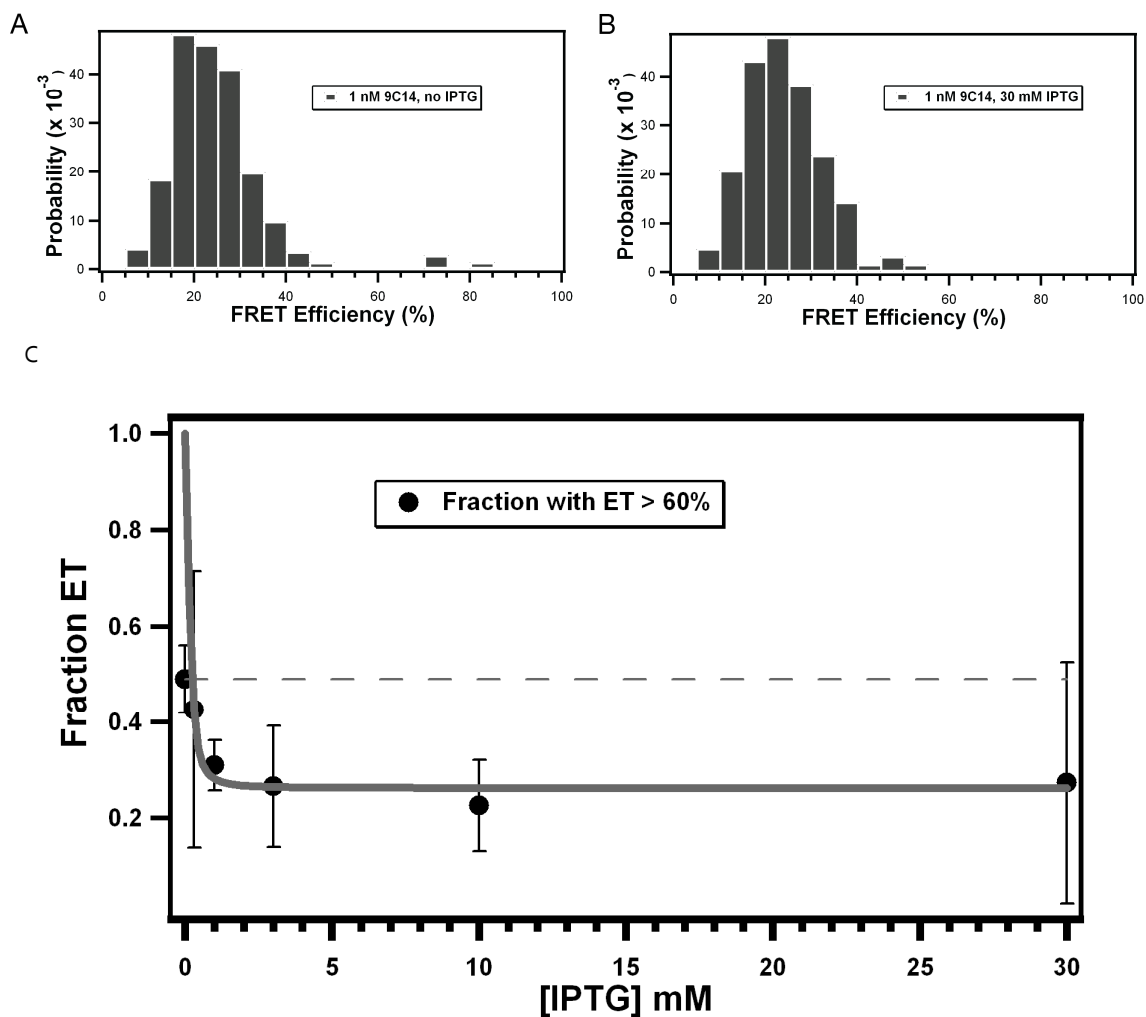


Figure 2.6 Single-molecule fluorescence titration experiments

Control SM-FRET experiments of freely diffusing 9C14 only in the (A) absence and (B) presence of IPTG. (C) The average (over multiple IPTG titration experiments) of the fraction of LacI-9C14 complexes in the sample that exhibit energy transfer (ET) efficiency above 60% plotted as a function of IPTG concentration (Appendix III).

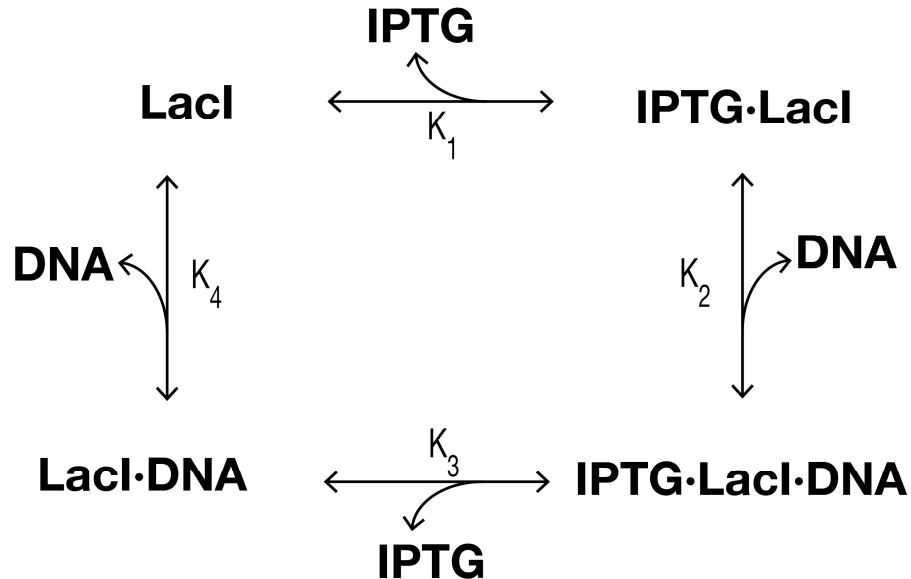


Figure 2.7 Binding cycle of LacI to IPTG and DNA.
Dissociation constants are represented by K.

2.3.3 SM-FRET Results on LacI-9C14 with LacI Pre-Incubated with IPTG

To confirm that the results above reflect equilibrium loop distributions, parallel studies in which LacI was mixed and preincubated with IPTG first, before addition of DNA were carried out (Figure 2.8). The same high-FRET and low-FRET peaks are still present at similar amplitudes, confirming that the essential results are independent of order of addition. The intermediate-efficiency apparent FRET values are more noticeable here, but the analysis discussed below suggests that this reflects different counting statistics in the two sets of experiments.

In other experiments similar to these (i.e. with or without preincubation with IPTG), histograms obtained at $0.5 \mu\text{M}$ and $5 \mu\text{M}$ IPTG are similar to those from the uninduced LacI-9C14 controls (Figure 2.9). Measurements at $50\text{-}300 \mu\text{M}$ IPTG are usually indistinguishable from the results shown in Figures 2.5 and 2.8, which are for

≥ 1 mM IPTG. We have occasionally observed distributions with intermediate amplitudes for the high-FRET peak, but given the variation apparent in Figures 2.5 and 2.8 these cannot be confidently assigned to actual mixtures of loops with and without IPTG. However, we have never observed a substantial shift in the position of the high-FRET peak. The transition between induced and uninduced loops would be expected to be quite sharp upon binding of inducer due to stabilization of the induced conformation of the repressor (Daber et al., 2009), displaying positive cooperativity for IPTG binding. The observed variability in the midpoint concentration of IPTG might also be due to variable adsorption of IPTG in the sample cell.

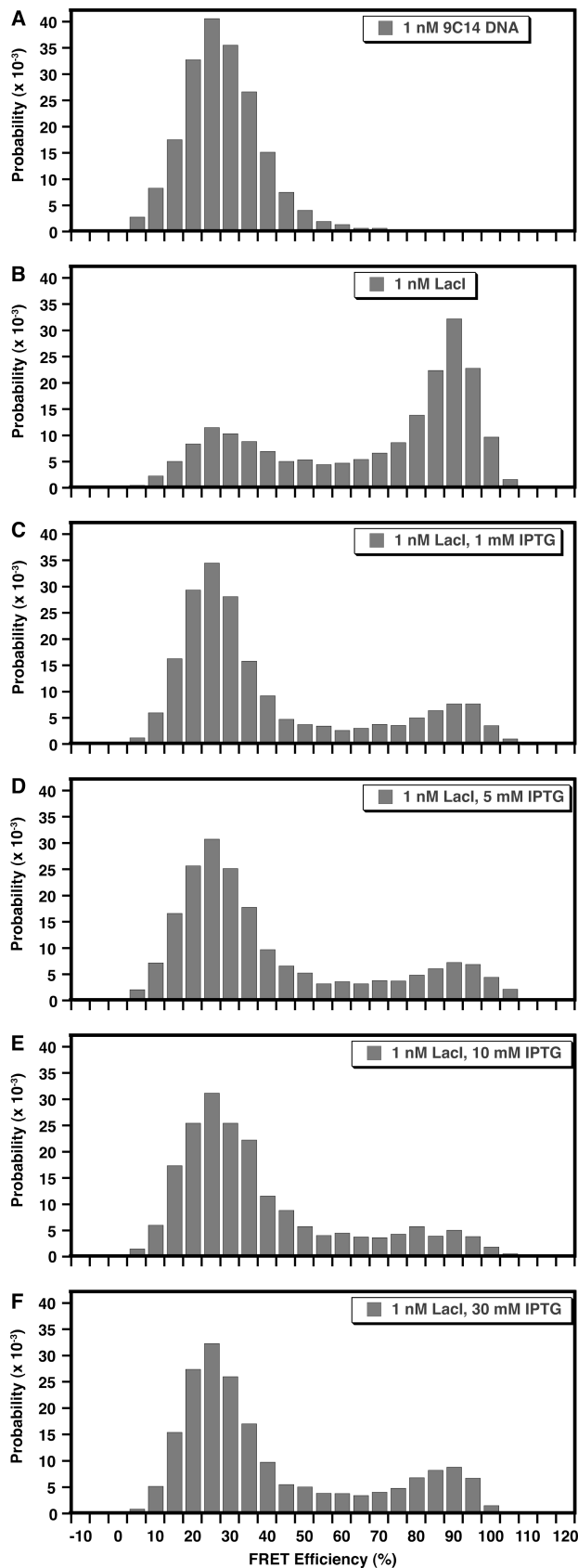


Figure 2.8 Single-molecule fluorescence experiments on freely diffusing LacI-9C14-IPTG complexes in which LacI was pre-incubated with IPTG.

The experiments were otherwise done as in Figure 2.6, and the similarity of the results demonstrates that the LacI-DNA-IPTG complexes observed are at equilibrium. (A) FRET histogram of 9C14 DNA alone. (B) LacI-9C14 complexes. (C-F) FRET histograms obtained at 1, 5, 10, and 30 mM IPTG. As in Figure 2.6, IPTG-bound looped complexes show a persistent high-efficiency peak. The low-amplitude intermediate apparent FRET efficiencies are discussed in Appendix II.

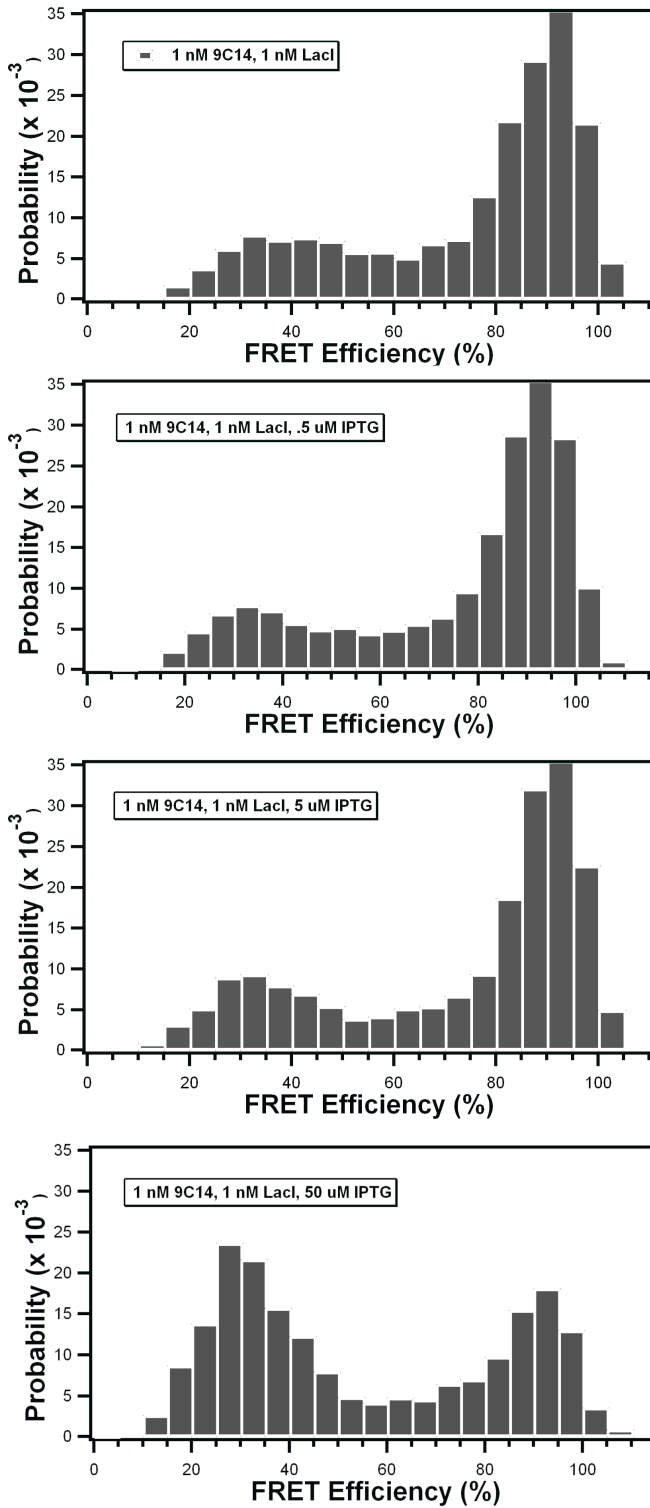


Figure 2.9 Single-molecule fluorescence experiments on freely diffusing LacI-9C14-IPTG complexes. Experiments with freely diffusing LacI-9C14-IPTG complexes in which LacI was pre-incubated with IPTG at the same concentrations were analogous to the ones shown here. Shown here are LacI-9C14 complexes with .5, 5, and 50 μ M IPTG. In this set of experiments we did not catch an intermediate; however, it clearly shows that we need greater than 5 μ M IPTG.

Bulk and single-molecule FRET measurements suggest that LacI-9C14-IPTG exists as at least two populations. One has a closed-form, high-efficiency FRET loop geometry similar to the uninduced LacI-9C14 loop. The other, which does not support FRET, could include loop states with more open LacI protein (moving the dyes apart), different loop topologies, and/or specific-nonspecific loops. In the bulk FRET experiments the addition of excess LacI did not further decrease the FRET, which is evidence for a molecule that is looped, but does not exhibit FRET (dark loop). The essential observation is that IPTG increases the diversity of loop shapes but under these conditions does not appear remove the ability of LacI to loop DNA. The free energy of the high-FRET LacI-DNA-IPTG loop is apparently comparable to the free energies of the other available states.

2.4 Discussion

Effector molecules and architectural DNA binding proteins regulate loop shape and stability (Dalma-Weiszhausz and Brenowitz, 1992; Hoover et al., 1990; Lobell and Schleif, 1991). Here, we apply EMSA and SM-FRET to investigate the modulation of LacI-DNA looping by IPTG *in vitro*, using the previously characterized 9C14 pre-bent DNA looping substrate that supports hyperstable loops. Inducer-bound Lac repressor undergoes a conformational change that allosterically shifts the headpiece and core domains of the structure (Lewis et al., 1996), resulting in dramatically decreased affinity for DNA. Previous *in vitro* and *in vivo* evidence does indicate that the IPTG-bound LacI is still capable of forming looped complexes. Here, a looped species with the same electrophoretic mobility is observed in the presence and absence of IPTG, presumably corresponding to the closed, parallel form

of the LacI-9C14 loop (Morgan et al., 2005). In single-molecule diffusing FRET experiments at saturating IPTG, the position but not the amplitude of a high-efficiency FRET peak is maintained. In both the EMSA and the single molecule FRET studies the addition of excess LacI to the LacI-9C14-IPTG complexes neither increased nor decreased the looped population, suggesting that the initial LacI-9C14-IPTG complexes that do not show FRET are also stable loops.

The DNA bending in the 9C14 model DNA construct is important to the stability of the induced loop. Tethered particle microscopy shows that IPTG breaks loops that lack DNA bending (Wong et al., 2008). We suggest that the bending in our DNA model constructs mimics the supercoiled DNA environment of an *E. coli* cell, in which the high local concentration of the operators allows the formation of LacI-DNA loops despite saturating IPTG concentration (Bond et al., 2010). We suggest that all of the looped forms are likely to be linked to at least one operator, since some extent of transcriptional repression is still observed.

The high-FRET LacI-9C14-IPTG loop presumably has the same closed geometry as the uninduced loop. The stable loops that do not show FRET could include an open form of the LacI protein, a different DNA loop topology (Haeusler et al., 2010; Lillian et al., 2008; Semsey et al., 2005), or looping between an operator and a non-specific DNA binding site. Open-form LacI or alternative loop topologies that still do not allow access of RNA polymerase will have more subtle biological effects. We propose that these inducer-bound LacI-DNA looped complexes may control the kinetics of induction and re-repression of the operon.

Chapter 3: SM-FRET Analysis of Freely Diffusing DNA-LacI Molecules with Proposed Alternative Loop Geometries

3.1 Introduction

The identification of V-shaped and extended Lac repressor conformations as influenced by DNA looping has been the focus of several experimental (Wong et al., 2008) and theoretical studies (Hirsh et al., 2011; Swigon et al., 2006). Distance and orientation of *lac* operators impacts the efficiency of repression (Bellomy et al., 1988; Müller et al., 1996). The bending flexibility of DNA as it relates to loop type can describe both the kinetics of looping and stability of looped complexes (Normanno et al., 2008). The Kahn lab has shown that sequence dependence curvature of DNA reduces the energetic cost of looping (Mehta and Kahn, 1999) and influences loop topology (Edelman et al., 2003; Haeusler et al., 2010; Morgan et al., 2005). These experiments demonstrate that operator phasing may modulate the preferred LacI geometry, allowing for exploration of distinct loop types. The exact degree to which the opening of the LacI tetramer from its proposed V-shape form mediates DNA loop formation remains an open question.

The studies presented in this chapter are the SM-FRET extensions of bulk FRET studies on a DNA sequence landscape of loop topologies from the dissertation research of Aaron Hausler (Haeusler, A., Goodson, K., Lillian, T., Goyal, S., Perkins, N., and Kahn, J. (2011). FRET Studies of Landscape of Lac Repressor Mediated DNA Loops. Nucl Acids Res, Accepted). The landscape (Figure 3.1) was created from the design rationale of the 9C14 and 11C12 model DNA constructs. The landscape provides for systematic study of accessible loop topologies and geometries

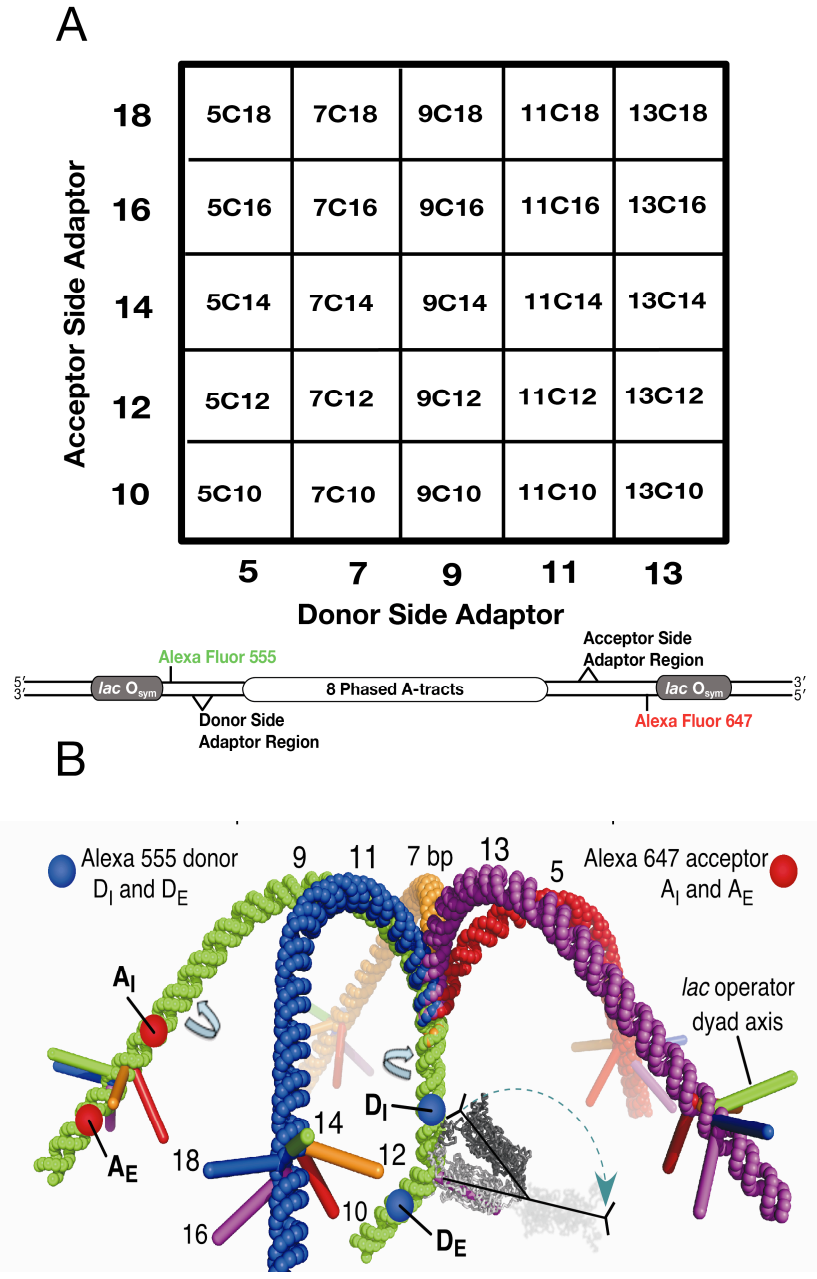


Figure 3.1 Layout and schematic of the model construct landscape.

(A and B) The landscape consists of a matrix of 25 pre-bent model constructs developed by rotating operators on both sides of the sequence directed bend of 9C14 by $0, \pm 2, \text{ or } \pm 4$ base pairs varying the degree of the operator dyad axis rotation with respect to 9C14 and is fully described in Haeusler, 2011. (B) is from Haeusler, A., Goodson, K., Lillian, T., Goyal, S., Perkins, N., and Kahn, J. (2011). FRET Studies of Landscape of Lac Repressor Mediated DNA Loops. Nucl Acids Res, Accepted.

defined by the operator phasing. Loop trajectories are defined by the direction of LacI binding sites in the DNA loop (Chapter 1, Figure 1.4).

In addition to the phasing of operator binding sites the positions of the fluorophores were expanded. The donor and acceptor fluorophores were repositioned from inside the operators to outside the operators on the model constructs (Figure 3.2). The repositioning of the fluorophores serves two purposes: (1) it can be used as

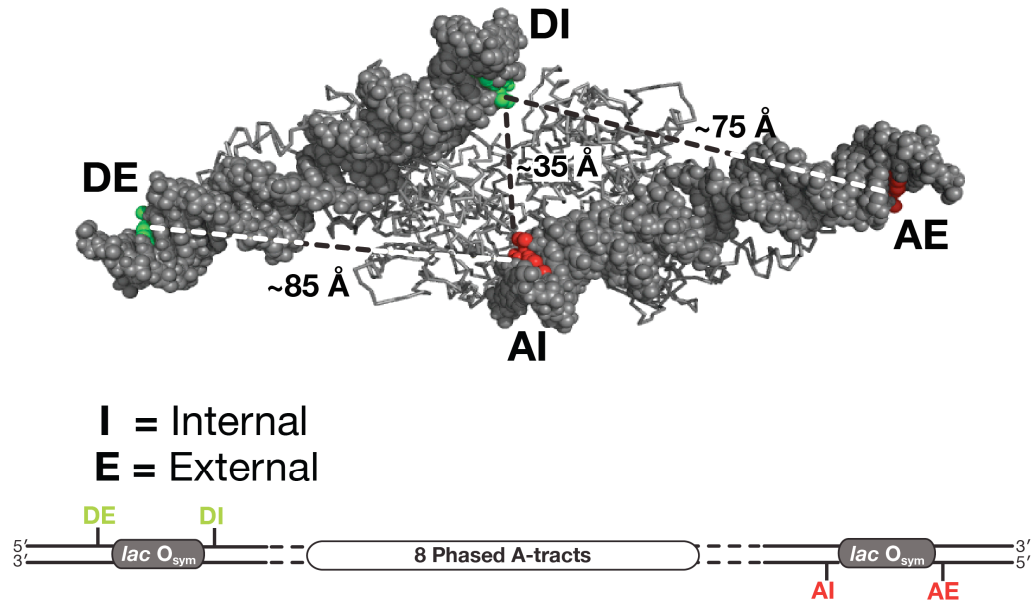


Figure 3.2 Top view of LacI bound to extended operator DNA with highlighted Alexa Fluor® 555 donor (green) and Alexa Fluor® 647 acceptor (red) fluorophore points of attachment.

The approximate distance between original donor and acceptor fluorophores is 35 Å in a closed form loop (Lewis et al., 1996; Morgan et al., 2005). Repositioning of either donor or acceptor fluorophores from the inside of the operator DNA (denoted DI and AI) to outside the operator DNA (denoted DE and AE) increases the approximate distance between donor and acceptor fluorophores to 75 and 85 Å respectively.

an internal control in single molecule experiments to provide an argument for assigning a population to a particular loop, and (2) it identifies possible looping conformations that may have been hidden due to the original placement of fluorophores in the initial experimental design (Figure 3.3).

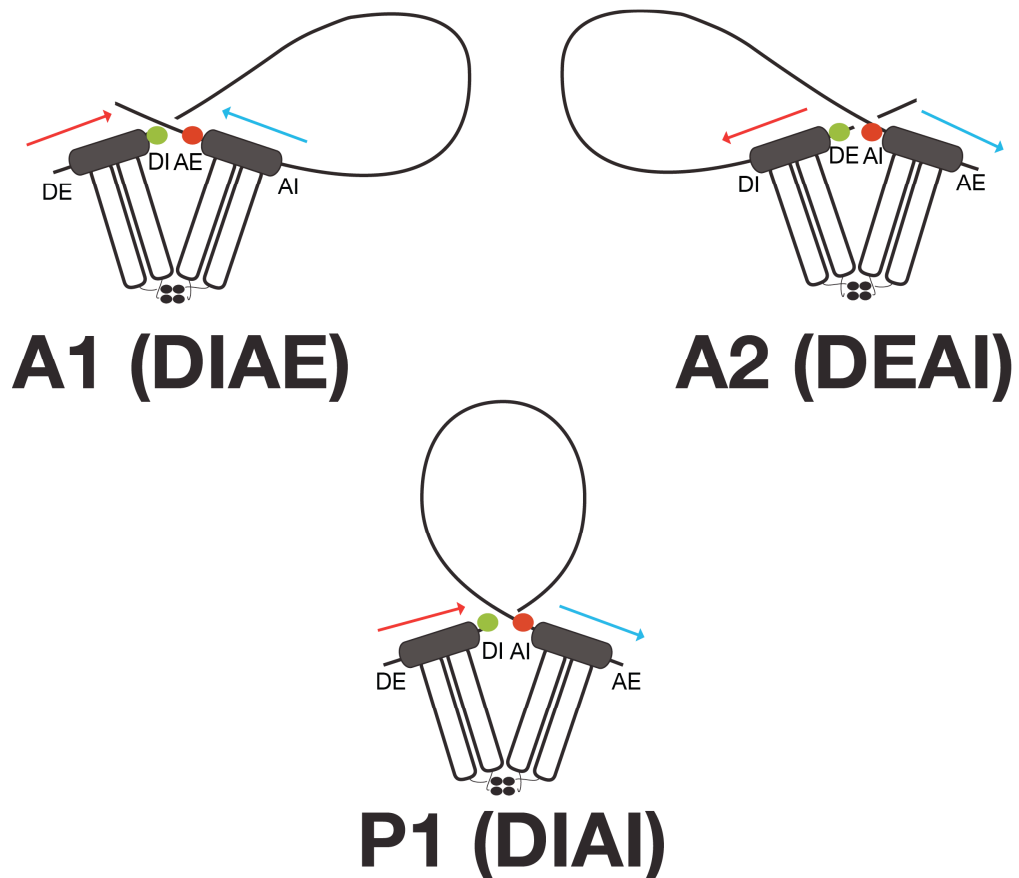


Figure 3.3 Models for LacI-DNA loops with fluorophores.

A schematic highlighting the combination of fluorophore positions that would provide for maximal energy transfer of each proposed loop type.

In the bulk FRET experiment, FRET efficiencies were measured for the 25 model constructs at all the following fluorophore positions DIAI, DIAE, DEAI, and DEAE with and without IPTG as summarized in the population maps of Figure 3.4.

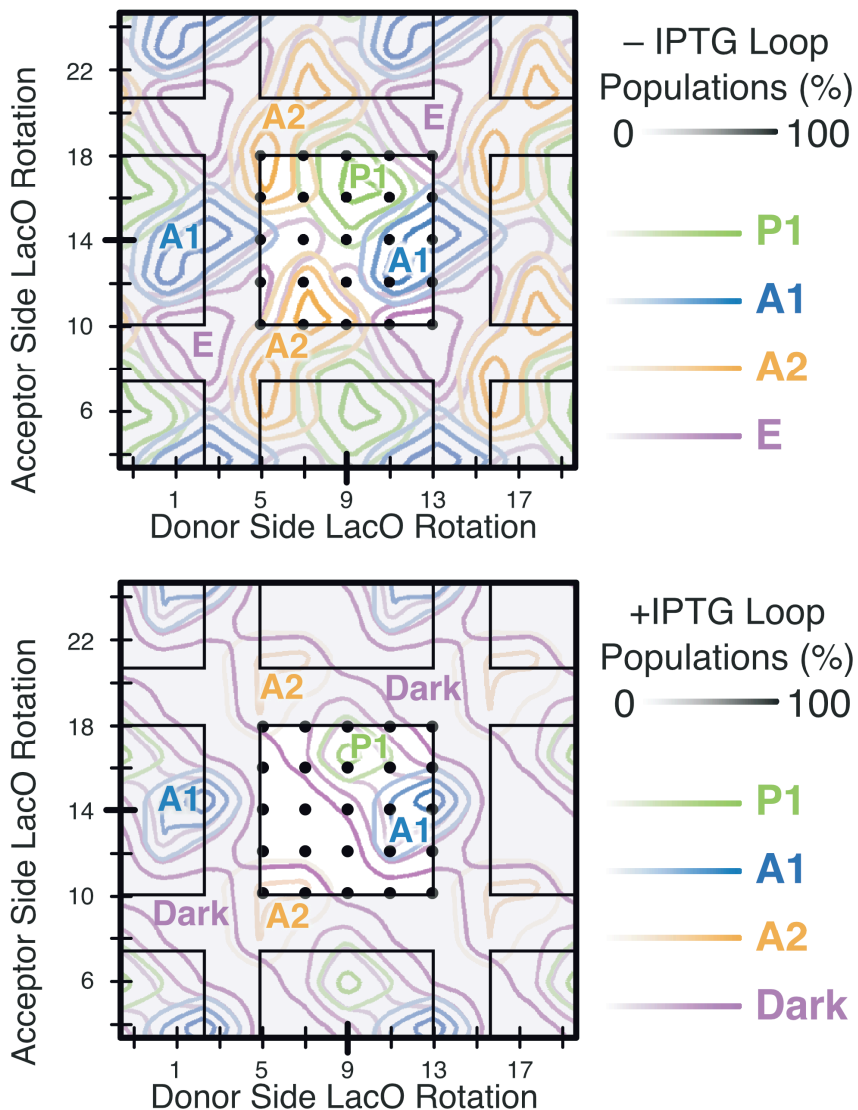


Figure 3.4 Bulk FRET population maps of LacI-landscape complexes.

Superposition of model constructs over the combined contour plot of the bulk FRET loop population distributions for the P1, A1, and A2 and E topologies calculated from the bulk landscape FRET efficiencies with and without IPTG from Haeusler, A., Goodson, K., Lillian, T., Goyal, S., Perkins, N., and Kahn, J. (2011). FRET Studies of Landscape of Lac Repressor Mediated DNA Loops. Nucl Acids Res, Accepted.

The goals of the bulk FRET work include: systematic study of accessible loops topologies, *in vitro* analysis of an extended form of the Lac repressor, and the effect of IPTG on loop topology. The bulk FRET experiments provide evidence for energy transfer in antiparallel (A1 and A2) loops and the ability for a construct to adopt more than one FRET population, however confirmation of the FRET values associated with these topologies may only be assessed using single molecule techniques. The bulk FRET experiments also address the effect of IPTG on alternative loop geometries. IPTG binding does not cause redistribution among loop topologies based on the work; however, more insight about the structural information may be gained from single molecule study.

Here, using SM-FRET we provide evidence for various loop topologies in LacI-DNA looped complexes. We study the antiparallel, A1 and A2, and parallel P1 (Figure 3.3) possible loop trajectory distributions. SM-FRET loop response to IPTG provides evidence for the effect of loop type on structural changes and the overall stability of looped complexes.

3.2 Materials and Methods

Samples were prepared and experiments were conducted essentially as described in Chapter 2. The additions and/or changes to the previously described methods are outlined below:

Fluorescently labeled oligonucleotides

The PCR primers for external fluorophore positions have an amino dT C-6 internal modification (T* below: iAmMC6T). The *lac* operator is underlined and the are as follows: 5'-CCGATATCTGCAGGTCAGTCTAGGTAATTGTGAGCGCTCACAATTAT*ATC T-3' (D_{External}) and 5-TTGATATCAAAGCTTTACCACAACGAATTGTGAGCGCTCACAATTAT*CTAGCTTCG -3' (A_{External}). The PCR primers with amino dT C-6 internal modification (T* below: iAmMC6T) moved internal to external positions of the *lac* operator (underlined) are 5'-CCGATATCTGCAGGTCAGTCTAGT*TAATTGTGAGCGC-3' (D_{Internal}) for donor incorporation and 5'-TTGATATCAAAGCTTTACCACAAT*GAATTGTGAGCGC-3' (A_{Internal}) for acceptor incorporation.

SM-FRET measurements

SM-FRET was done essentially as described Chapter 2. All SM-FRET measurements were conducted at 1 nM DNA and 1 nM LacI in LacI buffer. Samples were allowed to equilibrate at room temperature (20 °C) for at least 3 min. Excitation at 514 nm was from an argon ion laser at 35 μW power focused 10 μm into the sample from the glass-liquid interface. Photon counts were acquired in 1 ms or 100 μs time bins.

3.3 Results

3.3.1 Selection of Samples Based on Bulk FRET Results for LacI-Landscape Complexes

Bulk FRET study of the LacI-induced looped landscape complexes provided for analysis of antiparallel, A1 and A2, and parallel P1 (Figure 3.2) possible loop distributions (Haeusler, 2011) (Haeusler, A., Goodson, K., Lillian, T., Goyal, S., Perkins, N., and Kahn, J. (2011). FRET Studies of Landscape of Lac Repressor Mediated DNA Loops. Nucl Acids Res, Accepted). The work investigated the LacI-DNA and LacI-DNA-IPTG forms of all landscape molecules. The molecules with maximal energy transfer for each proposed loop type was selected for SM-FRET analysis (Figure 3.3), in order to ascertain peak FRET values for an individual loop type without the averaging effects as seen in a bulk experiment. In addition, molecules that are believed to adapt multiple loop types were analyzed, with the goal to monitor conversion of one loop type to another in the time scale of a single molecule experiment. The extended (E) loop distribution, as defined by an open form of the LacI tetramer that would provide for a zero FRET (or donor only FRET distribution) was not chosen for SM-FRET analysis (Figure 1.4). The selections of molecules for SM-FRET analysis are summarized in Table 1.

Table 1: Selection of molecules for SM-FRET analysis based on bulk FRET landscapes.

5C18 DEAI	Maximal energy transfer for the A2 loop population.
7C16 DIAI	Boundary between P1 and A2 loop populations.
7C16 DEAI	
9C16 DIAI	Maximal energy transfer for the P1 loop population.
13C14 DIAI	Control for crosstalk.
13C14 DIAE	Maximal energy transfer for the A1 loop population.

3.3.2 SM-FRET Results for LacI-Landscape Complexes

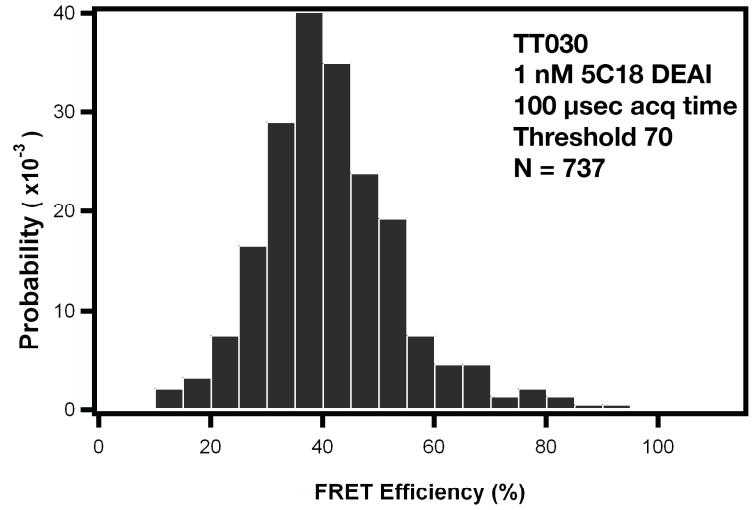
FRET efficiency was measured for the selected landscape DNA constructs in the presence of equimolar LacI (a 1:1 ratio of DNA:LacI). When used, IPTG was at saturating concentrations of IPTG (5 mM). DNA only controls show zero FRET, as seen in the molecules in Chapter 2. The SM-FRET histograms for the selected landscape DNA constructs are shown on the following pages (Figure 3.5).

Figure 3.5 SM-FRET histograms of LacI-landscape complexes.

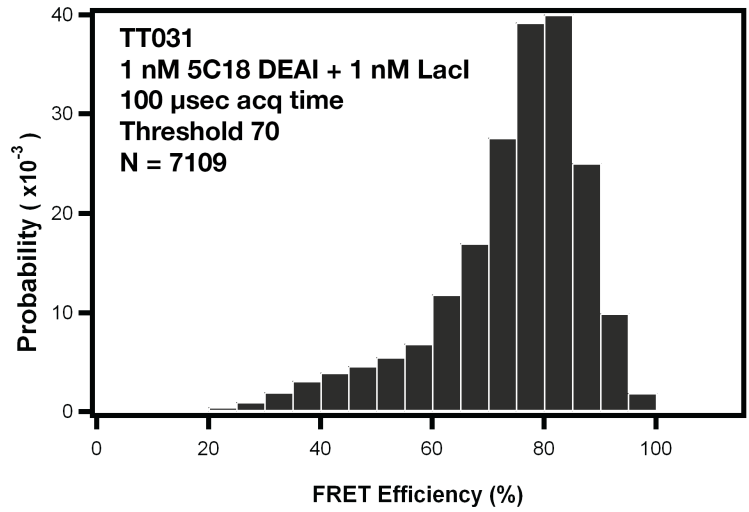
Individual SM-FRET histograms for the 5C18 DEAI (A2), 7C16 DIAI (P1), 7C16 DEAI (A2), 9C16 DIAI (P1), 13C14 DIAI (P1), and 13C14 DIAE (A1) DNA model constructs alone, with LacI, and with LacI and IPTG. The x-axis (FRET Efficiency (%)) of each histogram is scaled between 0-115 and the y-axis (Probability ($\times 10^{-3}$)) scale is between 0-40 or 0-60 varied due to the intensity given for an individual construct. All histograms shown have a bin size of 5 ms. The single molecule transient number (TT), experimental component description, acquisition time (acq), threshold, and number of event (N) are given in the inset of each individual histogram.

5C18 DEAI

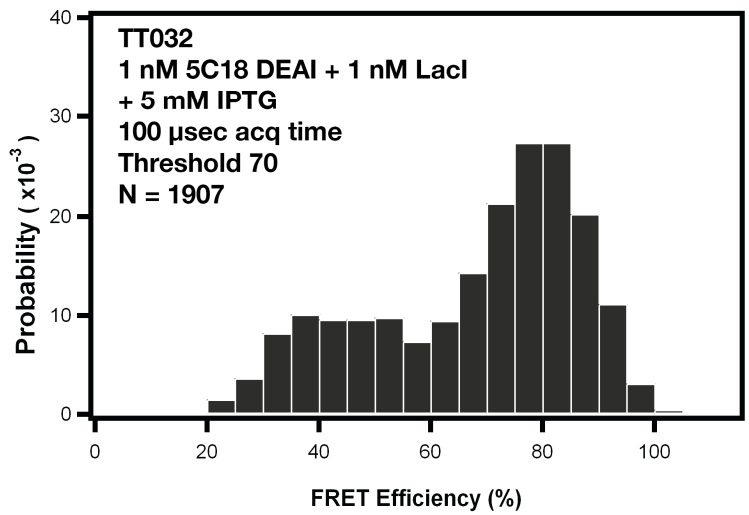
DNA Only



DNA + LacI

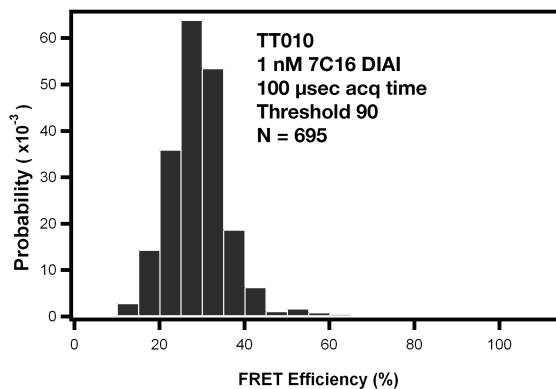


DNA + LacI
+ IPTG

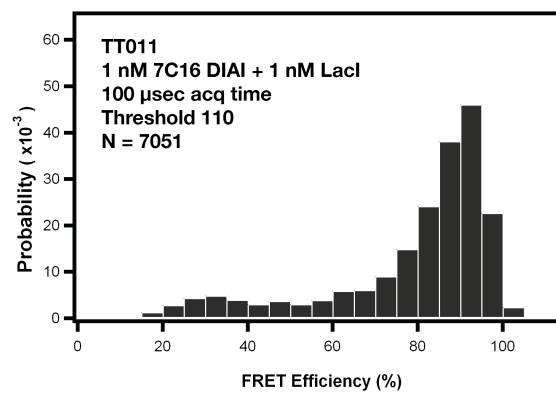


7C16 DIAI

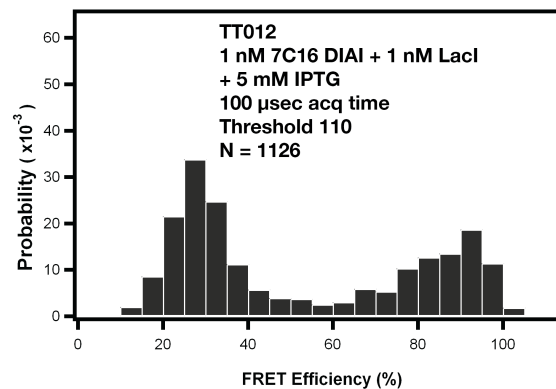
DNA Only



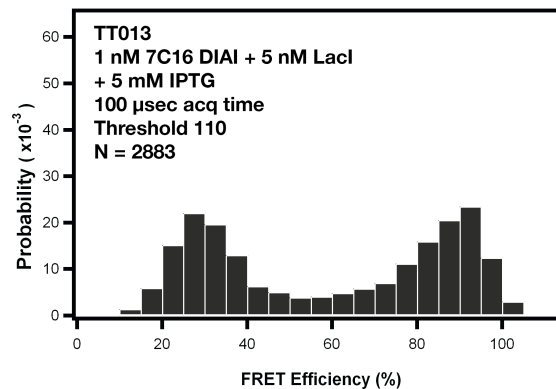
DNA + LacI



DNA + LacI
+ IPTG

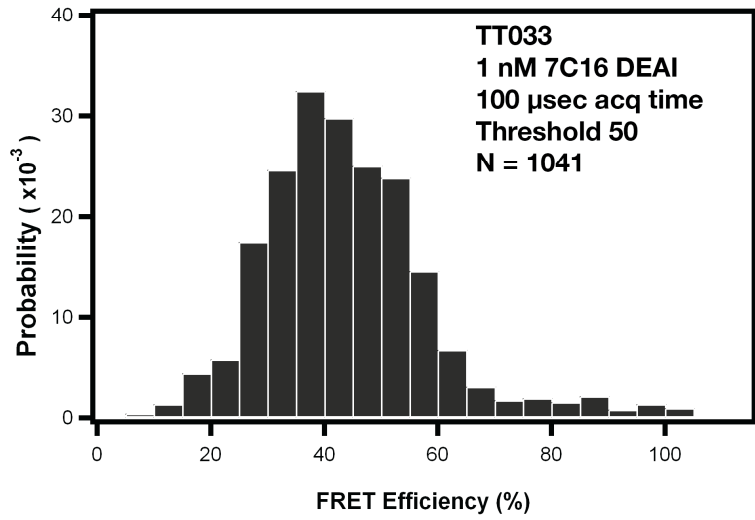


DNA + Excess LacI
+ IPTG

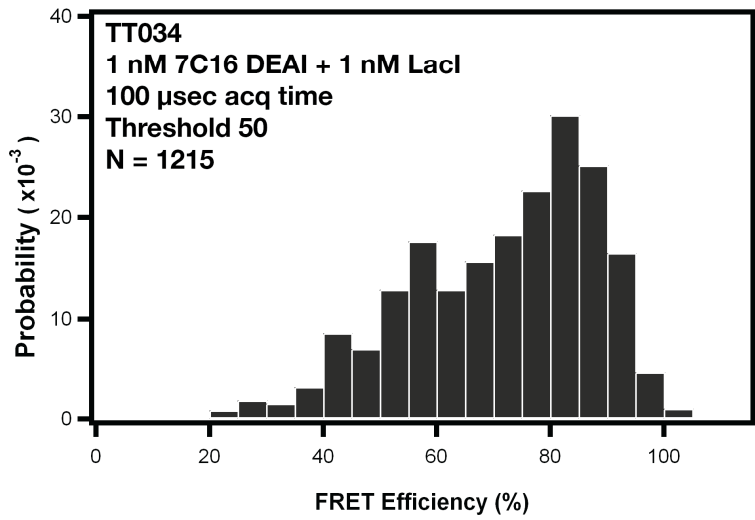


7C16 DEAI

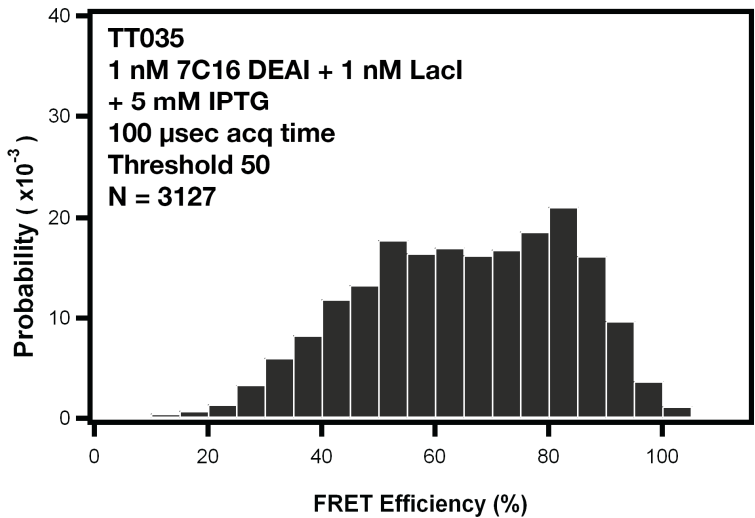
DNA Only



DNA + LacI

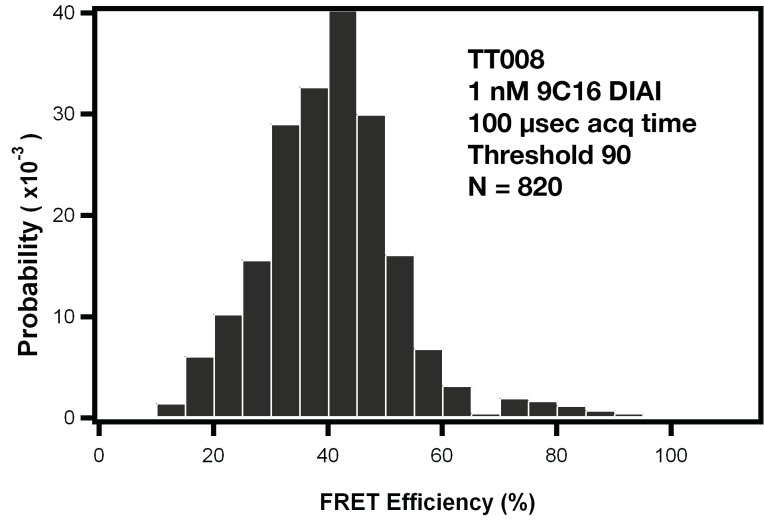


DNA + LacI
+ IPTG

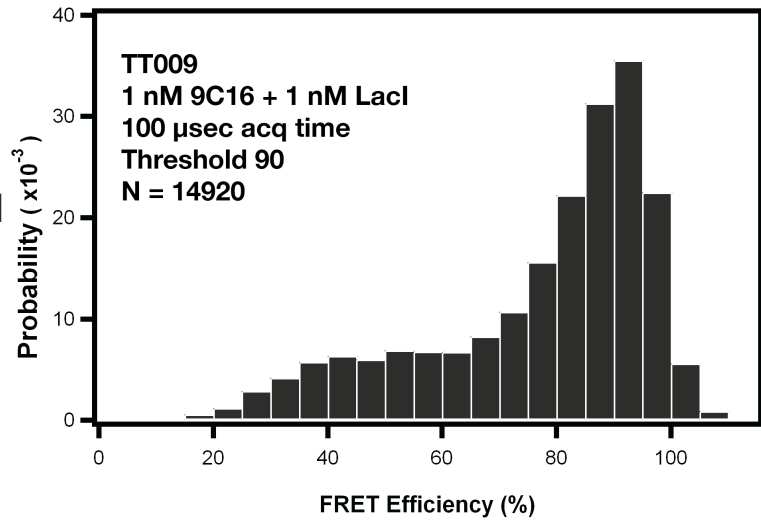


9C16 DIAI

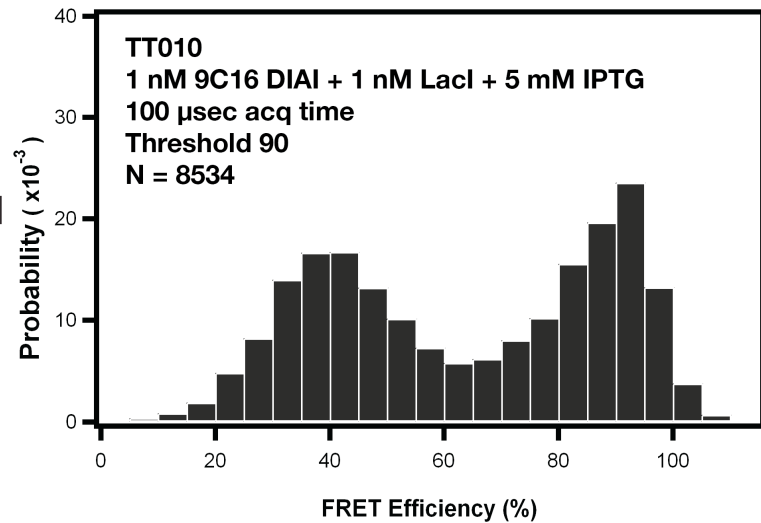
DNA Only



DNA + LacI

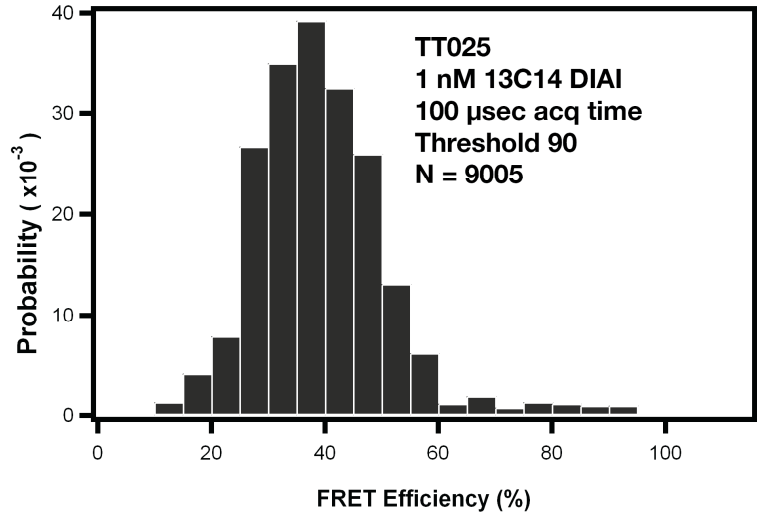


**DNA + LacI
+ IPTG**

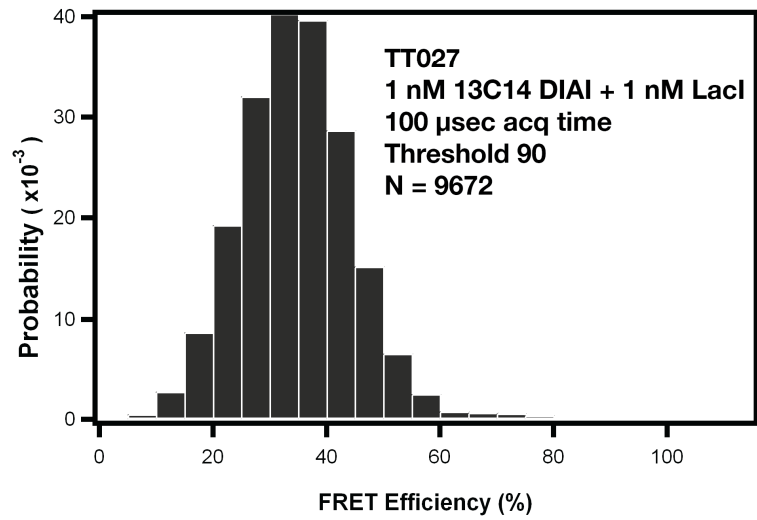


13C14 DIAI

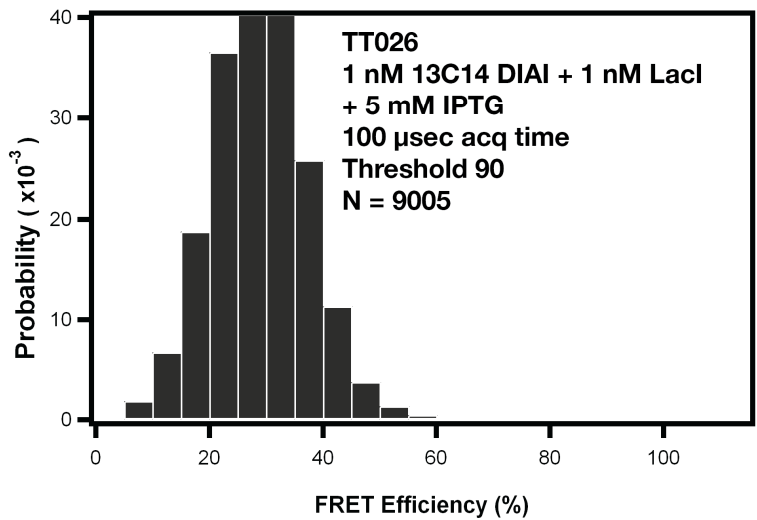
DNA Only



DNA + LacI

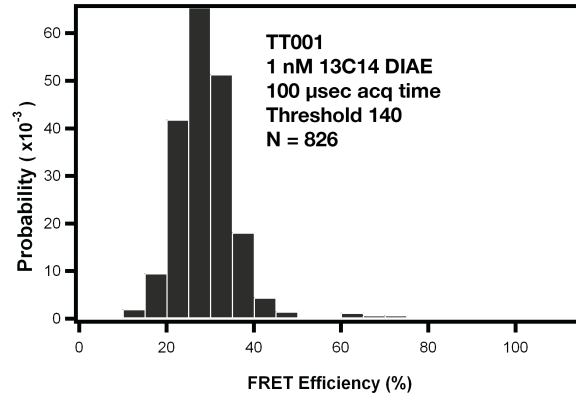


DNA + LacI
+ IPTG

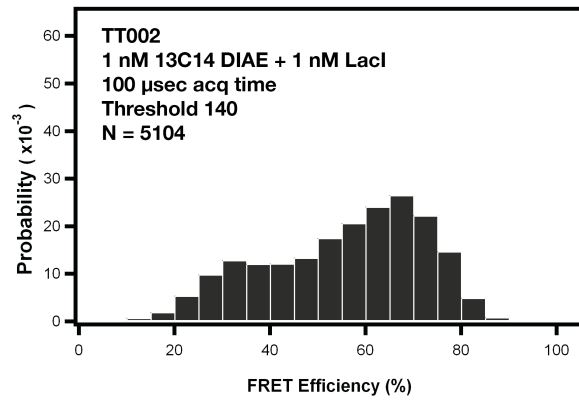


13C14 DIAE

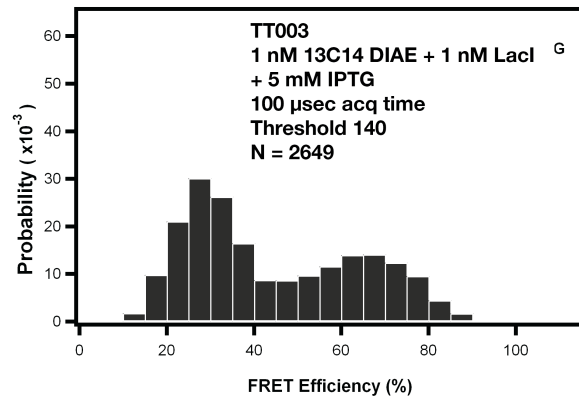
DNA Only



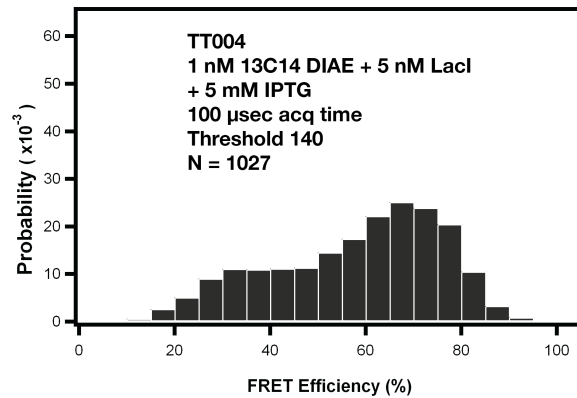
DNA + Lacl



DNA + Lacl
+ IPTG



DNA + Excess Lacl
+ IPTG



Based on their identification as P1 closed loop complexes, 9C16 DIAI constructs are expected to show at high FRET (~90% energy transfer) as seen in the previously discussed 9C14 DIAI model DNA construct (Chapter 2). Figure 3.6 confirms this prediction. Antiparallel loops (A1 and A2) are predicted to be more energetically favorable than P1 loops (Lillian et al., 2008; Mehta and Kahn, 1999). The histograms of 13C14 DIAE and 5C18 DEAI molecules with LacI display A1 and A2 loops with high FRET peaks at ~70% and ~80% energy transfer, respectively. The A1, A2, and P1 loop complexes appear to contain only a single species in a high FRET loop population because the SM-FRET histograms possess only a single high FRET peak. These values all represent efficient energy transfer, but they are different from each other. The centers of the high FRET peaks of all of the described loops are within 10% of each other, suggesting that all of them adopt a V-shaped conformation of the Lac repressor (Lillian et al., 2008). The calculated bulk FRET efficiencies for the peak A1, A2, and P1 constructs were 24%, 28%, and 29%, respectively.

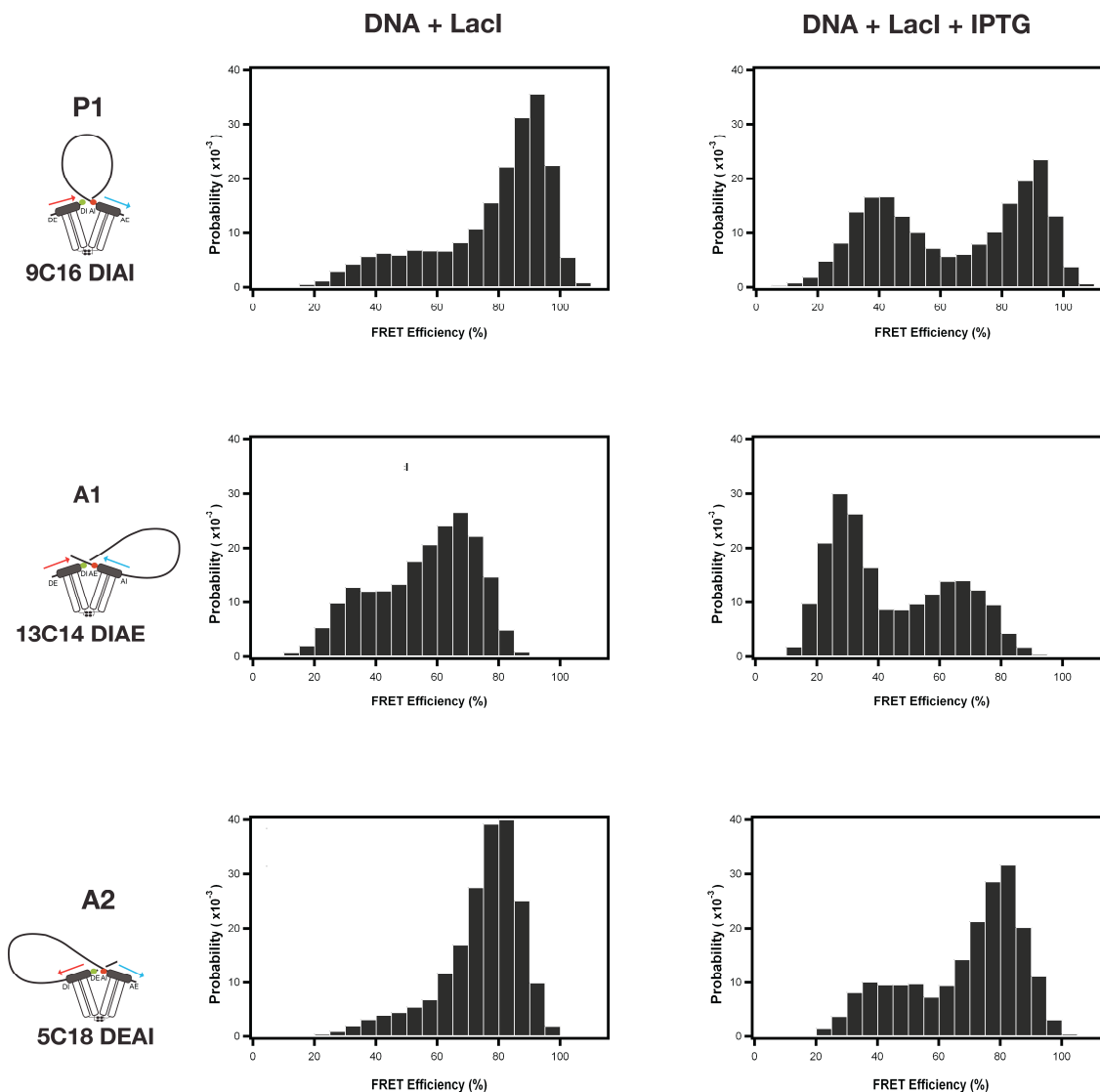


Figure 3.6 Single-molecule FRET experiments on freely diffusing LacI-landscape complexes.

For emphasis, we compare histograms shown in Figure 3.4. Peak landscape DNA model constructs are those that represent loops where more than 90% of the loop population represented the highlighted P1, A1, or A2 loop type based on bulk FRET analysis. Shown are the normalized histograms of FRET distributions for peak landscape DNA molecules in the presence of LacI (1 nM:1 nM ratio of DNA:LacI) and in the presence of LacI and 5 mM IPTG upon 514 nm laser excitation of samples dual-labeled with Alexa Fluor® 555 and Alexa Fluor® 647. Upon the addition of LacI all FRET histograms show a high FRET population of molecules. Amplitudes of the high FRET peaks are decreased but not eliminated upon the addition of saturating IPTG concentrations for all of the constructs shown.

Stable LacI-DNA-IPTG loops are indicated by the bulk FRET results. Here we compare the bulk FRET results with that of SM-FRET to further investigate loop conformation and stability among the loop topologies. The SM-FRET histograms show that all the loops from the peak A1, A2, and P1 FRET model constructs demonstrate destabilization of LacI-DNA looped complexes upon the addition of inducer. As seen for 9C14, a saturating concentration of IPTG causes a decrease in the amplitude but not in the position of the high-FRET peaks. For all the molecules assessed during the SM-FRET landscape studies, the addition of IPTG did not increase the amplitude of the high-FRET peak. The fact that the amplitude of the high FRET peak is reduced and not increased confirms we are seeing non-distribution of a population of one loop type to another in agreement with the bulk FRET studies. Significant high-efficiency FRET populations for the constructs remain at saturating IPTG concentrations. This persistence mirrors bulk FRET studies and is expected for in general based on the implications of the formation of stable closed form loops.

The 13C14 model construct shows the greatest transfer efficiency in the DIAE bulk FRET landscape (Figure 3.7). In addition, 13C14 was shown to have zero transfer efficiency in the DIAI bulk FRET landscape. The 13C14 DIAE SM-FRET histograms show a high FRET peak at $\sim 70\%$, thus indicating the formation of a loop even with the addition of IPTG. In the 13C14 DIAI SM-FRET histograms for the 13C14 construct there is no indication of FRET. Consistent with the bulk results, SM-FRET demonstrates absence of crosstalk. Crosstalk is denoted by weak FRET efficiency containing populations for molecules in more than one set of fluorophores

(i.e. between DIAI, DEAI, and DIAE landscapes). Physically crosstalk is defined by FRET between fluorophores that are nominally ≥ 75 Å apart as in figure 3.2 and therefore should show weak or no FRET. Overall, these results are in accord with the bulk FRET observations and assumptions. This affirms SM-FRET's ability to detect distinct topologies.

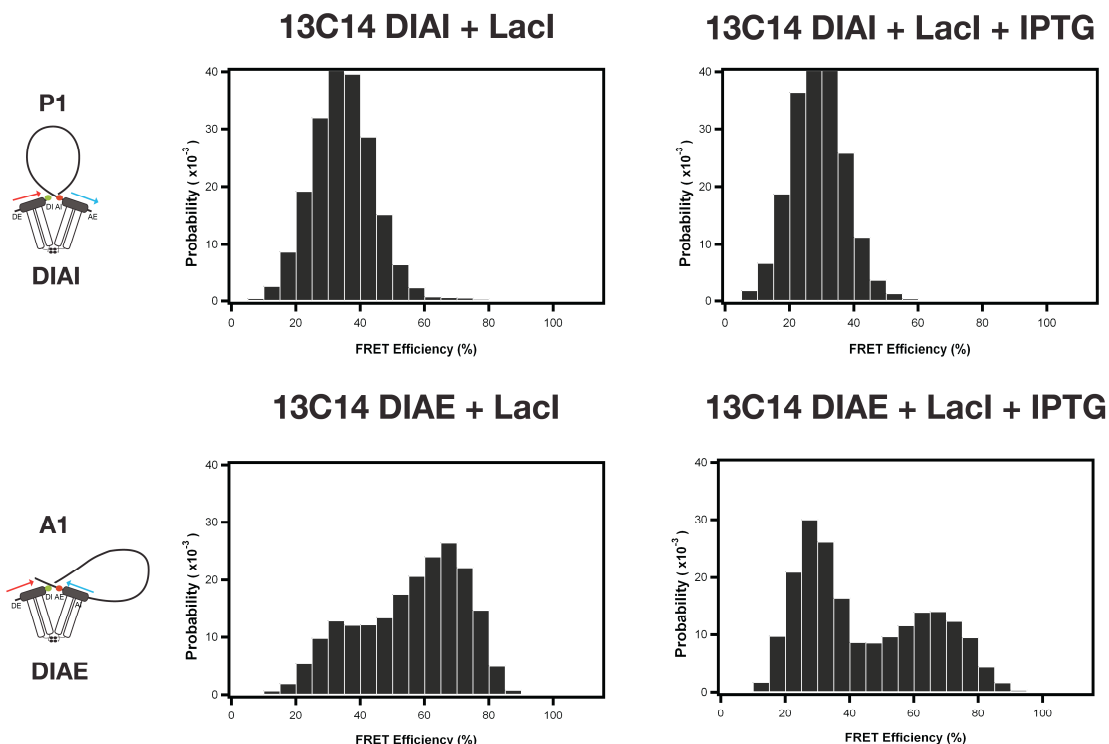


Figure 3.7 Single-molecule diffusing FRET experiments on freely diffusing 13C14 DIAI and 13C14 DIAE LacI-landscape complexes.

Energy transfer of the 13C14 construct with DIAI fluorophore positioning does not take place. Studies were performed with the same model construct with variable fluorophore positioning in order to directly assess possible calculated high-FRET peaks from distinct loop topologies. Shown here in the 13C14 model construct with fluorophore positioning internal to the operator binding sites (DIAI) and internal for the donor fluorophore and external for the acceptor fluorophore in regard to their perspective operator sites (DIAE). Constructs displaying maximal transfer for an individual loop topology of an apparent uniform population was only shown to do so with specific fluorophore positioning in the bulk FRET studies as confirmed here for the SM studies.

The 7C16 model construct lies on the boundary between the A2 and A1 populations as derived from the bulk FRET landscape (Figure 3.8). The SM-FRET confirms the ability of the 7C16 model construct to adopt both populations by the appearance of a high FRET peak in both the 7C16 DIAI and DEAI SM-FRET histograms. This is in contrast to the result for the 13C14 model construct, which is modeled to adopt a single topology.

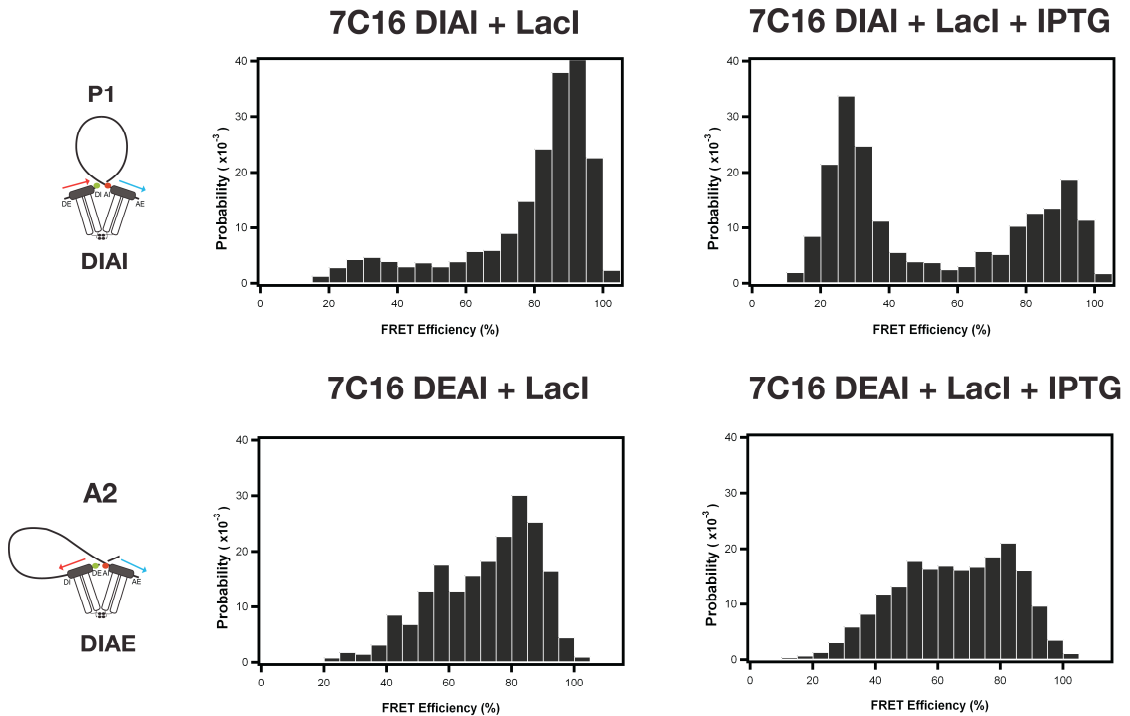


Figure 3.8 Single-molecule diffusing FRET experiments on freely diffusing 7C16 DIAI and 7C16 DEAI LacI-landscape complexes.

The 7C16 model construct lies on the boundary between a P1 and A2 loop topology. The 7C16 model construct showed significant FRET in more than one bulk FRET landscape. The SM-FRET histograms shown display the fact the 7C16 sequence may adopt more than one specific topology.

3.4 Discussion

Mapping variations in both DNA loop structure and stability is a key component in taking a quantitative approach in the study of gene regulatory systems. Here we have established that protein geometry mediates loop topology. We present evidence for stable alternative loop forms. The bulk FRET experiments were able to decipher explicit populations for loop topologies. SM-FRET experiments shown here resolves the FRET efficiency for a given loop topology. In addition, SM-FRET provides more structural information in terms of the identity the geometry of stable protein-DNA loops, since the bulk FRET studies are based on the result of averages of FRET efficiencies.

SM-FRET data demonstrate efficient energy transfer in both A1 and A2 loops, and the previously characterized P1 loops. It is highly probable that A1(or A2) and P1 loops would have different responses to DNA bending strain from each other. Antiparallel loops are generally thought to be more energetically favorable because they would require less bending energy (Geanacopoulos et al., 2001; Hirsh et al., 2011; Mehta and Kahn, 1999). Looping in antiparallel trajectories are proposed to bend DNA 180°, while a parallel trajectory would require DNA bending of 360°, paying a higher cost in terms of DNA deformation energy (Mehta and Kahn, 1999). The centers of the high FRET peaks for the molecule exhibiting maximal A1, A2, and P1 topologies are located at approximately 70%, 80%, and 90% FRET efficiency. The differences between the high FRET efficiency values may be interpreted in terms of the effect of DNA expansion on a particular loop topology. DNA expansion in antiparallel loops would open the LacI tetramer, increasing the distance between

donor and acceptor fluorophores, leading to decreased FRET efficiencies. However, DNA expansion in a P1 loop would contract the LacI tetramer bringing the DNA binding domains closer together, thus bringing the fluorophores closer together in our system as modeled in Figure 3.9. In addition, the calculated SM-FRET efficiencies provide evidence for stable V-shaped LacI DNA loops with alternative loop geometries.

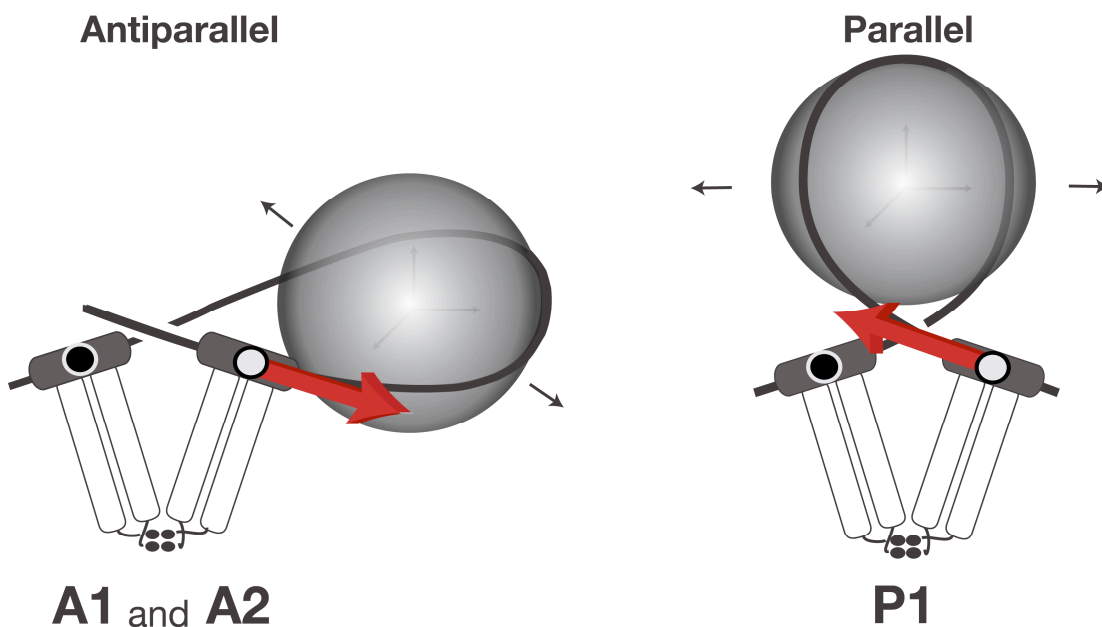


Figure 3.9 Model of LacI-DNA looped complex differential response to DNA expansion for antiparallel and parallel loop topologies.

In order to decrease the free energy of DNA bending (as represented by the expanding sphere in the model) the geometry of the looped complex would be altered. The degree and the manner in which this may occur is variable due to the response of the indicated loop type. If your prospective was anchored at the of the crossover of each loop, in the antiparallel loop DNA expansion would open the LacI tetramer and the fluorophores would be moved further apart leading to decreased FRET efficiencies. On the contrary, in a parallel loop the LacI tetramer would contract and the fluorophores would move closer together.

The SM-FRET analysis of LacI-induced looped landscape complexes has allowed for the calculation of a high-FRET efficiency value of a single molecule of a particular loop type. SM-FRET histograms of all looped complexes in the presence of saturating IPTG inducer reveal a decrease in the high efficiency FRET peak. The fact the high-FRET peak does not disappear suggests formation of stable LacI-DNA-IPTG. One hypothesis is that each loop becomes more dynamic in the presence of inducer but may not necessarily interconvert to another loop type. This may be attributed to interconversion between specific and non-specific binding interactions while the loops may retain their V-shaped geometry. The P1 loops are predicted to have the most fluctuation in the presence of inducer. This is a reasonable assessment because increased bending strain induced by the protein in P1 loops is greater than its A1 and A2 counterparts (Mehta and Kahn, 1999). In the current experimental results we do not detect interconversion of one loop type to another in the molecules that are proposed to be a mixture in population of two loops types (e.g. 7C16). Although we have not observed interconversion within the timescale of our experiment, we do have evidence for the both populations of the 7C16 loop. Loop lifetimes and interconversion from one loop type to another may be further explored with immobilized loop complexes.

Protein-DNA interactions may be directly mediated by loop trajectory (Lia et al., 2008). In general, there is evidence for variable stability in parallel and antiparallel loop trajectories in various systems (Geanacopoulos et al., 2001; Semsey et al., 2004). The sequence dependence of DNA elasticity has been well defined. *In vivo*, DNA bending and twisting occurs in a non-uniform manner attributed to global

and local recognition factors (Rohs et al., 2010). Identification of loop topology and stability can be used to model how intracellular environment mediates selection of prevalent loop types (Saiz and Vilar, 2006). Hence, the ability to detect and characterize variable loop structure as demonstrated through single molecule experiments is a key component in the study of gene regulatory systems.

Chapter 4: Implications of Presented Studies and Areas of Future Work

4.1 Introduction

DNA looping is a mechanism for a variety of biochemical interactions (Matthews, 1992; Schleif, 1992). In general, DNA loop formation is controlled by distance between binding sites, DNA deformation, and contacts with proteins. Combined, these are an indication that the physical properties of DNA may be used to control cellular behavioral pathways including gene regulation. The goal of the work presented was to add quantitative and systematic measurement to study the role of allosteric effectors on DNA looping in the *lac* operon system. We found that upon saturating inducer conditions, LacI-DNA loops were not abolished. The persistence of a viable DNA loop under these conditions is argument for inclusion of IPTG-bound loops in quantitative models for DNA strain and bending that explore DNA geometry. Ultimately, future study of DNA looping in this system will involve immobilized model DNA constructs that allow for the direct monitoring of dynamics through fluctuations of a fluorescent signal. A model for immobilization in our system is outlined in Appendix IV.

4.2 Biological Consequences of DNA-Protein Complexes, DNA Looping, and DNA Loop Topology

DNA supercoiling could stabilize a variety of loop shapes and sizes. For example, LacI binding to plectonemic DNA could form loops with the same V-shaped LacI seen in the high-FRET 9C14 loops, but an open form LacI could bridge operators in apical loops (Bond et al., 2010) (Figure 4.1). *In vivo* loop size may range on the order of under 100 bp or to the upper limits of thousands of bp (Ringrose et al., 1999). Thus, we believe that our loops are a good representation of the type and the size of DNA loops that may be found *in vivo*.

The actual or proposed role for looping should be compared to the regulation that could be carried out by a single-site protein (Schleif, 1987). Looping with a two-site protein confers several potential advantages. First, it allows for multiple simultaneous inputs from separate DNA binding sites, which may be essential for regulation of genes with complex responses to the environment, as in development or homeostasis. Furthermore, detailed experiments on the *lac* system suggest that induction increases the apparent torsional rigidity of looped DNA, indicating that the induced loop is more sensitive to poor alignment of operator sites (Becker et al., 2005). The control of loop stability by changes in DNA shape and supercoiling is an additional mechanism for modulation of gene regulation (Deniz and Mukhopadhyay, 2007; Lobell and Schleif, 1990, 1991; Whitson et al., 1987).

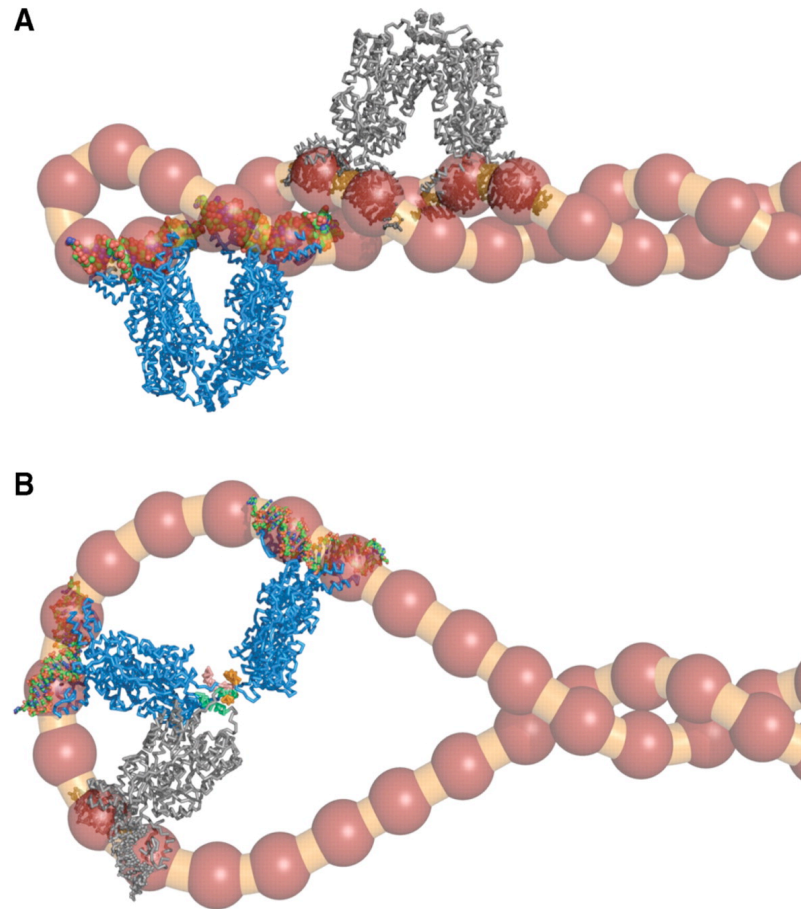


Figure 4.1 Schematic of proposed loop formation at the apex of a negatively supercoiled plectoneme.

Work from Bond et al., 2010, outlining the formation of short DNA loops. LacI is modeled as bound to operator DNA. The model is based on 500 bp DNA minicircle, every 10 bp is denoted by the red marker. Theoretical contracting (A) and expanding (B) the apical loop of the plectoneme would support models of open and closed loop forms of the Lac repressor. (A) is modeled with a superhelical density of -0.18 and (B) is modeled with a superhelical density of -0.06, which is more physiologically relevant.

An additional unique function of looping is that local concentration effects confer rapid on/off rates even at high affinity. In contrast, a single-site protein with a

larger binding surface would tend to require slow on/off rates for high affinity. Leibler has pointed out that looping is therefore useful to the cell because the low level of transcription initiation that escapes repression occurs at a relatively uniform rate instead of in stochastic bursts (Vilar and Leibler, 2003). Here we extend this idea to the induced state: loops in which one headpiece of the repressor is bound to nonspecific DNA instead of to the proximal operator would presumably allow induction, but the induced repressor would be retained in the DNA neighborhood through the other headpiece, able to respond rapidly to the disappearance of allolactose.

Figure. 4.2 illustrates this model for the biological consequences of alternative looping. The left half of the figure illustrates the advantage of fast on/off rates in the repressed state. The right half illustrates that continued localization of the repressor even during induction should accelerate re-repression when the inducer concentration drops. In addition, persistent looping during induction should suppress variability in rates of re-repression that would otherwise be caused by loss of LacI from the local DNA environment. The proposal that induced LacI will remain localized is testable with *in vivo* single molecule studies, but existing data do not address it because they have used dimeric repressors (Elf et al., 2007). When quantitative models for DNA strain and bending are extended to include IPTG-bound loops it will be possible for systems biology models to fully reflect the relevance of changes in looping cooperativity as well as simple binding affinity.

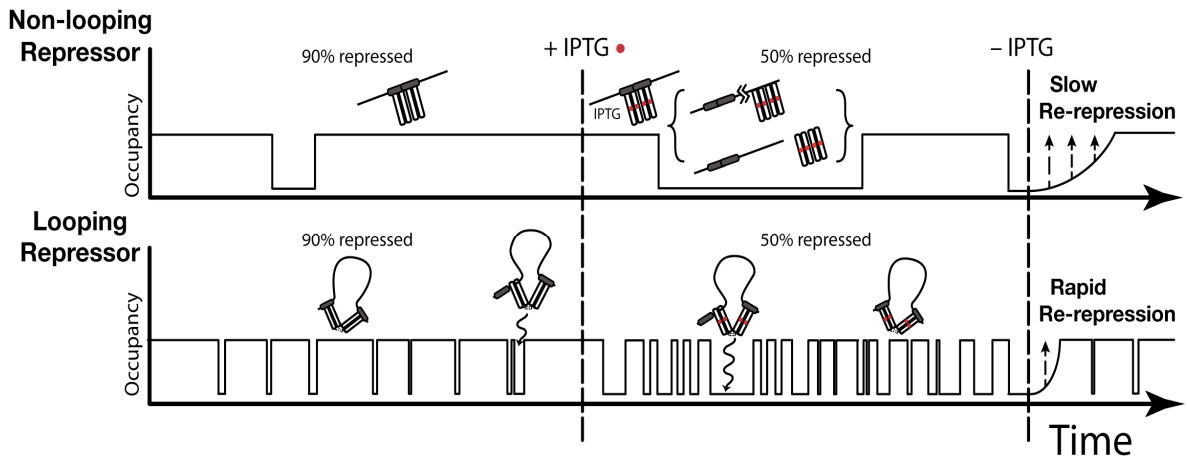


Figure 4.2 Stochastic model for the functions of alternative DNA loops during repression, induction, and re-repression.

Regulation carried out by the Lac repressor, with its proposed ability to form stable specific-nonspecific loops, is compared to regulation by a putative non-looping protein with the same binding affinity for its (longer) operator site. Equal affinity is indicated in the figure by equal ratios of on/off times for the two proteins. The on rate for a single-site protein is necessarily slower than that of a looping protein because it cannot locate its operator through direct transfer (von Hippel and Berg, 1989) and hence the off-rate is also slower at constant affinity. Upon induction, if the non-looping protein leaves its site there is no mechanism for retaining it nearby, whereas a specific-nonspecific loop allows for induction while maintaining nearby LacI. This is most critical to regulatory efficiency when the inducer is removed. The looping protein, being continually localized, can reoccupy its operator very rapidly, whereas the non-looping protein must diffuse back to the site from elsewhere in the cell. Hence, re-repression is accelerated by the proposed specific-nonspecific looping mechanism, and it also occurs at a more consistent rate.

4.3 Systems Biology Applications

Systems biology and single molecule spectroscopy both use physical and mathematical tools for answering the questions of biological processes. Thus, they are natural partners for studying the dynamics of biological complexes. From the single molecule perspective, complete systems may be dissected in order to quantitate a single constituent without average factors that mask identification. One such

emerging example is the single molecule imaging (SMI) of cells in living cells (Sako, 2006). *In vivo* SMI imaging of cells has allowed for noninvasive and non-synchronized monitoring of the finite effects such as diffusion coefficients and dissociation rates that are important for systems biology modeling (Sako, 2006). As single molecule spectroscopy technique makes its introduction to systems biology, its ability to make quantitations of stochastic events may be used to model trends in gene expression and regulation (Elf et al., 2007; Kuhlman et al., 2007).

The overall goal of our studies includes adding a quantitative approach to DNA looping in terms of gene regulation. Work in the Kahn lab has shown that the sequence specificity in combination with facilitation of protein-DNA interaction may be used to influence loop topology and geometry. The SM-FRET work explored here allows one to directly monitor a particular loop type. With the framework set forth here, we will extend SM diffusing studies to that of SM immobilization studies which may provide more insight to the role of LacI deformation energy role in loop formation, and the kinetic parameters of DNA loop formation in general.

Appendices

Appendix I LacI Purification

Goodson, Haeusler, Wang, English, and Kahn
“LacI-DNA-IPTG Loops: Equilibria among Conformations by Single-Molecule FRET”
Supporting Material for *Biophysical Journal*

LacI Expression and Purification

The protein expression and purification was adapted from unpublished work by L. M. Edelman, and published work (Brenowitz et al., 1991; Wilson et al., 2007) with modifications. LacI was expressed in *E. coli* BL21(DE3)pLysS transformed with pMDB1, a pET3a-derived plasmid that confers ampicillin resistance and contains the LacI gene in a T7 expression cassette, generously provided by Michael Brenowitz. Cells were grown from a single colony in 1 mL of LB medium overnight. The starter culture was added to 1 L of LB media containing 50 µg/mL each of ampicillin and chloramphenicol and grown for 2 hr at 37 °C. The cells were then induced with 0.1 mM IPTG and an additional 50 µg/mL of ampicillin was added, and growth was continued for 3 hr. The cells were harvested by pelleting at 8,000 g at 4°C for 10 min in a JLA-10.5 rotor (Beckman, Avanti J-25I). The cell pellet was resuspended to 0.25 g/mL in LacI Resuspension Buffer (200 mM Tris-HCl, 200 mM KCl, 10 mM MgCl₂, 5% (v/v) glycerol, 0.3 mM DTT, 1 mM NaN₃, 1 mM PMSF, pH 7.2) and lysed by four passes through a French Press (American Instrument Company). The lysed cells were mixed with 0.4 mg/mL of DNase I for 30 minutes on ice with constant rocking. The debris was pelleted from the lysate at 39,000 g at 4 °C for 20 min in a JA 25.5 rotor. The crude LacI was precipitated from the supernatant with ~35% ammonium

sulfate saturation at 4 °C (confirmed by SDS-PAGE), and then pelleted at 39,000 g for 20 min. The LacI pellet was resuspended in 20 mL of dialysis buffer (50 mM K₂HPO₄/KH₂PO₄, 0.1 mM EDTA, 5% (w/v) glucose, 0.3 mM DTT, 1 mM NaN₃, pH 7.2) and dialyzed overnight against the same buffer at 4 °C using a Slide-A-Lyzer 7K dialysis cassette (Pierce). The dialyzed sample was pelleted at 39,000 g for 20 min at 4 °C and the supernatant filtered through a 0.2 µm syringe filter (Millipore).

LacI was then purified on a Mono S HR 5/5 Column using a GE AKTA FPLC with a 50 mM to 500 mM K₂HPO₄/KH₂PO₄ 40-column volume linear gradient (in 0.1 mM EDTA, 5% (w/v) glucose, 0.3 mM DTT, 1 mM NaN₃, pH 7.2), at a 1.0 mL/min flow rate. The fractions containing LacI (usually eluting between 250 and 300 mM K₂HPO₄/KH₂PO₄) were pooled and concentrated (if required) with a Centricon (Amicon, Millipore). Fractions that contain < 95% purity (determined from a 1% SDS-PAGE silver staining analysis) were further purified using a Sephadex 300, 2 x 15 cm gel filtration column at 1.0 mL/min flow rate using LacI Storage Buffer (200 mM K₂HPO₄/KH₂PO₄, 2 mM EDTA, 400 mM NaCl, 1 mM DTT, 1 mM NaN₃, pH 7.2). The concentrated samples were dialyzed against LacI Storage Buffer G (LacI Storage buffer that includes 50% glycerol) with multiple changes at 4°C overnight.

The concentration of LacI tetramer was determined from the A₂₈₀ with an extinction coefficient of 22,500 per monomer, with a typical yield of 5 nmol (2 mL of 25 µM) LacI tetramer per liter of LB. The active protein concentration was determined by EMSA, using radiolabeled 9C14 DNA prepared as below (14.4 nM) incubated with [LacI] ranging from 0-32 nM in LacI buffer (25 mM Tris, 100 mM KCl, 5 mM MgCl₂, 2 mM DTT, 50 µg/µL BSA, 0.02% IGEPAL CA-630 (Sigma; replaces

nonionic detergent Nonidet P-40). Electrophoresis was in a 7.5% gel (75:1 acrylamide:*bis*-acrylamide) at 20 V/cm for 2 hours at 20 °C in TBE buffer. Samples were incubated for 15 min at room temperature before loading onto the gel. The fraction of DNA binding to LacI was used to calculate the active LacI concentration relative to the A_{280} .

Radiolabeled 9C14 DNA was prepared by labeling 100 μ M of the top primer (5' CTGCAGGTCAGTCTAGTTAATTGTGAGCGC 3') with 70 μ Ci γ -[32 P]-ATP (6000 Ci/mmol, Perkin-Elmer) with T4 polynucleotide kinase (New England Biolabs), in a 10 μ L reaction volume. The primer was separated from the ATP using a P6 column (BioRad). The labeled primer was combined with the unlabeled bottom primer (5' CAAGCTTTACCATCAATGAATTGTGAGCGC 3'), and end-labeled 9C14 was produced by PCR. PCR mixtures (50 μ L) contained 40 pg of *Bst**N I* digested pRM9C14 DNA template (3), 0.5 μ M each primer, 250 μ M each dNTP, and 2 U Phusion polymerase (New England Biolabs), in HF buffer. After an initial 3 min incubation at 95 °C, 35 cycles of 95 °C for 1 min, 63 °C for 30 sec, and 72 °C for 1 min were performed. The labeled product was visualized on a Phosphorimager (Storm 680, Molecular Dynamics) and gel purified. The final DNA concentration was determined by scintillation counting (Packard 1600TR) with the specific activity being known from that of the labeled primer, assuming complete recovery of primer from the P6 column. Typical specific activity is about 60 % upon purification, declining to 40 % after prolonged storage.

Appendix II Data Analysis and Error Propagation

Supporting Material for Paper Submission derived directly from the work of Dr. Douglas English and Zifan Wang.

Goodson, Haeusler, Wang, English, and Kahn “LacI-DNA-IPTG Loops: Equilibria among Conformations by Single-Molecule FRET”

Error Analysis

Standard error propagation was used to estimate the uncertainties associated with the FRET histograms shown in Figures 4 and 5. The purpose of this analysis was to evaluate the intermediate FRET values observed in the region of 40-80% FRET efficiency. Toward this end, estimations of the standard deviation associated with the calculation of the high and low FRET distributions were acquired by constructing photon counting histograms (Figure 1). These histograms show the donor (green) and acceptor (red) intensity distributions from millisecond bursts for which the total intensity (donor plus acceptor) exceeded a threshold of 30 photons per millisecond. Once constructed, the photon counting histograms were fit to a superposition of two log normal distributions:

$$P(I) = \frac{A_1}{\sigma_1 I \sqrt{2\pi}} e^{-(\ln(I) - \mu_1)^2 / 2\sigma_1^2} + \frac{A_2}{\sigma_2 I \sqrt{2\pi}} e^{-(\ln(I) - \mu_2)^2 / 2\sigma_2^2} \quad (1)$$

where I is the intensity value (x -axes in Figure 1). The solid black lines in the panels of Figure 1 indicate the results of the fits to Equation 1. The log normal fit parameters were used to calculate the peak intensity along with the mean and variances of the intensity distributions using the following relationships:

$$\bar{I}_X = e^{\mu_x + \sigma^2 x / 2} \quad (2)$$

$$\sigma_X^2 = (e^{\sigma_X^2} - 1) e^{2\mu_X + \sigma_X^2} \quad (3)$$

where x represents either the acceptor or donor. The variance and mean values as obtained from Equations 2 and 3 were used to find the estimated variance for apparent FRET values using Equations 4 and 5.

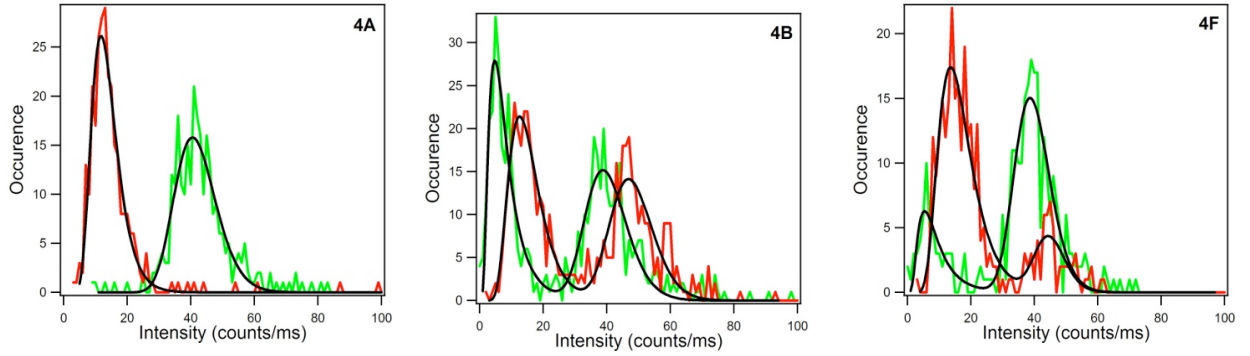


Figure 1: Photon counting histograms for bursts above a threshold of 30 total counts per millisecond. Red traces and green traces correspond to acceptor photons and donor photons respectively. Each panel is labeled with the figure number of the corresponding figure in the main text.

$$\sigma_{E_{app}}^2 = \left(\frac{\partial E_{app}}{\partial I_A} \right)^2 \sigma_{I_A}^2 + \left(\frac{\partial E_{app}}{\partial I_D} \right)^2 \sigma_{I_D}^2 \quad (4)$$

$$\sigma_{E_{app}}^2 = \left[\left(1 + \frac{I_D}{I_A} \right)^{-2} \left(\frac{I_D}{I_A^2} \right) \right]^2 \sigma_{I_A}^2 + \left[\left(1 + \frac{I_D}{I_A} \right)^{-2} \left(\frac{1}{I_A} \right) \right]^2 \sigma_{I_D}^2 \quad (5)$$

Results from this error analysis are given in Table 1. The values in columns designated *Low FRET* were acquired from low intensity acceptor and high intensity donor photon count distributions and the values in columns labeled *High FRET* were acquired from high intensity acceptor and low intensity donor photon count distributions. For instance, in the panel labeled 4A of Supplemental Figure 1, only low intensity acceptor and high intensity donor distributions are observed, hence only *Low Fret* values are calculated. In the panel labeled 4B in Fig. S1 both the acceptor and donor histograms show two clear distributions and these were fit to a sum of two log normal distributions (Equation 1) after which error was propagated for two FRET distributions using the values obtained from the four intensity distributions.

The average intensities and the standard deviation for E_{App} are given in Table 1. Only six sets of FRET data were modeled using this approach because the remaining sets did not yield photon counting histograms that could be well-fit to log normal distributions due to overlap of high and low intensity distributions. To judge the quality of the error propagation approach for these five sets of data, the peak intensities for donor and acceptor and $\sigma_{E_{App}}$ were used to generate Gaussian distributions for E_{App} . These distributions are shown along with their experimentally-acquired counterparts in Figure 2 (solid black lines). Figure 2 illustrates the limits to standard error analysis using photon counting histograms. In Figure 2, the panels for 4A and 5A the low FRET efficiency peak is modeled well by a Gaussian function constructed using the mean donor and acceptor intensities acquired from the photon counting histograms. For the remaining histograms, showing two FRET efficiency

distributions, two fits are provided. One composed of the sum of two Gaussians (solid black line) and the other a sum including a Gaussian for the low FRET peak and the β function for the high FRET distribution (solid blue line). The β function has been used previously to describe FRET distributions near their limits (Dahan et al., 2001; Morgan et al., 2005):

$$\beta = \frac{E^{I_A} (1 - E)^{I_D}}{a} \quad (6)$$

I_A is the acceptor intensity, I_D is the donor intensity, and E is the efficiency. The quantity a is an amplitude scaling factor and is the only fitting variable used.

In the panels of Figure 2 for 4B, 4D, 4F and 5B the high FRET peak is fit fairly well but the sum of the two distributions do not capture the amplitude of the histogram at FRET values near 60%. The error propagation method also predicts a broader peak width than the β function.

Corresponding Panel in Figure 2	<i>Low FRET</i>			<i>High FRET</i>		
	$I_A \pm s$ (counts per ms)	$I_D \pm s$ (counts per ms)	$\sigma_{E_{App}}$	$I_A \pm s$ (counts per ms)	$I_D \pm s$ (counts per ms)	$\sigma_{E_{App}}$
4A	14 \pm 5	42 \pm 7	0.070			
4B	16 \pm 6	40 \pm 8	0.087	48 \pm 7	8 \pm 6	0.087
4C	11 \pm 5	39 \pm 7	0.081	44 \pm 10	5 \pm 10	0.19
4D	13 \pm 6	39 \pm 7	0.091	45 \pm 7	5 \pm 5	0.093
4E	14 \pm 5	39 \pm 15	0.10	45 \pm 7	N.F.	N.F.
4F	17 \pm 7	40 \pm 7	0.089	45 \pm 5	9 \pm 6	0.081
5A	14 \pm 6	31 \pm 7	0.096			
5B	20 \pm 8	37 \pm 12	0.12	47 \pm 12	11 \pm 9	0.13
5C	15 \pm 7	36 \pm 16	0.23	46 \pm 10	N.F.	N.F.
5D	14 \pm 7	34 \pm 18	0.15	44 \pm 11	N.F.	N.F.
5E	14 \pm 7	35 \pm 14	0.12	38 \pm 9	N.F.	N.F.
5F	14 \pm 8	35 \pm 20	0.16	41 \pm 13	N.F.	N.F.

Table 1: Values obtained from photon counting histograms and error analysis. Values for the mean and standard deviations of acceptor and donor intensities were determined from the log normal fits of photon counting histograms. The estimated standard deviation for the apparent FRET distributions was determined using Equation 5.

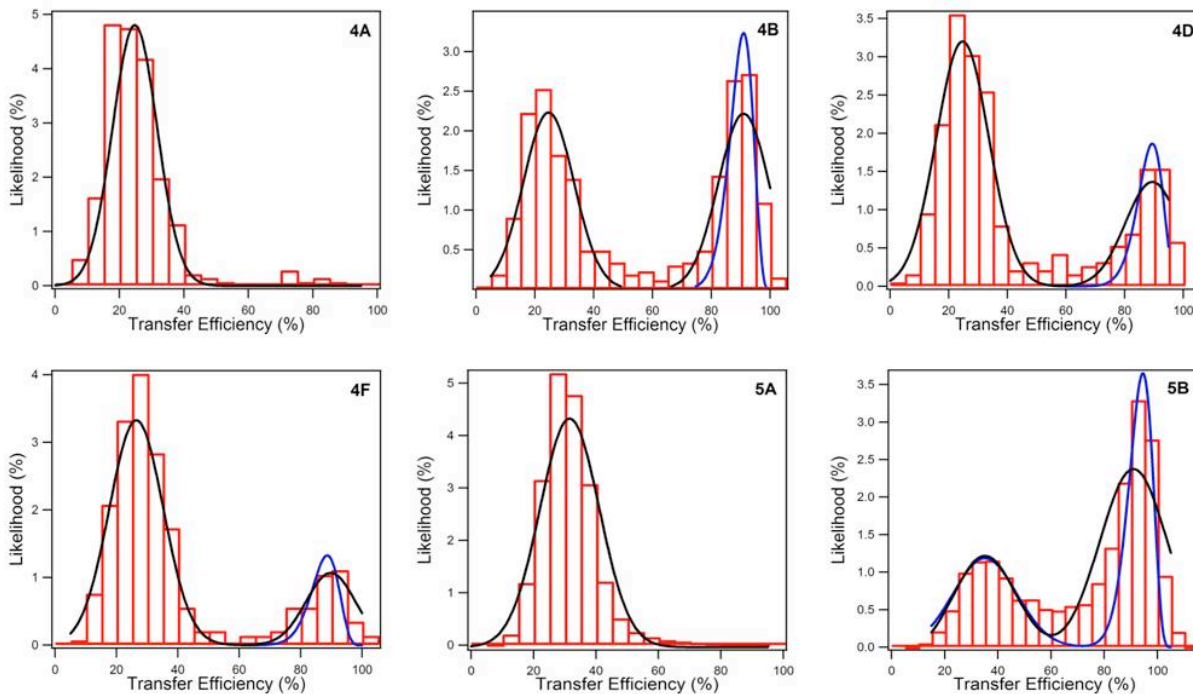


Figure 2: Experimentally-derived apparent FRET efficiency histograms (red bars) overlaid with estimated distributions from error analysis. The sum of two Gaussians is shown in black and a sum including a Gaussian for the low FRET peak and the β function for the high FRET distribution is shown in blue.

A main goal of this error analysis is to address the origin of intermediate FRET values in the range of 40-80% transfer efficiency. There are several possible molecular-level mechanisms for molecules with FRET efficiencies in this range: 1) there could be stable LacI-9C14-IPTG complexes with intermediate transfer efficiencies, 2) LacI-9C14-IPTG complexes could undergo a conversion from closed-to-open or open-to-closed looped complex while present in the observation volume of the microscope, and 3) the acceptor fluorophore could bleach during the observation time. The match between our predicted and actual distributions in Figure 2B suggests

that the intermediate FRET values near 60% are not due to the predicted uncertainties in the low and high efficiency peaks of the FRET distributions but actually originate from molecular-level mechanisms that contribute to additional broadening in the FRET distributions. The likely source for these intermediate values is the third scenario listed, acceptor bleaching during observation. The first scenario is unlikely since LacI-9C14-IPTG loops with alternative geometries would exhibit a distinct, Gaussian distribution. The second scenario is also unlikely since it would require that the complexes interconvert on a time scale faster than the millisecond time scale of the observations. Hence, we assign the intermediate FRET population to event in which the acceptor fluorophore photobleaches during the observation period.

Appendix III Fit to IPTG Saturation Curve

The fit of the plot of the average fraction of molecules exhibiting a FRET efficiency above 60% vs. IPTG concentration from Chapter 2 figure 2.6C (also shown bellow) is based on the measurable component in our system, fluorescence of the 9C14 model construct. The normalized area under the curve for the fraction of molecules that exhibited between 60%-100% energy transfer were plotted against IPTG concentration, represented as C and F in Figure 1 below. SM-FRET data from 9C14, LacI, and IPTG at the concentration of 0, .3, 1, 3, 10, 30 mM IPTG over three experiments were used in the plot (Figure 2).

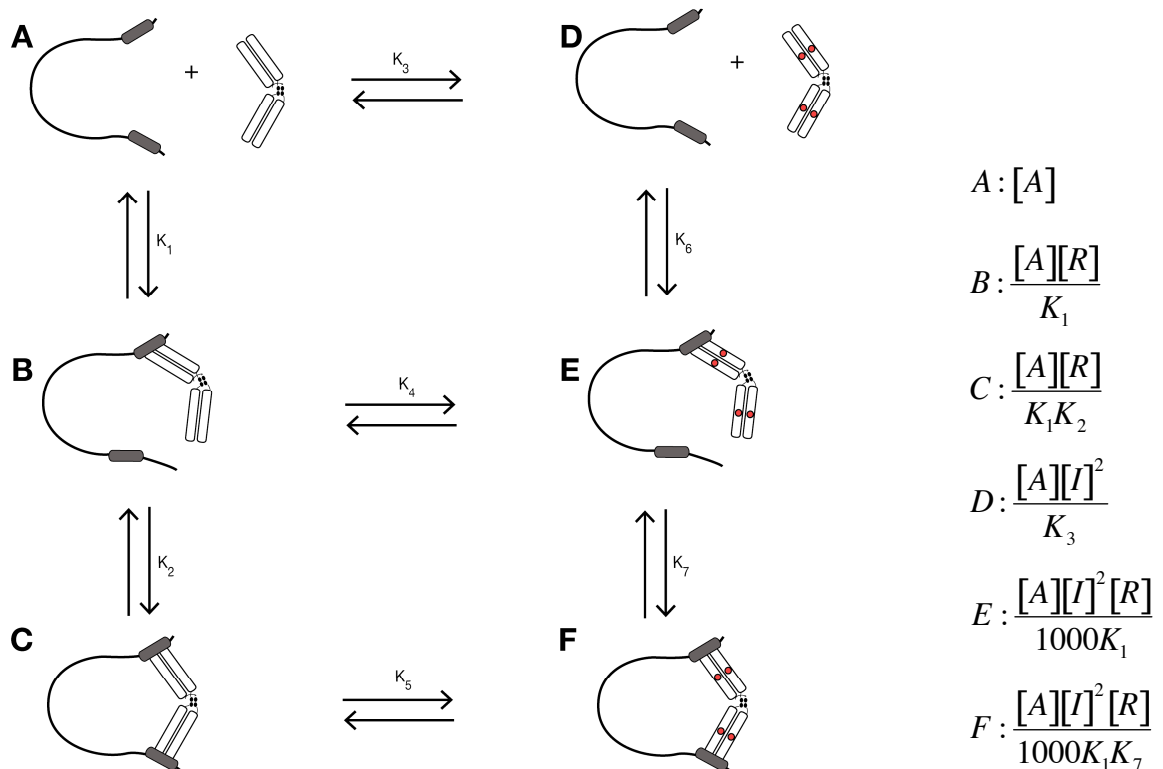


Figure 1: Model equilibrium of IPTG and operator binding in the case of saturating IPTG concentration. $[R]$ represents the tetrameric LacI concentration.

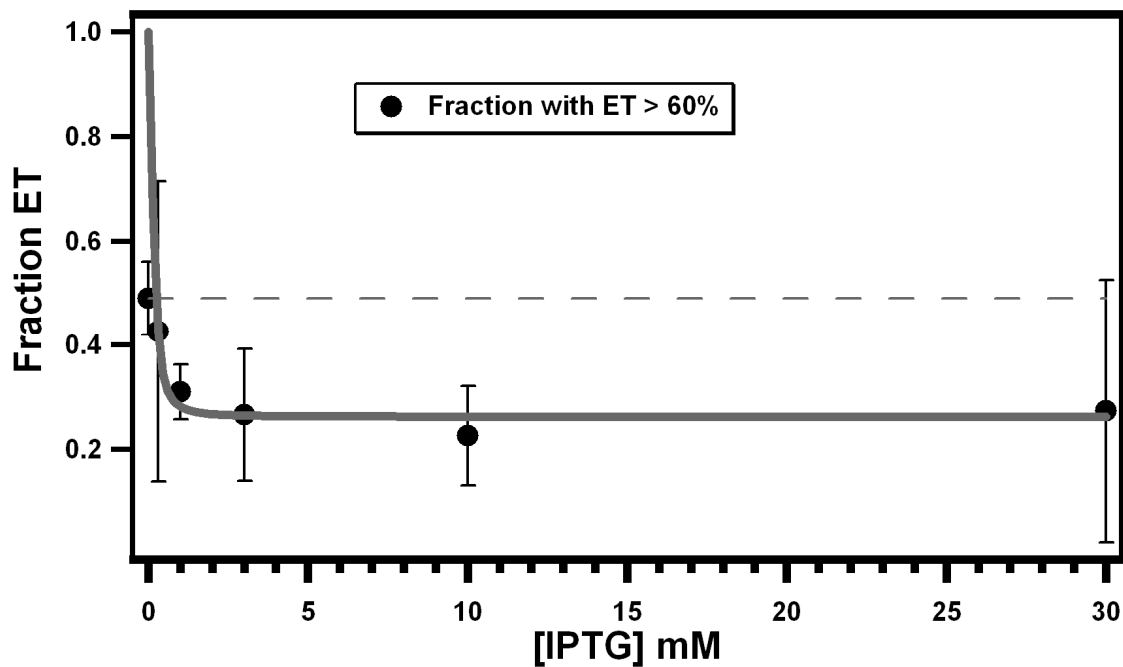


Figure 2: The above plot is fit to the following equation, with the defined parameters (C and F refer to Figure 1):

$$\text{Measurable: } \frac{C + F}{[9CT+]} = \frac{[\text{loop}] + [\text{loop} \cdot I]}{[DNA]_{\text{tot}}} = \frac{a + b[I]^2}{c + d[I]^2} \left(\frac{1}{1/b} \right) = \frac{(a/b) + [I]^2}{(c/b) + (d/b)[I]^2} = \frac{f + [I]^2}{g + [I]^2}$$

a = looped DNA

b = looped DNA + inducer

c = free DNA ± inducer

d = looped DNA ± inducer

$[I]^2 = 0 = a/c = \text{for normalized data}$

$d/b \neq 1$ and is represented as g

$a/b = f$ and $a = c$ in the case of no free DNA

Appendix IV Immobilization of Model DNA Constructs

In order to make direct comparisons of diffusing and immobilized experiments and as a means to directly monitor loop formation, we will employ an immobilization technique to our study that does not involve protein-surface interaction, which could interfere with dynamics. Several immobilization research methods are available including hydrogels (Tang et al., 2004), agarose gels (Huang et al., 2001; Lu et al., 1998; Peterman et al., 1999), acrylamide gels (Peterman et al., 1999), surface-tethered vesicles (Boukobza et al., 2001; Rhoades et al., 2003) and attachment to a surface using biotin and streptavidin (Joo et al., 2004; Lesoine et al., 2006). Attachment to a glass surface has been a prevailing technique used to study single molecule immobilized biological molecules. The Haran group has immobilized biomolecules using vesicles through a technique that encompasses vesicle encapsulation of probe molecules with bilayer/avidin immobilization of the vesicles (Boukobza et al., 2001). The Ha group has directly immobilized biotinylated DNA to avidin-coated surfaces (Joo et al., 2004).

Our technique will involve tethering the 9C14 construct to a glass surface via a biotin/streptavidin linkage, with the biotin linked to the DNA far away from the loop. Our method will involve immobilizing biotinylated 9C14 to a biotin/polyethylene glycol (PEG) streptavidin intermediate treated coverslip (MicroSurfaces, Inc.). The model for the immobilized DNA model construct is a the 9C14 fluorophore conjugated DNA linked to a long tailed biotinylated DNA molecule linked via linker as shown in the following in Figure 1:

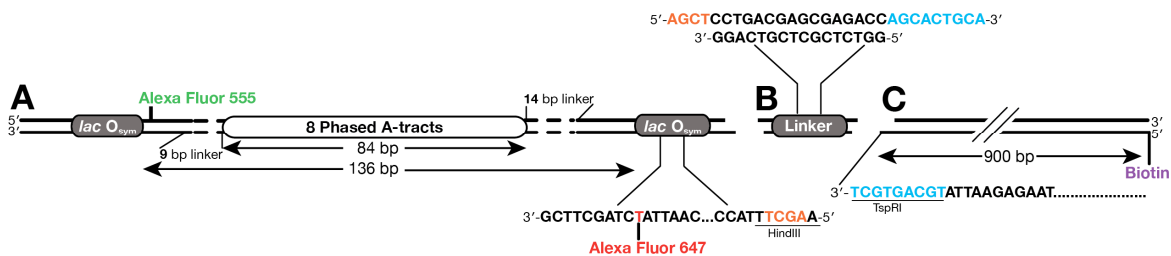


Figure 1: The schematic of fluorophore labeled immobilized DNA looping constructs. The A, B, and C labels represent the three DNA components of the construct and are fully outlined in the text below.

The following includes the experimental preparation conducted to date for our immobilized method:

(A) Fluorescently labeled 9C14 product

PCR Product from EcoRV restricted pRM9C14:

```

ATCTGCAGGTCAGTCTAGGTAATTGTGAGCGCTCACAATTAGATCTCAAT
TCGTACGGATCCGGTTTTTTGCCCCTTTTTTGCCGTTTTTTGCCCCTTTT
TTGCCGTTTTTTGCCCCTTTTTTTGCCGTTTTTTGCCCCTTTTTTTGCGCTG
AACGCGTCCTAGAATCGAAGCTAGCTAATTGTGAGCGCTCACAATTCGTT
GTGGTAAAGCTTTGAT

```

Fluorophores were conjugated to oligonucleotides synthesized with an amino dT C-6 internal modification (T* below: iAmMC6T). PCR was performed using the previously described conditions for fluorescently labeled 9C14 from Chapter 2 with the following primers: 9C14- Alexa Fluor® 555: 5'-CCGATATCTGCAGGTCAGTCTAGGTAATTGTGAGCGCTCACAATTAT*ATC-3' 9C14- Alexa Fluor® 647: 5'-TTGATATCAAAGCTTTACCACAACGAATTGTGAGCGCTCACAATTAT*CTAGCTTCG-3'. Immediately following PCR the product was restricted with HindIII under NEB conditions followed by heat inactivation. The PCR product was isolated on a 7.5 % polyacrylamide (40:1 (w/w) acrylamide: bis-acrylamide), native gel. The

DNA was excised and eluted overnight into 50 mM NaOAc (pH 7.0) and 1 mM EDTA, phenol-chloroform extracted, ethanol precipitated, and resuspended in T4 DNA ligase buffer.

(B) Linker

Annealed linker product is composed of the following ssDNA:

5'-AGCTCCTGACGAGCGAGACCAGCACTGCA-3' and 3'-GGACTGCTCGCTCTGG-5'. Oligonucleotides were purified on a 12% polyacrylamide (40:1 (w/w) acrylamide: bis-acrylamide), 8 M urea gel. Oligonucleotides were excised, eluted, phenol-chloroform extracted and ethanol precipitated. The T4 polynucleotide kinase reaction was performed with each individual purified oligonucleotides under the recommended NEB conditions in T4 DNA ligase buffer. This was followed by an annealing reaction under Sigma-Aldrich conditions in ligase buffer. Outlined as follows:

1. Mix corresponding volumes of both ssDNA
2. Place tube in a standard heatblock at 90–95 °C for 3–5 minutes.
3. Slow cool to room temperature (45–60 minutes).
4. Store at 4 °C

Annealing of the purified single strands of the linker in a 1:1 ratio were successful as shown in Figure 3.

(C) 905 bp Product

PCR Product from pARH:

```
GGCCGCAGTGTTATCACTCATGGTTATGGCAGCACTGCATAAATCTCTTA
CTGTCATGCCATCCGTAAGATGCTTTTCTGTGACTGGTGAGTACTCAACC
AAGTCATTCTGAGAATAGTGTATGCGGCGACCGAGTTGCTCTTGCCCGGC
GTCAATACGGGATAATACCGCGCCACATAGCAGAACTTTAAAAGTGCTCA
TCATTGGAAAACGTTCTTCGGGGCGAAAACCTCTCAAGGATCTTACCGCTG
TTGAGATCCAGTTCGATGTAACCCACTCGTGCACCCAACCTGATCTTCAGC
ATCTTTTACTTTACCAGCGTTTCTGGGTGAGCAAAAACAGGAAGGCAAA
ATGCCGCAAAAAGGGAATAAGGGCGACACGGAAATGTTGAATACTCATA
CTCTTCCTTTTTCAATATATTGAAGCATTTATCAGGGTTATTGTCTCAT
GAGCGGATACATATTTGAATGTATTTAGAAAAATAAACAAATAGGGGTTC
CGCGCACATTTCCCGAAAAGTGCCACCTGACGTCTAAGAAACCATTATT
ATCATGACATTAACCTATAAAAATAGGCGTATCACGAGGCCCTTTCGTCT
CGCGCGTTTCGGTGATGACGGTGAAAACCTCTGACACATGCAGCTCCCGG
AGACGGTCACAGCTTGTCTGTAAGCGGATGCCGGGAGCAGACAAGCCCGT
CAGGGCGCGTCAGCGGGTGTGGCGGGTGTGGGGCTGGCTTAACTATGC
GGCATCAGAGCAGATTGTAAGTGCAGAGTGCACCATATGCGGTGTGAAATAC
CGCACAGATGCGTAAGGAGAAAATACCGCATCAGGCGCCATTGCCATTC
AGGCTGCGCAACTGTTGGGAAGGGCGATCGGTGCGGGCCTCTTCGCTATT
ACGCC
```

PCR cycling conditions were the following: 94.0°C for 1 min, 55.0°C for 30 s, 60.0°C for 30 s, 72°C for 1 min, for 35 cycles. The following primers were used Primer Top 5'-GGCCGCAGTGTTATCACTCATGG-3' and Primer Bottom 5' /5Biosg/GGCGTAATAGCGAAGAGGCCCGC-3.' PCR reactions (50 µL) contained 40 picograms of template, 250 µM of each dNTP, 1 µM of each primer above, 1X Phusion™ HF Reaction Buffer, and 2 units of Phusion™ High-Fidelity DNA Polymerase. Due to low recovery during the purification process multiple PCR reactions should be run.

Immediately following PCR the product (Figure 2) was restricted with TspRI under NEB conditions overnight. The PCR product was isolated on a 7.5 %

polyacrylamide (40:1 (w/w) acrylamide: bis-acrylamide), native gel. The DNA was excised and eluted overnight into 50 mM NaOAc (pH 7.0) and 1 mM EDTA, phenol-chloroform extracted, ethanol precipitated, and resuspended in TE buffer. Incorporation of the TspRI site has been seen in the work of Poirier (Poirier et al., 2009).

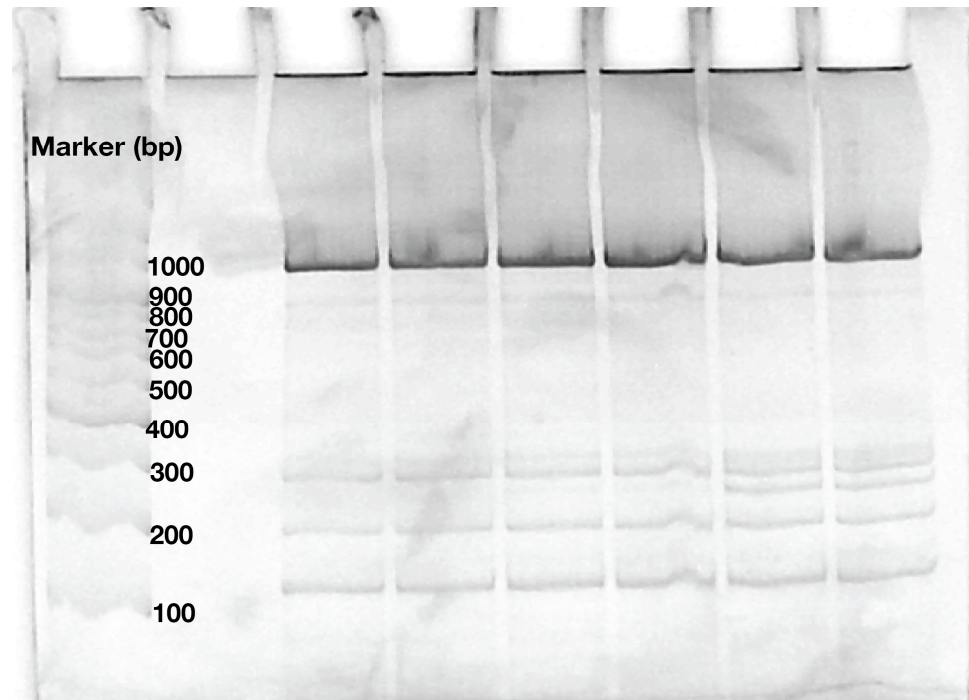


Figure 2: 905 bp PCR product analysis on a 7.5 % polyacrylamide (40:1 (w/w) acrylamide: bis-acrylamide) native gel. Variation in gel percentage used for purification was performed in order to maximize recovery of product. Low recovery is probably due the length of product.

(A + B) Product

Ligation reactions were run overnight at 16°C following NEB conditions. Controls were run of self ligations of single stranded linker, annealed linker, and restricted 9C14, example of some are shown in Figure 3. The ligations of restricted

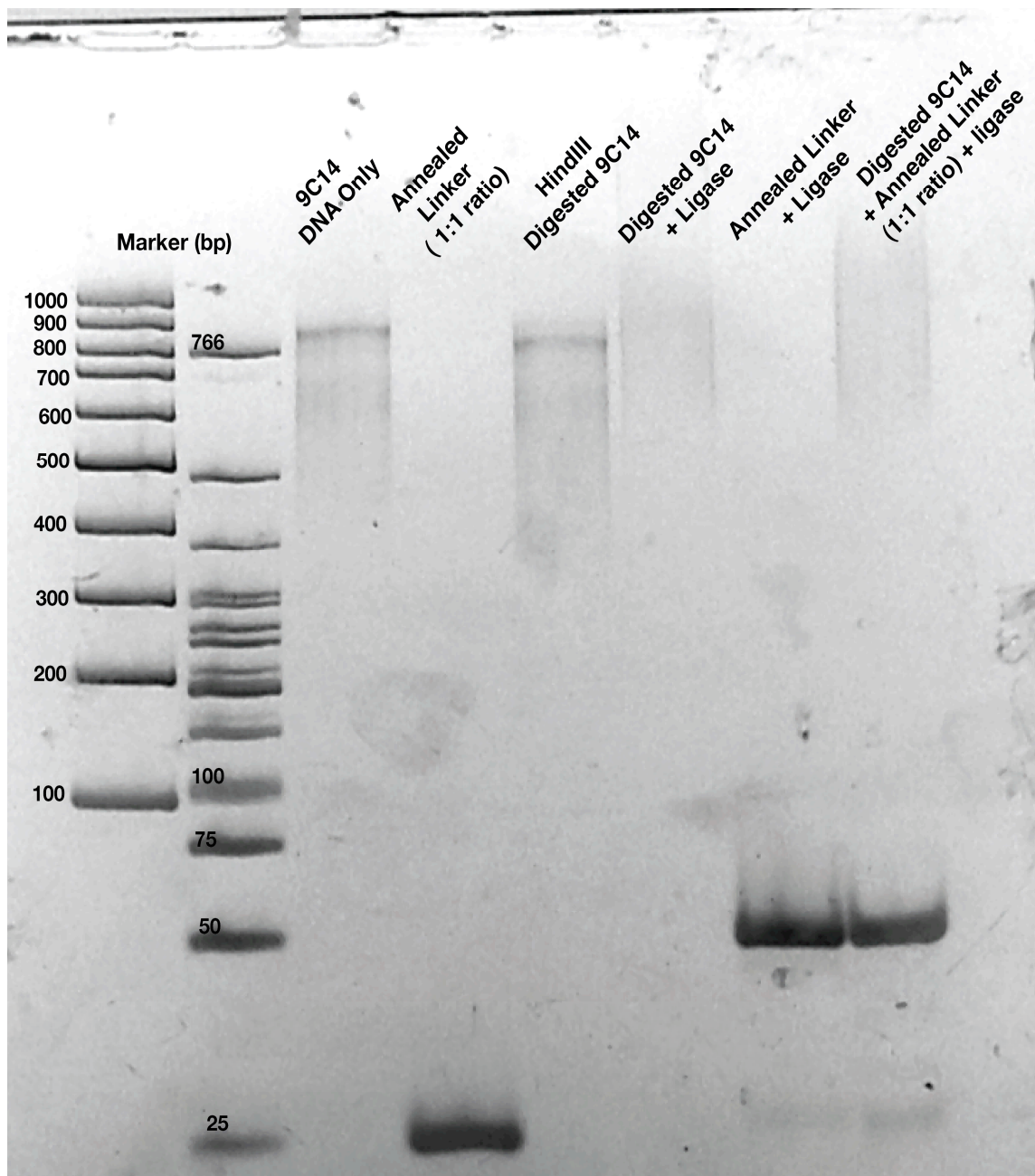


Figure 3: 7.5 % polyacrylamide (40:1 (w/w) acrylamide: bis-acrylamide) native gel analysis of components of immobilized looping construct. The ligation of the digested 9C14 and annealed linker shown here reveal smearing. Other control studies (not shown) have indicated that the multiple products above 1200 bp have formed with ligations of digested 9C14 and the annealed linker in multiple ratios.

9C14:annealed linker at various conditions gave multiple products in MW ranges above the expected product.

Future work will include ligations of A, B, and C (Figure 1). Ligation studies varying the ratio of 9C14 (A) and annealed linker (B) should be conducted to improve the yield of the reaction. The A+B purified ligation product can then be ligated to the TspRI restricted 905 bp biotin PCR product (C). The final ligation product (A+B+C) does not have to be purified because only final products with both incorporation of the biotin label (C) and fluorophores (A) will be detected in the immobilized SM-FRET studies (A). In addition, the three components (A+B+C) can be ligated in a single reaction, again without a final gel purification step.

Bibliography

- Ambrose, W.P., Goodwin, P.M., Jett, J.H., Van Orden, A., Werner, J.H., and Keller, R.A. (1999). Single molecule fluorescence spectroscopy at ambient temperature. *Chem Rev* 99, 2929-2956.
- Becker, N.A., Kahn, J.D., and Maher III, L.J. (2005). Bacterial repression loops require enhanced DNA flexibility. *J Mol Biol* 349, 716-730.
- Bell, C.E., Barry, J., Matthews, K.S., and Lewis, M. (2001). Structure of a variant of lac repressor with increased thermostability and decreased affinity for operator. *J Mol Biol* 313, 99-109.
- Bell, C.E., and Lewis, M. (2000). A closer view of the conformation of the Lac repressor bound to operator. *Nat Struct Biol* 7, 209-214.
- Bellomy, G.R., Mossing, M.C., and Record, M.T., Jr. (1988). Physical properties of DNA *in vivo* as probed by the length dependence of the lac operator looping process. *Biochemistry* 27, 3900-3906.
- Bellomy, G.R., and Record, M.T., Jr. (1990). Stable DNA loops *in vivo* and *in vitro*: roles in gene regulation at a distance and in biophysical characterization of DNA. *Progress in Nucleic Acid Research and Molecular Biology* 39, 81-128.
- Berlier, J.E., Rothe, A., Buller, G., Bradford, J., Gray, D.R., Filanoski, B.J., Telford, W.G., Yue, S., Liu, J., Cheung, C.-Y., *et al.* (2003). Quantitative comparison of long-wavelength Alexa fluor dyes to Cy dyes: fluorescence of the dyes and their bioconjugates. *J Histochem Cytochem* 51, 1699-1712.
- Binnig, G., Quate, C.F., and Gerber, C. (1986). Atomic Force Microscope. *Phys Rev Lett* 56, 930-933.
- Binnig, G., Rohrer, H., Gerber, C., and Weibel, E. (1982). Surface Studies by Scanning Tunneling Microscopy. *Phys Rev Lett* 49, 57-61.
- Blackwood, E.M., and Kadonaga, J.T. (1998). Going the distance: a current view of enhancer action. *Science (New York, N Y)* 281, 60-63.
- Boezi, J.A., and Cowie, D.B. (1961). Kinetic studies of beta-galactosidase induction. *Biophys J* 1, 639-647.
- Bond, L.M., Peters, J.P., Becker, N.A., Kahn, J.D., and Maher, L.J. (2010). Gene repression by minimal *lac* loops *in vivo*. *Nucl Acids Res* 38, 8072-8082.
- Boukobza, E., Sonnenfeld, A., and Haran, G. (2001). Immobilization in surface-tethered lipid vesicles as a new tool for single biomolecule spectroscopy. *J Phys Chem B* 105, 12165-12170.

- Brenowitz, M., Mandal, N., Pickar, A., Jamison, E., and Adhya, S. (1991). DNA-binding properties of a lac repressor mutant incapable of forming tetramers. *J Biol Chem* 266, 1281-1288.
- Chargaff, E. (1950). Chemical specificity of nucleic acids and mechanism of their enzymatic degradation. *Experientia* 6, 201-209.
- Chatterjee, S., Zhou, Y.N., Roy, S., and Adhya, S. (1997). Interaction of gal repressor with inducer and operator: induction of gal transcription from repressor-bound DNA. *Proc Natl Acad Sci USA* 94, 2957-2962.
- Chung, H.S., Louis, J.M., and Eaton, W.A. (2009). Experimental determination of upper bound for transition path times in protein folding from single-molecule photon-by-photon trajectories. *Proc Natl Acad Sci USA* 106, 11837-11844.
- Condon, A. (2006). Designed DNA molecules: principles and applications of molecular nanotechnology. *Nat Rev Gen* 7, 565-575.
- Cordes, T., Maiser, A., Steinhauer, C., Schermelleh, L., and Tinnefeld, P. (2011). Mechanisms and advancement of antifading agents for fluorescence microscopy and single-molecule spectroscopy. *Phys Chem Chem Phys* 13, 6699-6709.
- Crothers, D.M., Haran, T.E., and Nadeau, J.G. (1990). Intrinsically bent DNA. *J Biol Chem* 265, 7093-7096.
- Daber, R., Stayrook, S., Rosenberg, A., and Lewis, M. (2007). Structural analysis of lac repressor bound to allosteric effectors. *J Mol Biol* 370, 609-619.
- Dahan, M., Deniz, A.A., Ha, T., Chemla, D.S., Schulz, P.G., and Weiss, S. (2001). Ratiometric measurement and identification of single diffusing molecules. *Chem Phys* 247, 85-106.
- Deniz, A.A., Dahan, M., Grunwell, J.R., Ha, T., Faulhaber, A.E., Chemla, D.S., Weiss, S., and Schultz, P.G. (1999). Single-pair fluorescence resonance energy transfer on freely diffusing molecules: observation of Förster distance dependence and subpopulations. *Proc Natl Acad Sci USA* 96, 3670-3675.
- Deniz, A.A., and Mukhopadhyay, S. (2007). Fluorescence from diffusing single molecules illuminates biomolecular structure and dynamics. *J Fluorescence* 17, 775-783.
- Donner, J., Caruthers, M.H., and Gill, S.J. (1982). A calorimetric investigation of the interaction of the lac repressor with inducer. *J Biol Chem* 257, 14826-14829.
- Edelman, L.M., Cheong, R., and Kahn, J.D. (2003). Fluorescence resonance energy transfer over ~130 basepairs in hyperstable Lac repressor-DNA loops. *Biophys J* 84, 1131-1145.

- Elf, J., Li, G.W., and Xie, X.S. (2007). Probing transcription factor dynamics at the single-molecule level in a living cell. *Science* *316*, 1191-1194.
- Emmer, M., deCrombrughe, B., Pastan, I., and Perlman, R. (1970). Cyclic AMP receptor protein of *E. coli*: its role in the synthesis of inducible enzymes. *Proc Natl Acad Sci USA* *66*, 480-487.
- Eslami-Mossallam, B., and Ejtehadi, M.R. (2009). Asymmetric elastic rod model for DNA. *Phys Rev E* *80*.
- Finzi, L., and Gelles, J. (1995). Measurement of lactose repressor-mediated loop formation and breakdown in single DNA-molecules. *Science* *267*, 378-380.
- Flynn, T.C., Swint-Kruse, L., Kong, Y.F., Booth, C., Matthews, K.S., and Ma, J.P. (2003). Allosteric transition pathways in the lactose repressor protein core domains: asymmetric motions in a homodimer. *Protein Sci* *12*, 2523-2541.
- Friedman, A.M., Fischmann, T.O., and Steitz, T.A. (1995). Crystal structure of lac repressor core tetramer and its implications for DNA looping. *Science* *268*, 1721-1727.
- Geanacopoulos, M., Vasmatzis, G., Zhurkin, V.B., and Adhya, S. (2001). Gal repressosome contains an antiparallel DNA loop. *Nat Struct Biol* *8*, 432-436.
- Gilbert, W., and Maxam, A. (1973). The nucleotide sequence of the lac operator. *Proc Natl Acad Sci USA* *70*, 3581-3584.
- Ha, T., Enderle, T., Ogletree, D.F., Chemla, D.S., Selvin, P.R., and Weiss, S. (1996). Probing the interaction between two single molecules: fluorescence resonance energy transfer between a single donor and a single acceptor. *Proc Natl Acad Sci USA* *93*, 6264-6268.
- Haeusler, A. (2011). Differentiating a landscape of lac repressor mediated DNA loops using FRET. PhD Dissertation (College Park, University of Maryland).
- Haeusler, A.R., Goodson, K., and Kahn, J.D. (2010). A LacI-DNA looping landscape and allosteric effects on the loop shapes. *Biophys J* *98*, 72a.
- Hagerman, P.J. (1988). Flexibility of DNA. *Annu Rev Biophys Bio Chem* *17*, 265-286.
- Harekrushna, S. (2011). Förster resonance energy transfer-spectroscopic nanoruler: principle and applications. *JPPC* *12*, 20-30.
- Hirsh, A.D., Lillian, T.D., Lionberger, T.A., and Perkins, N.C. (2011). DNA modeling reveals an extended lac repressor conformation in classic in vitro binding assays. *Biophys J* *101*, 718-726.

- Hoefling, M., Lima, N., Haenni, D., Seidel, C.A.M., Schuler, B., and Grubmuller, H. (2011). Structural Heterogeneity and Quantitative FRET Efficiency Distributions of Polyprolines through a Hybrid Atomistic Simulation and Monte Carlo Approach. *PLoS ONE* 6.
- Horowitz, D.S., and Wang, J.C. (1984). Torsional rigidity of DNA and length dependence of the free energy of DNA supercoiling. *J Mol Biol* 173, 75-91.
- Huang, S., Hayes, S.J., and Serwer, P. (2001). Fluorescence microscopy of single viral capsids. *J Struct Biol* 135, 270-280.
- Jacob, F., and Monod, J. (1961a). Genetic regulatory mechanisms in the synthesis of proteins. *J Mol Biol* 3, 318-356.
- Jacob, F., and Monod, J. (1961b). On the regulation of gene activity. *Cold Spring Harbor Symp Quant Biol* 26, 193-211.
- Joo, C., McKinney, S.A., Lilley, D.M.J., and Ha, T. (2004). Exploring Rare Conformational Species and Ionic Effects in DNA Holliday Junctions Using Single-molecule Spectroscopy. *Journal of Molecular Biology* 341, 739-751.
- Kahn, J.D., Cheong, R., Mehta, R.A., Edelman, L.M., and Morgan, M.A. (2006). Flexibility and control of protein-DNA loops. *Biophys Rev Lett* 1, 327-341.
- Kalodimos, C.G., Boelens, R., and Kaptein, R. (2004). Toward an integrated model of protein-DNA recognition as inferred from NMR studies on the Lac repressor system. *Chem Rev* 104, 3567-3586.
- Kao-Huang, Y., Revzin, A., Butler, A.P., O'Conner, P., Noble, D.W., and von Hippel, P.H. (1977). Nonspecific DNA binding of genome-regulating proteins as a biological control mechanism: Measurement of DNA-bound *Escherichia coli* lac repressor *in vivo*. *Proc Natl Acad Sci USA* 74, 4228-4232.
- Koo, H.S., Drak, J., Rice, J.A., and Crothers, D.M. (1990). Determination of the extent of DNA bending by an adenine thymine tract. *Biochemistry* 29, 4227-4234.
- Kramer, H., Amouyal, M., Nordheim, A., and Müller-Hill, B. (1988). DNA supercoiling changes the spacing requirement of two lac operators for DNA loop formation with lac repressor. *EMBO J* 7, 547-556.
- Kuhlman, T., Zhang, Z., Saier, M.H., and Hwa, T. (2007). Combinatorial transcriptional control of the lactose operon of *Escherichia coli*. *Proc Natl Acad Sci USA* 104, 6043-6048.
- Lakowicz, J.R. (2006). *Principles of Fluorescence Spectroscopy*, 3rd edn (New York, Springer).

- Lesoine, J.F., Holmberg, B., Maloney, P., Wang, X., Novotny, L., and Knauf, P.A. (2006). Development of an spFRET method to measure structure changes in ion exchange proteins. *Acta Physiol (Oxf)* 187, 141-147.
- Levandoski, M. M., O. V. Tsodikov, D. E. Frank, S. E. Melcher, R. M. Saecker, and M. T. Record, Jr. (1996). Cooperative and anticooperative effects in binding of the first and second plasmid O_{sym} operators to a LacI tetramer: Evidence for contributions of non-operator DNA binding by wrapping and looping. *J Mol Biol* 260, 697-717.
- Lewis, M. (1996). Response: DNA Looping and Lac Repressor--CAP Interaction. *Science* 274, 1931-1932.
- Lewis, M. (2005). The lac repressor. *C R Biol* 328, 521-548.
- Lewis, M., Chang, G., Horton, N.C., Kercher, M.A., Pace, H.C., Schumacher, M.A., Brennan, R.G., and Lu, P. (1996). Crystal structure of the lactose operon repressor and its complexes with DNA and inducer. *Science* 271, 1247-1254.
- Lillian, T.D., Goyal, S., Kahn, J.D., Meyhöfer, E., and Perkins, N.C. (2008). Computational analysis of looping of a large family of highly bent DNA by LacI. *Biophys J* 95, 5832-5842.
- Lobell, R.B., and Schleif, R.F. (1990). DNA looping and unlooping by AraC protein. *Science* 250, 528-532.
- Lobell, R.B., and Schleif, R.F. (1991). AraC DNA looping: orientation and distance-dependent loop breaking by the cyclic AMP receptor protein. *J Mol Biol* 218, 45-54.
- Lodish, H., Berk, A., Zipursky, S.L., Matsudaira, P., Baltimore, D., and Darnell, J. (2000). *Molecular Cell Biology* (4th edition)
- Lodish, H.F. (2000). *Molecular cell biology, 4th edn* (New York, W.H. Freeman).
- Lu, H.P., Xun, L., and Xie, X.S. (1998). Single-Molecule Enzymatic Dynamics 10.1126/science.282.5395.1877. *Science* 282, 1877-1882.
- Matthews, K.S., Wilson, C.J., Zhan, H., and Swint-Kruse, L. (2007). The lactose repressor system: paradigms for regulation, allosteric behavior and protein folding. *Cell Mol Life Sci* 64, 3-16.
- McKay, D.B., Pickover, C.A., and Steitz, T.A. (1982). Escherichia coli lac repressor is elongated with its operator DNA binding domains located at both ends. *J Mol Biol* 156, 175-183.
- Mehta, R.A., and Kahn, J.D. (1999). Designed hyperstable Lac repressor-DNA loop topologies suggest alternative loop geometries. *J Mol Biol* 294, 67-77.

- Moerner, W.E. (2002). A Dozen Years of Single-Molecule Spectroscopy in Physics, Chemistry, and Biophysics. *The Journal of Physical Chemistry B* 106, 910-927.
- Moerner, W.E., and Orrit, M. (1999). Illuminating single molecules in condensed matter. *Science* 283, 1670-1676.
- Morgan, M.A., Okamoto, K., Kahn, J.D., and English, D.S. (2005). Single-molecule spectroscopic determination of lac repressor-DNA loop conformation. *Biophys J* 89, 2588-2596.
- Mossing, M.C., and Record, M.T. (1986). Upstream operators enhance repression of the lac promoter. *Science* 233, 889-892.
- Müller, J., Oehler, S., and Müller-Hill, B. (1996). Repression of lac promoter as a function of distance, phase and quality of an auxiliary lac operator. *J Mol Biol* 257, 21-29.
- Nie, S.M., and Zare, R.N. (1997). Optical detection of single molecules. *Annu Rev Biophys Biomol Struct* 26, 567-596.
- Normanno, D., Vanzi, F., and Pavone, F.S. (2008). Single-molecule manipulation reveals supercoiling-dependent modulation of lac repressor-mediated DNA looping. *Nucl Acids Res* 36, 2505-2513.
- O'Gorman, R.B., Rosenberg, J.M., Kallai, O.B., Dickerson, R.E., Itakura, K., Riggs, A.D., and Matthews, K.S. (1980). Equilibrium Binding of Inducer to Lac Repressor - Operator DNA Complex. *J Biol Chem* 255, 107-114.
- O'Gorman, R.B., Rosenberg, J.M., Kallai, O.B., Dickerson, R.E., Itakura, K., Riggs, A.D., and Matthews, K.S. (1980). Equilibrium binding of inducer to lac repressor•operator DNA complex. *J Biol Chem* 255, 10107-10114.
- Oehler, S., Amouyal, M., Kolkhof, P., von Wilcken-Bergmann, B., and Müller-Hill, B. (1994). Quality and position of the three *lac* operators of *E. coli* define efficiency of repression. *EMBO J* 13, 3348-3355.
- Oehler, S., Eismann, E.R., Kramer, H., and Müller-Hill, B. (1990). The three operators of the lac operon cooperate in repression. *EMBO J* 9, 973-979.
- Ohshima, Y., Mizokoshi, T., and Horiuchi, T. (1974). Binding of an inducer to the lac repressor. *J Mol Biol* 89, 127-136.
- Periasamy, A. (2001). Fluorescence resonance energy transfer microscopy: a mini review. *J Biomed Opt* 6, 287-291.
- Peterman, E.J.G., Brasselet, S., and Moerner, W.E. (1999). The fluorescence dynamics of single molecules of green fluorescent protein. *J Phys Chem A* 103, 10553-10560.

- Pfahl, M., Gulde, V., and Bourgeois, S. (1979). "Second" and "third operator" of the lac operon: An investigation of their role in the regulatory mechanism. *J Mol Biol* *127*, 339-344.
- Poirier, M.G., Oh, E., Tims, H.S., and Widom, J. (2009). Dynamics and function of compact nucleosome arrays. *NSMB* *16*, 938-944.
- Purohit, P.K., and Nelson, P.C. (2006). Effect of supercoiling on formation of protein-mediated DNA loops. *PhysR_E* *74*, 061907-061901-061914.
- Reznikoff, W.S., Winter, R.B., and Hurley, C.K. (1974). The location of the repressor binding sites in the lac operon. *Proc Natl Acad Sci USA* *71*, 2314-2318.
- Rhoades, E., Gussakovsky, E., and Haran, G. (2003). Watching proteins fold one molecule at a time. *Proc Natl Acad Sci USA* *100*, 3197-3202.
- Rippe, K., von Hippel, P.H., and Langowski, J. (1995). Action at a distance: DNA-looping and initiation of transcription. *Trends Biochem Sci* *20*, 500-506.
- Ruben, G.C., and Roos, T.B. (1997). Conformation of Lac repressor tetramer in solution, bound and unbound to operator DNA. *Microsc Res Tech* *36*, 400-416.
- Sadler, J.R., Sasmor, H., and Betz, J.L. (1983). A perfectly symmetric lac operator binds the lac repressor very tightly. *Proc Natl Acad Sci USA* *80*, 6785-6789.
- Sako, Y. (2006). Imaging single molecules in living cells for systems biology. *Mol Syst Biol* *2*, 56.
- Sandison, D.R., Piston, D.W., Williams, R.M., and Webb, W.W. (1995). Quantitative comparison of background rejection, signal-to-noise ratio, and resolution in confocal and full-field laser-scanning microscopes. *Applied Optics* *34*, 3576-3588.
- Sasmor, H.M., and Betz, J.L. (1990). Symmetric lac operator derivatives - effects of half-operator sequence and spacing on repressor affinity. *Gene* *89*, 1-6.
- Schafer, D.A., Gelles, J., Sheetz, M.P., and Landick, R. (1991). Transcription by single molecules of RNA polymerase observed by light microscopy. *Nature* *352*, 444-448.
- Schleif, R. (1987). Why should DNA loop? *Nature* *327*, 369-370.
- Schleif, R. (1992). DNA looping. *ARB* *61*, 199-223.
- Semsey, S., Virnik, K., and Adhya, S. (2005). A gamut of loops: meandering DNA. *Trends Biochem Sci* *30*, 334-341.
- Shore, D., and Baldwin, R.L. (1983). Energetics of DNA twisting. I. Relation between twist and cyclization probability. *J Mol Biol* *170*, 957-981.

- Shore, D., Langowski, J., and Baldwin, R.L. (1981). DNA flexibility studied by covalent closure of short fragments into circles. *Proc Natl Acad Sci USA* *78*, 4833-4837.
- Spronk, C.A., Bonvin, A.M., Radha, P.K., Melacini, G., Boelens, R., and Kaptein, R. (1999). The solution structure of Lac repressor headpiece 62 complexed to a symmetrical lac operator. *Structure* *7*, 1483-1492.
- Swigon, D., Coleman, B.D., and Olson, W.K. (2006). Modeling the Lac repressor-operator assembly: The influence of DNA looping on Lac repressor conformation. *Proc Natl Acad Sci USA* *103*, 9879-9884.
- Tang, J.Y., Mei, E., Green, C., Kaplan, J., DeGrado, W.F., Smith, A.B., and Hochstrasser, R.M. (2004). Probing structural dynamics of individual calmodulin : Peptide complexes in hydrogels by single-molecule confocal microscopy. *Journal of Physical Chemistry B* *108*, 15910-15918.
- van der Meer, B.W. (2002). Kappa-squared: from nuisance to new sense. *Rev Mol Biotechnol* *82*, 181-196.
- Vanzi, F., Broggio, C., Sacconi, L., and Pavone, F.S. (2006). Lac repressor hinge flexibility and DNA looping: single molecule kinetics by tethered particle motion. *Nucl Acids Res* *34*, 3409-3420.
- Vilar, J.M., and Leibler, S. (2003). DNA looping and physical constraints on transcription regulation. *J Mol Biol* *331*, 981-989.
- Vilar, J.M.G., and Saiz, L. (2005). DNA looping in gene regulation: from the assembly of macromolecular complexes to the control of transcriptional noise. *CODV* *15*, 136-144.
- Vologodskii, A., and Cozzarelli, N.R. (1996). Effect of supercoiling on the juxtaposition and relative orientation of DNA sites. *Biophys J* *70*, 2548-2556.
- Vologodskii, A.V., Levene, S.D., Klenin, K.V., Frank-Kamenetskii, M., and Cozzarelli, N.R. (1992). Conformational and thermodynamic properties of supercoiled DNA. *J Mol Biol* *227*, 1224-1243.
- von Hippel, P.H., and Berg, O.G. (1989). Facilitated target location in biological systems. *J Biol Chem* *264*, 675-678.
- Wang, Y.M., Tegenfeldt, J.O., Reisner, W., Riehn, R., Guan, X.J., Guo, L., Golding, I., Cox, E.C., Sturm, J., and Austin, R.H. (2005). Single-molecule studies of repressor-DNA interactions show long-range interactions. *Proc Natl Acad Sci USA* *102*, 9796-9801.
- Watson, J.D., and Crick, F.H.C. (1953). Molecular Structure of Nucleic Acids - a Structure for Deoxyribose Nucleic Acid. *Nature* *171*, 737-738.

- Weiss, S. (1999). Fluorescence spectroscopy of single biomolecules. *Science* 283, 1676-1683.
- Weiss, S. (2000). Measuring conformational dynamics of biomolecules by single molecule fluorescence spectroscopy. *Nat Struct Biol* 7, 724-729.
- Whitson, P.A., Hsieh, W.T., Wells, R.D., and Matthews, K.S. (1987). Influence of supercoiling and sequence context on operator DNA binding with lac repressor. *J Biol Chem* 262, 14592-14599.
- Wilson, C.J., Zhan, H., Swint-Kruse, L., and Matthews, K.S. (2007). Ligand interactions with lactose repressor protein and the repressor-operator complex: the effects of ionization and oligomerization on binding. *Biophys Chem* 126, 94-105.
- Wong, O.K., Guthold, M., Erie, D.A., and Gelles, J. (2008). Interconvertible lac repressor-DNA loops revealed by single-molecule experiments. *PLoS Biol* 6, e232.
- Xie, X.S., and Trautman, J.K. (1998). Optical studies of single molecules at room temperature. *Annu Rev Phys Chem* 49, 441-480.
- Yagil, G., and Yagil, E. (1971). On the relation between effector concentration and the rate of induced enzyme synthesis. *Biophys J* 11, 11-27.
- Zechiedrich, E.L., and Osheroff, N. (1990). Eukaryotic Topoisomerases Recognize Nucleic-Acid Topology by Preferentially Interacting with DNA Crossovers. *EMBO J* 9, 4555-4562.